Doctor of Philosophy

SCR 시스템에서 NOx 전환 효율 향상 연구

A study of improving NOx conversion efficiency in SCR System

The Graduate School of
University of Ulsan

Department of Mechanical Engineering

Muhammad Khristamto Aditya Wardana

A study of improving NOx conversion efficiency in SCR System

Supervisor: Prof. Lim, Ock Taeck

A Dissertation

Submitted to
the Graduate School of the University of Ulsan
in partial Fulfillment of the Requirements
for the degree of

Doctor of Philosophy

By

Muhammad Khristamto Aditya Wardana

Department of Mechanical Engineering
University of Ulsan, Republic of Korea
June 2021

A study of improving NOx conversion efficiency in SCR System

This certifies that the disertation of
Muhammad Khristamto Aditya Wardana is approved

Committee Chair	**Prof. Lee, Yoon Ho**
Committee Member	**Prof. Lim, Ocktaeck**
Committee Member	**Prof. Chang, Kyoungsik**
Committee Member	**Dr. Lee, Young Jae**
Committee Member	**Prof. Chun, Doo-Man**

Department of Mechanical Engineering
University of Ulsan, Republic of Korea
June 2021

Acknowledgements

First and foremost, I express my sincere gratitude to Almighty “Allah”.

I would like to express my unfeigned thanks to my respected supervisor Prof. Lim, OckTaeck for his continuous support in every possible way. His fruitful comments during research progress meeting to help me prepare my experimental facility. I am always thankful to him for providing a well-equipped experimental laboratory with a highly enjoyable working environment. His motivation, immense knowledge and continuous guidance encouraged me all the time for amalgamating my total research work in this dissertation paper. And the important think was his attention to me and my family, he a like father to me. He always supports and help me, when i was in adversity and trouble. Thank you professor, i will never forget your kindness in my entire life.

Besides my advisor, I am gratefully obligated to the rest of my dissertation committee: Prof. Lee, Yoon Ho, Prof. Chang, Kyoungsik, Dr. Lee, Young Jae and Prof. Chun, Doo-Man for their strenuous efforts to go through my dissertation. Also, their insightful comments and encouragement on my dissertation presentation motivate me to widen my research area on SCR system from various perspectives.

An exceptional thanks to Mr. Ardhika S. Ph.D. candidate, Mr. Cahyani W. Ph.D. candidate and Mr. Binyamin Ph.D. candidate, who advise and supports me a lot during my experimental setup preparation. In addition, I'd want to express my gratitude to my Smart Powertrain Laboratory colleagues for their friendship and support. Members of the Internal Combustion Engine Laboratory and the Director of LIPI Bandung's Research Centre for Electrical Power and Mechatronics deserve special gratitude for their exceptional cooperation, inspiration, and support during this work. I am very much grateful to the University of Ulsan for giving me such an excellent research environment and financial support.

The meaning “being at home” is something can learn when you are away from it too often. Many special thanks to my beloved father (Mulyono) and mother (Louis Sriwanti), I love you a lot. I am ever grateful to my parents for teaching me what’s right and wrong. I acknowledge the sincerity of my parents-in-law (Muchnizon Chaniago and Sri Bintarti), who consistently encouraged me to carry on my higher studies in Korea. Furthermore, I would like to express to my wife (Melita Dyah K.) and my kids (Permata Wardana and Arya Wardana) thanks to them. Because they already show me the right path thorough my entire life and always support me more than anyone in my life. Last but not the least, I would like to thank my extended family members and close friends for their love, support and understanding.

This Ph.D dissertation is written during the spring semester of 2021 which contains total research work conducted during the Ph. D study period. All the contents of this dissertation are written for partially fulfilling the degree requirement of Ph.D of Science in Mechanical and Automotive Engineering at the University of Ulsan.

University of Ulsan

June, 2021

Muhammad Khristamto Aditya Wardana

ABSTRACT

A study of improving NOx conversion efficiency in SCR System

Department of Mechanical Engineering

Muhammad Khristamto Aditya Wardana

The diesel engine is utilized in most of Korea's transportation vehicles to convey goods from various companies; nevertheless, diesel engines emit large amounts of nitrogen oxide (NOx), which is harmful to human health. A common approach for reducing NOx emissions from diesel engines is the selective catalytic reduction (SCR) system; however, many factor create difficulties to reduce NOx emission. The urea particles often get stuck in the injector and cannot spread through the system; the injector often struggles to spray urea in small droplets; the large urea particles from the injector easily attach to the system; the exhaust temperature and wall temperature (Tw) make it difficult to evaporate the urea droplet, which produces solid deposit formations in the system. This study dealing with optical chamber and commercial SCR system from 3L diesel engine and 12L diesel engine. The optical chamber can observe the gas distribution and spray pattern as can't show in the commercial SCR system; this study was investigate the effects of urea injection timing on prediction NOx conversion in SCR system; the effects of urea injection strategy on solid deposit formation; the analysis of ammonia uniformity to forecast NOx conversion efficiency; and the analysis of different types of urea injectors in an SCR system. 19 gas sensors on the catalyst surface were used to validate the presence of ammonia gas in this study; NOx conversion values from a gas analyzer were used to evaluate the effectiveness of the mixing process between ammonia gas and NOx emission. These evidence shows to improve NOx conversion efficiency in an SCR system, it is necessary to optimize important factors such as temperature, gas flow, wall material, urea injection distribution, urea evaporation, ammonia gas distribution and mixing process as shown in this study.

Keyword : emissions; ammonia; selective catalytic reduction (SCR); urea injector; heavy-duty diesel engine; urea water solution (UWS)

Table of Contents

Index of Figures

Index of Tables

List of Abbreviations

UWS	Urea water solution
CFD	Computational fluid dynamics
SMD	Sauter mean diameter
UDF	User defined function
SCR	Selective catalytic reduction
DNS	Direct numerical simulation
LISA	Linearized instability sheet atomization
RANS	Reynolds-averaged Navier Stokes
T^*	Critical transition temperature
T_w	Wall temperature
T_{sat}	Saturation temperature
m_p	Mass of atomized particles
$V_{p,i}$	Velocity of atomized particles
F_i	Force acting on the particles
$m_{p,i}$	Quasi steady evaporation rate of droplets
B	Spalding transfer number
A_S	Surface area of droplets
ζ_i	Fractional mass transfer rate of droplets
T_{DL}	Deposition temperature
T^*_{DL}	Critical deposition temperature
P_{inj}	Injection pressure
T_g	Ambient temperature
P_g	Ambient pressure
d_{inj}	Injector nozzle hole diameter

Θ	Injection angle
PM	Particulate matter
HD	Heavy duty
DPF	Diesel Particulate Filter
LNT	Lean NOx Trap
FTIR	Fourier-transformed infrared spectroscopy
TGA	Thermogravimetric analysis
RGB	Red, green and blue
UV	Ultra violet
ASOI	After start of injection
AEOI	After end of injection
μ	Viscosity of the fluid
ρ_ρ	Density of the particle
β	Temperature exponent (dimensionless)
Δs	Grid spacing near the boundary layer (mm)
dp	Diameter of the particle
Re	Relative Reynolds number
up	Velocity of the particle
u	Velocity of the fluid
CD	Drag coefficient
$\dot{m}_p$	Mass flow rate of the particles
Δt	Time step
F_{Other}	Other interaction forces
m_{pin}	Mass of the particle on cell entry (kg)
m_{pOut}	Mass of the particle on cell exit (kg)
Cp_p	Heat capacity of the particle (J/kg-K)
H_{pyro}	Heat of pyrolysis as volatiles are evolved (J/kg)

T_{pin}	Temperature of the particle on cell entry (K)
T_{pout}	Temperature of the particle on cell exit (K)
T_{ref}	Reference temperature for enthalpy (K)
H_{latref}	Latent heat at reference conditions (J/kg)
C_{pg}	Heat capacity of gas product species (J/kg-K)
T_{bp}	Boiling point temperature (K)
H_{lat}	Latent heat at the boiling point temperature (J/kg)
M_p	Mass of the particle (kg)
C_p	Heat capacity of the particle (J/kg-K)
Ap	Surface area of the particle (m^2)
T_∞	Local temperature of the continuous phase (K)
$h*$	Convective heat transfer coefficient (W/m^2-K)
Ni	Molar flux of vapor ($kgmol/m^2$-s)
kc	Mass transfer coefficient (m/s)
$C_{i;s}$	Vapor concentration at the droplet surface ($kgmol/m^3$)
$C_{i;\infty}$	Vapor concentration in the bulk gas ($kgmol/m^3$)
Di,m	Diffusion coefficient of vapor in the bulk (m^2/s)
Sc	The Schmidt number
d_p	Particle (droplet) diameter
$M_{w,i}$	Molecular weight of species i (kg/kgmol)
mp	Mass of the droplet (kg)
A_p	Surface area of the droplet (m^2)
$C_{j,r}$	Molar concentration of species j in reaction r ($kgmol/m^3$)
n_{jr}	Rate exponent for reactant species j in reaction r
m_{jr}	Rate exponent for product species j in reaction r
Ar	Pre-exponential factor (consistent units)

E	Activation energy for the reaction (J/kgmol)
R	Universal gas constant (J/kgmol-K)
Xc	Mole fraction of CO^2
Xmc	Mole fraction of MEA Carbamate
h	Enthaply (J/kg)
njr	Rate exponent for reactant species j in reaction r
mjr	Rate exponent for product species j in reaction r
t	Time (s)
Lp	Longitudinal position (m)
DeNOx	NO_x removal ratio
E_a	Activation energy
f_{DeNox}	The possible NO_x removal rate
f_{NFM}	The NO_x formation model
f_a	Seed ratio
f_O	Surface coverage
p	Pressure
k	Pre-exponential factor
n	Molar amount
n^*	Molar flow

List of Chemical Species

CO_2	Carbon dioxide
CO	Carbon monoxide
HC	Hydrocarbon
H_2O	Water
NH_3	Ammonia
HNCO	Isocyanic acid
N_2	Nitrogen
NO	Reynolds-averaged Navier Stokes
NO_2	Nitric oxide
NO_X	Nitrogen oxide, sum of NO and NO_2
N_2O	Nitrous oxide
O_2	Oxygen
SO_X	Sulfur oxide

List of Subscripts

A	Air
Ads	Absoption
AF	Air filter
amb	Ambient
art	Artificial
BP	Boiling point
C	Catalytic converter, or controller, or compressor
Cb	Combustion
C_{ond}	Convestion
des	Desired
Des	Desoption
filt	Filtered
inj	Injection
IR	Inlet reciver
meas	Measurement
N	Normal condition
NFM	Nitrogen oxide formation model
OC	Oxidation cell
OF	Output filter
OR	Outlet receiver
Ox	Oxidation
SCR	Selective catalytic reduction
sim	Simulated
U	Urea

UD	Urea decomposition
US	Urea solution
USE	Urea solution evaporation

Chapter 1

Introduction

1.1 Background

The decrease of emissions and the lowering of fuel consumption have been driving forces in engine development during the last few decades. The primary goal is in the vehicle owners' best financial interests. The second is enacted by law, which is sometimes bolstered by tax breaks or customer requests for cleaner engines. Lower caps, a shift from steady-state to transient cycles, and the control of additional components are all trends in emission legislation/certification. They are driven by a better understanding of the environmental impact of the emitted species and a desire to solve the problems as quickly as possible.

Any pollutant's impact on the atmosphere is determined by its water solubility, volatility, and reactivity. The less soluble, volatile, and reactive a species is, the more extensive and long-lasting its effect becomes. Several potentials, such as the photochemical ozone production potential, the global warming potential, and the ozone depletion potential, have been created in order to characterize the contribution of certain pollutants to certain problems. Air pollution also significant impact on human health and environment, so maintaining the air quality is very important, especially in highly dense populated urban and industrial areas. Authorities and environmental agencies are trying to introduce new emission legislation to control air pollution. Though air pollution is reducing over last few years due to strict emission legislation, there is still a serious air quality problem because of the number of the vehicle is increasing day by day. Citizens are more and more worried about the problem.

Diesel engines are widely used because of having several advantages like, high thermal efficiency, better fuel economy and low greenhouse gases emissions. Regarding heavy duty transportation there are no effective alternatives to diesel engine vehicles. In new generation diesel engine, fuel economy is improved as well as the NOx emission also increased. This dangerous NOx is one of the most serious environmental pollutants caused by the transportation industry. To reduce NOx emissions while retaining a superior fuel economy, an effective after-treatment system is required. Engine tuning can meet the current EURO 3 emission regulations for heavy-duty diesel automobiles. Various in-engine technologies, such as combustion system optimization, intercooling, turbocharging, injection pressure increases, injection timing retardation, development of smart electronic controllers, injection rate shaping, and exhaust gas recirculation, have been used to meet legislation requirements (EGR). Although some of these technologies are still in the early stages of development and others, such as homogeneous charge compression ignition (HCCI), indicate that future legislation will require

an aftertreatment system to reduce NOx and/or abate PM emissions to the required levels, indications are that future legislation will require an aftertreatment system to reduce NOx and/or abate PM emissions to the required levels. Limitations imposed by the combustion process, development expenses, or a large fuel penalty imposed by in-engine pollution abatement technology are among the causes.

DPFs (diesel particulate filters) appear to be quite successful in removing PM. They must be regenerated, which can be accomplished either by fuel injection or catalysis. Their disadvantages include a rise in back pressure and a fuel penalty, as well as the fact that they have a limited lifespan owing to ash collection. While DPFs have little effect on NOx levels, SCR converters decrease PM. DPFs also require a specific quantity of NOx to function correctly. Engine manufacturers are being obliged to incorporate exhaust after-treatment equipment to address the mounting issue of implementing progressive compact emission requirements, such as Euro 6. Selective catalytic reduction (SCR) is the most well-liked nitrogen oxides (NOx) emissions reduction method in the automobile industry, capable of fulfilling the majority of emission regulations[1]. The NOx element is converted to nitrogen (N_2) gas and water (H_2O) [2] when ammonia (NH3) gas combines with the exhaust gas going into the SCR device. Despite the fact that NH3 is a toxic chemical component that is damaging to human health, urea is employed as the precursor of NH_3 gas, which is easy to handle and transport [3]. AdBlue, a urea-water solution with 32.5 percent urea by weight, is injected into the exhaust gas stream through an injector, and the urea is then degraded to ammonia (NH_3) gas [4].

1.2 Problem

Urea water solution droplets decomposition is a thermally activated phenomenon, it begins by water evaporation from the solution, separating the urea components. Then urea molecules are decomposed into ammonia gas. Urea decomposition is not always uniform. During the decomposition process intermediate phases can react with undecomposed urea and produce various unwanted complex polymer [5,6]. These urea deposits build up on the injector tip, exhaust pipe wall, catalyst surface, and mixing element, reducing catalyst activity, raising engine backpressure, and eventually rendering the system useless. Although urea deposits dissolve at extremely high exhaust temperatures, sustaining these temperatures might increase fuel consumption [7–9].

The uniform distribution of urea, as well as the reduction of solid deposit development, are the most difficult aspects of urea SCR systems to implement [10,11]. Though current urea-SCR systems necessitate a small exhaust pipe design because urea thermal breakdown is a time-consuming process, droplet spray impingement on the exhaust pipe wall or on the mixer is difficult to prevent. The likelihood of deposit formation increases when the liquid coating evaporates, causing additional temperature reductions. Low injection pressure is used in traditional pressure assisted SCR injectors,

which prevents secondary breakage and produces droplets of a large size. The wall surface condition also can be a parameter for assist the urea droplet for breakup to achieve small size of droplet[12,13]. As a result, spray wall impingement occurs, and spray cooling occurs throughout the injection phase. Spray cooling causes the creation of a liquid film, which is the prelude to the production of a solid deposit [14,15]. Temperature distribution is the main point for getting the good evaporation in the system. The prediction for urea injection timing can be a good solving for solid deposit phenomena in SCR system.

However, basic phenomena, mechanisms of droplet spray, urea droplet break-up, urea distribution, temperature quality, gas distribution, ammonia uniformity, solid deposits formation and NOx conversion process are not properly discussed yet. Therefore, it is of great interest to get a good understanding on fundamental spray characteristics of urea water solution, thermal and fluid dynamic factors that affects on urea decomposition process, urea solid deposits are formed and decompose to obtain an efficient injection strategy that can mitigate deposit formation. The different model of SCR system also can effect to the difference result of study. This study dealing with optical chamber and commercial SCR system from 3L diesel engine and 12L diesel engine. Thus, this study is a good reference for future research into decreasing NOx emissions diesel engine and heavy-duty diesel engines, especially engines with similar parameters.

1.3 Aims and Objective

This study focuses on the ammonia generation process to improve NOx reduction efficiency in selective catalytic reduction systems in an optical chamber and commercial SCR system commercial SCR system from 3L diesel engine and 12L heavy-duty diesel engine.

The main objective of this study focusing on the technical part is given below:

- The Impact of Urea Injection Timing on NOx Conversion Prediction in SCR Systems.
  - Design and construction of the SCR system.
    - To investigate the effect of exhaust gas temperature in the chamber and commercial SCR system from 3L diesel engine.
    - To investigate the urea injector spray distribution in the chamber.
    - To investigate the urea evaporation process quality.
  - Performing experiments result.
    - Capture the thermal distribution gas in the optical chamber.
    - Capture the ammonia homogenization in the catalyst surface.

- Capture the NOx conversion value in the catalyst outlet.

❖ Analyzing the experimental results.

- Measure the urea injection timing for increase ammonia generation process.
- Measure the gas distribution quality in the system.
- Measure the evaporation process quality.

☐ Effects of Urea Injection Strategy on Solid Deposit Phenomenon.

❖ Design and construction of the SCR system.

- To investigate the spray distribution and urea droplet.
- To investigate the urea injection phenomenon in low dan high wall temperature.
- To investigate solid deposit formation.
- To investigate the urea evaporation process quality.

❖ Performing experiments result.

- Capture the solid deposits formed.
- Capture the wall surface effect to urea evaporation process.
- Capture the quality of super hydrophobic material to decrease solid deposit formed.

❖ Analyzing the experimental results.

- Measure the wall impingement images to obtain the axial and radial distances and area of the spray after impingement.
- Measure the quality of super hydrophobic material.
- Measure the evaporation process quality in the system.

☐ Ammonia uniformity to predict NOx conversion efficiency in an SCR System.

❖ Design and construction of the SCR system.

- To investigate the effect of exhaust gas temperature.
- To investigate urea evaporation quality.
- To investigate ammonia gas distribution.
- To investigate the quality of mixer fan with 16 blades in the system.

❖ Performing experiments result in the SCR system.

- Identify the gas distribution quality at the outlet of SCR system.
- Identify the ammonia uniformity on the catalyst surface.
- Identify NOx conversion at the outlet of SCR system.

❖ Analyzing the experimental results.

- Measure the gas distribution quality in the system.
- Measure the ammonia uniformity on the catalyst surface.
- Measure NOx conversion at the catalyst outlet.

❖ Analyzing the numerical results

- Measure the gas distribution phenomena inside the SCR system
- Measure the ammonia uniformity on the catalyst surface
- Measure the urea evaporation quality based on vaporization and saturation value
- Measure the NOx conversion value
- Validate the simulation result with the experiment result

☐ Investigation of Different Types of Urea Injectors in an SCR System.

❖ Design and construction of the SCR system.

- To investigate exhaust gas temperature and gas distribution.
- To investigate the distribution of 2 type of urea injector spray.
- To investigate the urea injector quality.
- To investigate the solid deposit in the system.
- To investigate the urea evaporation process from 2 type injectors.
- To investigate the ammonia uniformity quality based on 2 difference type of injector.

❖ Performing experiments result in the SCR system.

- Identify the quality of 2 type of urea injectors.
- Identify the gas distribution quality in SCR system.
- Identify the ammonia uniformity on the catalyst surface by 19 sensors.
- Identify the evaporation quality based on the NOx conversion quantity.

❖ Analyzing the experimental results

- Measure the gas distribution quality in the system.
- Measure the ammonia uniformity on the catalyst surface.
- Measure NOx reduction quality at the catalyst outlet.

❖ Analyzing the numerical results.

- Measure the gas distribution phenomena inside the SCR system
- Measure the ammonia uniformity on the catalyst surface
- Measure the urea evaporation quality based on vaporization and saturation value
- Measure the NOx conversion value
- Validate the simulation result with the experiment result.

From the academic point of view, the study covers,

☐ Carrying out a literature review on overall selective catalytic reduction (SCR) systems

- Getting to know the NOx components emission and their aftertreatment solution
- Studying about the current and future emission standards
- Studying about the state of art in diesel and heavy duty SCR systems
- Learning about the SCR system problems and influential parameters behind these

☐ Getting knowledge about various numerical models related to spray, turbulent flow, wall impingement and droplet evaporation

☐ Increase the knowledge in design of experiments

☐ Learn about the analysis of results obtained from the experiment

1.4 Disertation Outline

Chapter 1 describe the topic introduction and the context with preccesing studies. The research objective can shows the guideline in this study.

Chapter 2 explains the emissions of nitrogen oxides, its impact on human health and environment, current emission standards, various NOx after-treatment techniques, fundamental characteristics of UWS spray, theories of exhaust temperature, super-hydrophobic surface, ammonia uniformity and NOx conversion in the system.

Chapter 3 describes the detailed step to step of the research work. The experimental setup from optical access, 3L diesel engine and 12L Heavy-duty diesel engine, detail of instrumentation, measurement method, simulation model, boundary condition and initial value.

Chapter 4 describes the numerical simulation and experimental to investigate the improving NOx conversion efficiency in SCR system by the urea injection timing strategy. The urea characteristic, effects of exhaust gas temperature, gas distribution value and ammonia uniformity can improve the NOx conversion efficiency value.

Chapter 5 describes the investigation of solid deposit formation in the SCR system by the super-hydrophobic surface. This chapter can inform the urea injection phenomenon in low and high wall temperature condition, ammonia evaporation process and solid deposit effected to improving NOx conversion efficiency value in SCR system.

Chapter 6 describes the investigation of ammonia uniformity value in 3L diesel engine to predict NOx conversion efficiency in SCR system. This chapter inform the distribution of gas value, the concentration of mass fraction and multi-component gas distribution, ammonia uniformity value and engine speed operation and mixer fan strategy in order to improve NOx conversion efficiency in SCR system.

Chapter 7 describes the investigation of different type of urea injector in 12L Heavy-duty diesel engine in order to increase NOx conversion in SCR system. This chapter shows the saturation and vaporization process to produce ammonia gas, urea distribution, gas distribution in the system, ammonia uniformity value and NOx conversion value in 12L Heavy-duty diesel engine.

Chapter 8 Contains the summary of this study and conclusion as well as some concluding remarks and suggestions to further work.

1.5 Flow-chart of the Overall process

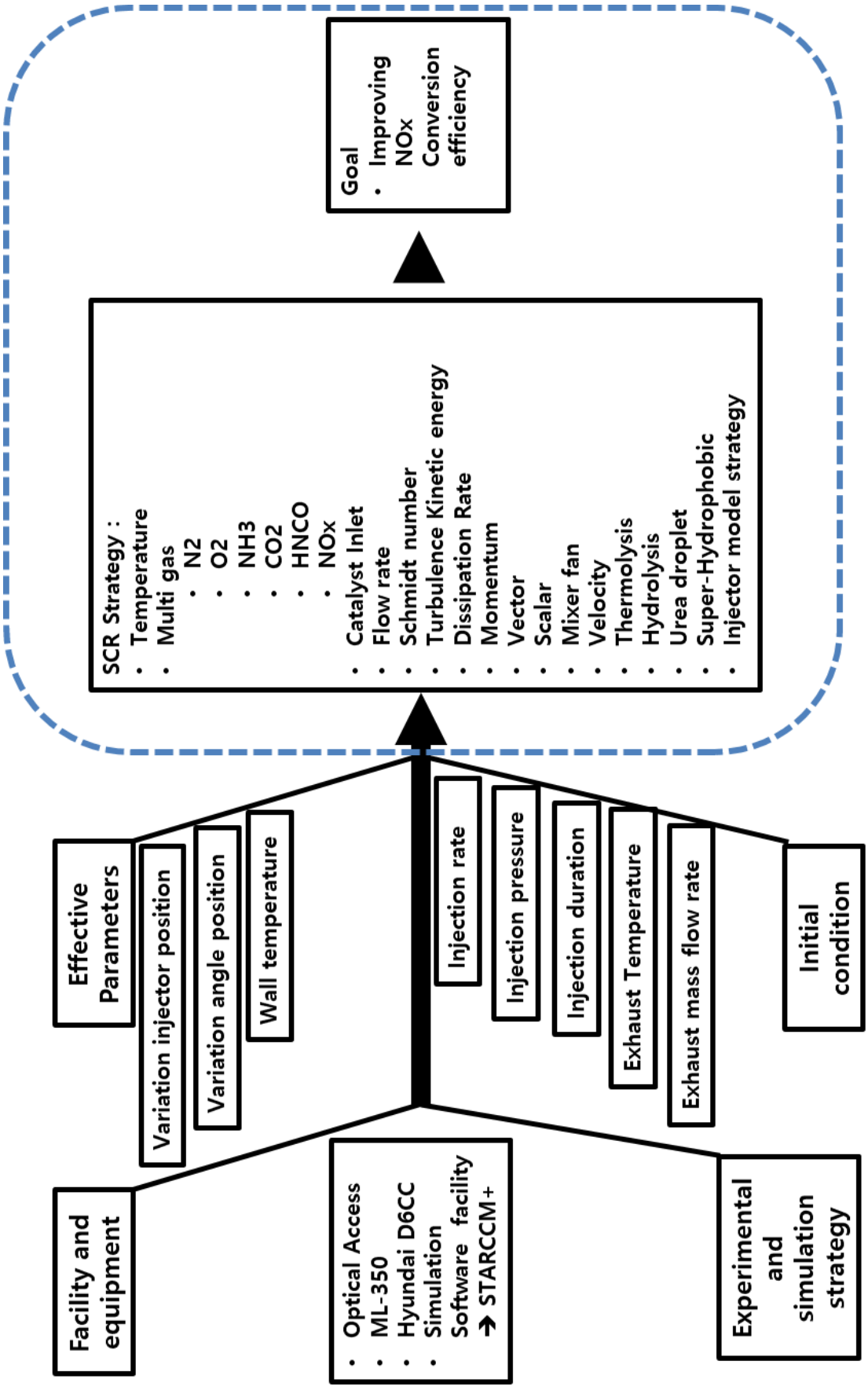

Chapter 2

Literature Review

This chapter explains the emissions of nitrogen oxides, its impact on human health and environment, current emission standards, various NOx after-treatment techniques, fundamental characteristics of UWS spray, theories of exhaust temperature, super-hydrophobic surface, ammonia uniformity and NOx conversion in the system.

2.1 Introduction

2.1.1 Emissions of Nitrogen Oxides

In SI engines the combustible air-fuel mixture is entirely homogeneous, but in diesel combustion, the mixture is heterogeneous in nature. A high-pressure injection system, which is packed with high-temperature compressed air, injects diesel fuel into the engine cylinder. In a diesel engine, combustion is started by compressing the low air-fuel combination until the charge has gathered enough energy to initiate the combustion. Engine emissions are produced due to the combustion of this heterogeneous air fuel mixture by relying on the governing conditions not only at combustion phase, but also in the expansion stroke to before the opening of the exhaust valve[16]. Several parameters such as air-fuel mixture formed during the ignition delay, expansion stroke duration, residence time at various combustion temperatures and other design parameters of the engine are responsible for emissions formation. High combustion temperature and excess air lead to react with atmospheric nitrogen thus form NOx [17]. The reaction mechanism is given below:

$$\mathbf{O + N_2 = NO + N} \qquad (1)$$

$$\mathbf{N + O_2 = NO + O} \qquad (2)$$

$$\mathbf{N + OH = NO + H} \qquad (3)$$

Although the creation of NOx is dependent on combustion parameters, nitric oxide is the most common cause of NOx. As a result of NO oxidation, NO_2 can account for 5-30% of total NOx emissions based on engine emission measurements, and the NOx production mechanism is very temperature dependent.

2.1.2 Emission Standards

The harmful effects on health and environment led to introduce emission legislation that prescribes the allowed emission levels. Most of the vehicle types along with passenger cars, bus, trucks, trains, lorries, sea going ships etc. should meet the existing standards. Vehicles which are already on roads are excluded from the new standards. European emission standards had been introduced and acting science the beginning of 1990's[18,19]. The emissions regulations are gradually implemented by means of stages and becoming stricter throughout the years. For light duty vehicles, the stages are known as Euro 1, Euro 2, Euro 3, and so on, whereas for heavy duty vehicles (HDV), the stages are known as Euro I, Euro II, Euro III, and so on. Euro VI is the current emission standard for HDVs. The Working Party on Pollution and Energy approved it in January 2012, and the World Forum approved it in June 2012. It began operating progressively in January 2013 and was completely installed in January 2014. The allowed nitrogen oxide emissions were reduced by 55% from the previous Euro V standard to the current Euro VI standard, posing a significant technological challenge for engine makers [20].

Euro VI initiated globally combined test procedures including conventional driving conditions in the European Union, Australia and Korea. Even not used same regulation, others country like Japan, USA, Brazil, India and China also has emission regulation to limited their emission as shown in figure 2.2. A second based series of normalized torque and speed measurements is included in the world Heavy-Duty Transient Cycle (WHTC). The World Heavy-Duty Steady-State Cycle (WHSC) tests contain 13 modes of operation for heavy-duty vehicles that mix varied weights and speeds. Because SI engines (Gasoline engines) only employ transient cycle testing, CI engines (Diesel engines) follow both tests. For the period 2017-2020, the impending Euro 6 emission standard will feature Real Driving Emission (RDE). The principle of RDE is that the vehicle will be evaluated across a broad variety of performance maps, rather than using a planned driving cycle, i.e. RDE will be done in real-world traffic using a random driving path.

Emission standard	Year of introduction	Operating cycles	Maximum emissions (g/kWh)					
			CO	HC	NMHC	CH4	NOx	PM
Euro I	1991	Steady state	4.5	1.1	-	-	8	0.36
Euro II	1996	Steady state	4	1.1	-	-	7	0.15
Euro III	2000	Steady state	2.1	0.66	-	-	5	0.1
		Transient	5.45	-	0.78	1.6	5	0.16
Euro IV	2005	Steady state	1.5	0.46	-	-	3.5	0.02
		Transient	4	-	0.55	1.1	3.5	0.03
Euro V	2008	Steady state	1.5	0.46	-	-	2	0.02
		Transient	4	-	0.55	1.1	2	0.03
Euro VI	2014	Steady state	1.5	0.13	-	-	0.4	0.01
		Transient	4	-	0.16	0.5	0.46	0.01

Figure 2.1: Euro standards [17]

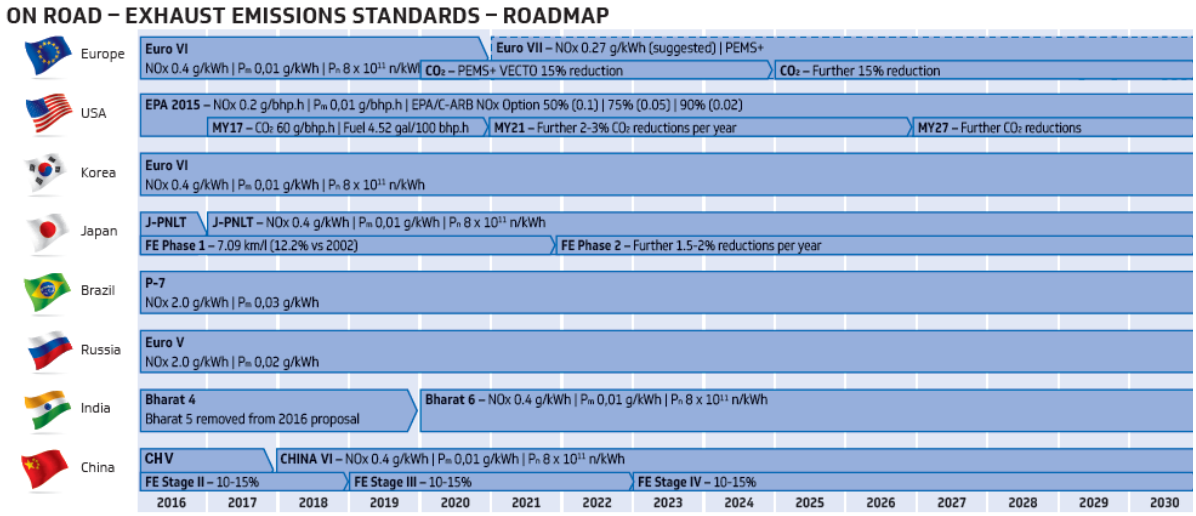

Figure 2.2: Emission regulation standard from all country [21]

2.1.3 NOx After-treatment Techniques

To meet the upcoming strengthen emission legislation concerning NOx emission, effective aftertreatment solution is mandatory. There are several types of NOx aftertreatment solution are introduced and some of the popular techniques are described below:

Lean NOx catalysts: The exhaust gas flow contains hydrocarbons. When exhaust gas combines with hydrocarbons, nitrogen, carbon dioxide, and water are produced. Although this strategy may be a viable strategy to reduce NOx emissions, it does have some significant drawbacks. The biggest issue with this technology is the poor NOx conversion rate (10-20%). This concept cannot meet the existing emission standards, so it can not be recommended for possible NOx reduction application [22].

NOx adsorbers: To minimize NOx emissions from partial lean burn SI engines and diesel-fueled engines, NOx adsorber exhaust systems have been introduced. During lean engine running, NOx adsorbers and catalyst wash-coat chemically collect NOx components from the exhaust gas flow.[1]. When the adsorber's capturing capacity get saturated, regeneration of the system is occurred in the rich operation period and captured NOx is catalytically converted to nitrogen. Repetitive desulfation is also required, as sulfur is also captured in the catalytic wash-coat. This sulfur poisoning results in irreversible catalyst deactivation. For this reason, NOx adsorbers type catalysts are not implemented for deNOx application [3].

Selective catalytic reduction (SCR): is the most well-liked NOx aftertreatment option used by the majority of automotive manufacturers. Below is a detailed description of the SCR system.

2.1.4 SCR System

SCR (selective catalytic reduction) is a well-established after-treatment technology for lowering NOx emissions from diesel engines. The reducing agent ammonia (NH_3) transforms the NOx components into nitrogen (N_2) gas and water (H_2O) [23]. Ammonia can be used directly as the reductant for stationary application. The most secure manner of providing ammonia to a diesel SCR system, particularly a mobile SCR system, is through a urea-water solution, known in Europe as AdBlue and in North America as Diesel exhaust fluid (DEF), which includes 32.5% urea by weight in water. SCR delivers superior fuel efficiency and a high NOx conversion rate when compared to other current technologies such as EGR and NOx-absorbers (90% or higher) [24].

2.2 Urea reduction agent in SCR system

The use of various reducing agents has been discussed in detail for SCR applications [M. Koebel]. A summary follow:

- Although gaseous ammonia is immediately available for SCR, it is difficult to handle properly due to its toxicity.
- A caustic aqueous solution containing 10 to 35% ammonia that crystallizes.
- Solid urea, a fertilizer used in agriculture, in pellet form that is ground or melted and then injected into the tailpipe. The challenge here is determining the right dose.
- 32.5% urea in an aqueous solution. The freezing point of this eutectic solution is -11ºC.
- Solid ammonia carbamate ($NH_4CO_2NH_2$) sublimates and decomposes into ammonia (NH_3) and carbon dioxide when heated to 80°C in a pressure container (CO_2).

Ammonia is the ultimate reactive species when any of the reducing agents described above are used. Because no conditioning is required after injection into the tailpipe, gaseous ammonia is the most efficient reducing agent. The evaporation of the water, which results in a modest drop in the exhaust gas temperature, is the first phase in the conditioning if an aqueous solution is employed as a reducing agent. If the reducing agent comprises urea, the urea molecules must first be thermally degraded into isocyanic acid (HNCO) and NH_3 in the tailpipe.

$$\mathbf{(NH_2)2CO(molten) \rightarrow NH_3(gaseous) + HNCO(gaseous)} \qquad (4)$$

2.3 Urea Decomposition Process

Due to safety concerns, direct ammonia injection cannot be used in portable SCR. A urea-water solution commonly known as adblue is injected into the hot exhaust flow instead of ammonia. This solution is made up of 32.5% urea and 67.5% water.[5]. In the SCR system, urea breakdown and hence ammonia creation take place in three phases. Water is evaporated from the adblue droplets in the first stage. In the second process, urea degradation occurs owing to the thermolysis process, which produces ammonia and iso-cyanic acid (HNCO). This was questionable when urea is solid or molten. The decomposition of urea, according to Birkhold et al., can occur in two ways [25]:

- In the gas phase, solid urea evaporates to gaseous urea, which decomposes into ammonia and iso-cyanic acid.
- Solid urea decomposes into ammonia gas and iso-cyanic acid.

Since gaseous urea is unstable, the breakdown process will take place in the droplet's border layer. [25]. Gaseous iso-cyanic acid is stable, but it can be converted to ammonia and carbon dioxide easily by hydrolysis reaction when the temperature is high enough (400 C or higher) or on the surface of metal oxides at lower temperature [26].

Water evaporation from the droplets:

$$\mathbf{(NH_2)_2CO\ (aq) = (NH_2)_2CO\ (s\ or\ g) + 6.9\ H_2O\ (g)} \quad (5)$$

Thermolysis of urea into ammonia and iso-cyanic acid:

$$\mathbf{(NH_2)CO\ (s\ or\ g) = NH_3\ (g) + HCNO\ (g)} \quad (6)$$

Hydrolysis of iso-cyanic acid:

$$\mathbf{HNCO\ (g) + H_2O = NH_3\ (g) + CO_2\ (g)} \quad (7)$$

In SCR, one mole of urea yields two moles of ammonia when the circumstances are right. Because urea is the only source of ammonia, urea breakdown is critical for evaluating the overall effectiveness of the SCR system. Because ammonia and iso-cyanic acid both react with NOx in SCR, they are referred to as the active substance. The total enthalpy change for the urea decomposition depends on the state of the urea, whether it is solid or as water solution. It also depends on the reaction path and final temperature. The required heat is lower if thermolysis and hydrolysis reactions occur simultaneously. The required heat for the decomposition of one mole of urea for different conditions is given below [27]:

Table 2.1: Heat required to decompose urea (kJ/mol)

	Thermolysis only		Thermo-hydrolysis	
	Tfinal = 500 K	Tfinal = 600 K	Tfinal = 500 K	Tfinal = 600 K

Urea (solid)	203.4	213.4	106.5	116.2
76.93% urea	241.7	255.3	144.8	158.1
50% urea	360	382	263.1	284.8
32.5% urea	541.5	576.3	444.6	479.1

Table 2.2: Compariosn of the properties of urea water solution (UWS) and water [28,29].

	UWS	Water
Property (unit)	Value	Value
Melting temperature, Tm (ºC)	-11.4	0
Specific latent heat, hls (kJ/kg)	152.86	226
Specific heat, solid, Cs (kJ/kg K)	1.6	2.108
liquid, Cl (kJ/kg K)	3.4	4.187
Density solid ρs (kg/m3)	1010	916.7
Density liquid, ρl (kg/m3)	1090	999.975
Thermal conductivity, solid, ks (W/m K)	0.75	1.6
liquid, kl (W/m K)	0.57	0.6
Dynamic viscosity, liquid, µl (mPa s)	1.4	0.89004
Thermal expansion coefficient, ß (1/K)	4.5x10-4	4.2x10-2

2.4 Urea Injector Sprays Strategy

In general, a spray causes a liquid dispersion in a gaseous phase, resulting in a considerable increase in the interface between the two fluids, which is beneficial for mass and heat transfer [30]. An injector injects the urea-water solution (UWS) into the hot exhaust flow ahead of the catalyst. Liquid atomization is a generic process unit action that converts a bulk fluid into a spray system. The goal of the atomization process is to increase the surface area of the gas-liquid interface since all transport mechanisms are directly reliant on it, and greater surface area improves the exchange between the two phases. When the liquid is not fragmented by atomization, the interchange between the phases in a spray system rises by several orders of magnitude [30].

2.4.1 Urea Size Distribution

To describe the droplet sizes of the spray an empirical droplet size distribution function may be used [31]. There are several empirical functions for achieving a droplet size distribution and the choice of function depends significantly on the disintegration mechanism for the situation. One function that has been widely used (and is used in the spray simulations of this study) is the Rosin-Rammler distribution which may be expressed as shown in equation:

$$1 - Q = \exp(-(\frac{D_p}{X})^q) \qquad (8)$$

The percentage of total holding drop volume with a diameter smaller than Dp is denoted by Q. The spread is measured by the exponent value q, and a greater value indicates a more uniform spray. The reference droplet diameter is denoted by the letter X.

2.4.2 Spray-wall Interaction

Calculate the physical mechanisms that occur during spray wall contact. The fundamental spray wall impingement model was created by Bai-Gosman [32]. Because the impinging droplet behavior is influenced by several parameters such as droplet diameter, velocity, fluid and thermodynamic properties, and wall surface properties such as wall surface temperature, wall film thickness, and surface roughness, the UWS spray interaction with the wall is a very complex phenomenon [33][34]. Different thermal and dynamic regimes can be generated based on the dynamics of the liquid and its physical qualities. Wetting, for example, causes a liquid layer to develop on the wall, but boiling causes droplet evaporation. The influence parameters underlying these events include wall temperature, wall state, Weber number, and Laplace number [31]. Kuhnke [35] presented a critical temperature connection for the processes that occur during spray wall impingement,

$$T^* = \frac{T_w}{T_{sat}} \qquad (9)$$

Here, T* is the critical transition temperature, Tw is the wall temperature, Tsat is the saturation temperature, and T* 1.1 is the range discovered for various fluids. The saturation temperature of UWS is higher than that of water, resulting in a greater tendency for wall wetting and film formation. Spray impingement causes local cooling, lowering the crucial transition temperature T* and increasing the chance of wall wetness. When the wall temperature is higher than the boiling point of the UWS liquid, the spray droplets splash and break apart spontaneously. When spray droplets impact on an existing wall film at a temperature below that of boiling water, the droplets splash into secondary droplets, increasing the thickness of the film. Birkhold [36] The critical transition temperature T* range of splash and breakdown for lower and higher wall temperatures was 40-45^o C and 130-200^o C, respectively, in experiments. The current study implemented Bai-Gosman [32] wall impingement model and Kuhnke [35] the spray wall impingement simulation of scattered droplets with Lagrangian particle tracking has a critical temperature limit. The critical temperature value is implemented in the 0.9 to 1.5 range since the present study's working wall temperature range is 338 K to 573 K. The potential consequences and crucial temperature regimes of UWS spray wall impingement are depicted in Figures 2.3 (a) and (b).

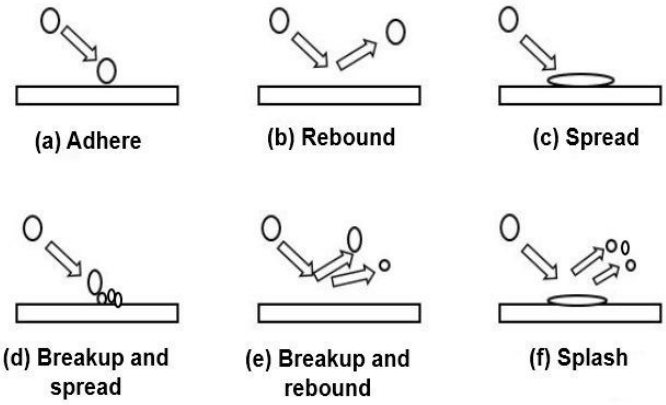

(a)

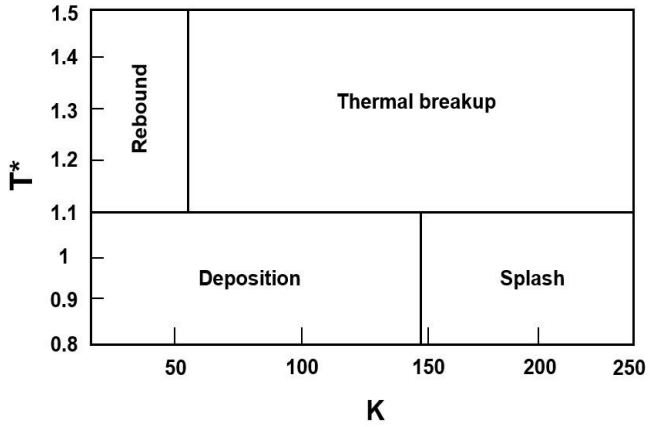

(b)

Figure 2.3 (a) (b): Schematic figure of depicting the potential impact of droplet impingement on a solid wall.[37]

2.5 Urea Evaporation Process

For evaporation to proceed, there has to be a vapor concentration difference between the droplet surface and the continuous phase [31]. In most cases the continuous phase surrounding the droplet is assumed to be a binary mixture of the gas and the droplet vapor [38]. The rate of the evaporation process will be determined by the droplet size, temperature, pressure, material properties of the surrounding gas and relative velocity between the phases. One common way to describe steady-state evaporation i.e. when the droplet has reached the wet-bulb temperature that corresponds to the current conditions, is the so called D^2 law stated in equation :

$$D_o^2 - D_p^2 = \lambda t \qquad (10)$$

Where D_0 is the initial droplet diameter, D_p is the droplet diameter at time t and λ represents the evaporation constant [39].

2.5.1 Temperature Strategy on deposit formation

If a UWS droplet lands on a hot surface, the temperature will drop; if another drop lands in the same area before the surface has restored its original temperature, the last droplet will induce additional cooling. In the experimental study of Xu et al. [40], The temperature of the impingement site was cooled down to roughly 5-30^{o} C, and it took approximately 5 seconds for it to recover. Based on the geographical and temporal development of the wall temperature, Yujun L. et al. evaluated the spray cooling effect and discovered that the temperature reduced from 164^{o} C to 115^{o} C at the front cone of the impact zone [41]. The temperature of the wall has a major impact on urea decomposition, and local cooling caused by spray impingement can have a major impact on urea breakdown, resulting in solid deposits. Several polymers are generated during urea breakdown, the first of which is Biuret, which is generated about 150-190^{o} C and melts and decomposes at 193-250^{o} C [42]. As a result, it's critical to add a deposition limit temperature to distinguish between the wetting and non-wetting regimes for practical purposes, so that the production of wall films and solid deposits can be predicted. Different parameters, such as the droplet weber number, impact the wall wetting [34], surface roughness [33], specific impact mass flux [43] etc. However, it has become common practice to define critical surface temperatures as a function of the injected fluid's saturation temperature [32][44][35][29].

T^{*}_{DL} is the critical surface temperature, and consequently the relative deposition limit temperature.,

$$T_{DL} = T^{*}_{DL} T_{sat} \qquad (11)$$

The above equation can be used to calculate the critical temperature. When the UWS saturation pressure exceeds the local pressure, boiling is likely. The separate saturation curves for water [28] and urea [44] may be used to compute the saturation pressure of the UWS combination, using Raoult's law as a guide. In his work, Henrik Smith et al. reviewed the findings on deposition limit temperature [45]. In his investigation, Birkhold demonstrated that wall wetting occurs at the same time that the temperature reaches the Leidenfrost temperature threshold, and he connected the Leidenfrost temperature with the deposition limit, resulting in T*DL = 1.43.....1.47. When it comes to CFD simulations, most research rely on the values provided by Birkhold [44] and the experimentally harmonized to match the simulation results.

2.6 Super-hydrophobic surface to decrease solid deposit formation

In a conventional SCR system for diesel engine, the urea evaporation and saturation process is the main process to identify the quality of SCR system. In the common SCR system, the generation process from urea become ammonia difficult to reach the good performance. Many researchers change

the urea injector with varies pressure and angle, but still didn't found the significant improvement. Urea solid deposited still high and under control, especially for SCR system with high quantity of urea.

The urea water solution (UWS) in SCR system has composition of 40% of urea and 60% of water. Even the UWS has liquid shape, the density was difference with pure water. The UWS easily solid when influence with temperature. That solid deposit will grow with the function of time. Finally, that problem will decrease the SCR quality to reduce NOx from diesel engine. To solve that problem, this study will insert new surface with micro pattern. The micro pattern will produce the super-hydrophobic surface and that material will have inserted in front of urea injector. The super-hydrophobic surface will assist the break up process in the SCR system.

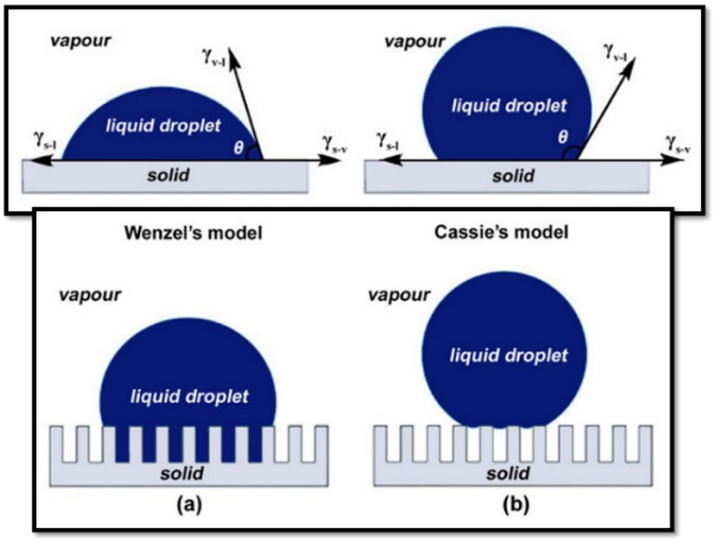

Figure 2.4: The fundamental theory of super-hydrophobic surface.[46]

Figure 2.4 is the fundamental theory of super-hydrophobic surface[47,48]. That diagram illustrated the equation theory using Young's model equation. The tensions s-l and v-l in that equation try to make the droplet smaller, while the tension s-v tries to spread the droplet out over the surface. The angle between the solid/liquid interface and the liquid/vapor interface was dubbed contact angle (θ) when the droplets on the surface attained equilibrium. The super-hydrophobic surface may be used in the SCR system based on the Young's equation model.

$$cos\theta = \frac{ys-v-ys-I}{Yv-I} \qquad (12)$$

The Wenzel equation, as shown in Eq. (12), can be used to explain the fully wetted state on a hydrophilic material with a rough surface, where ue is the equilibrium contact angle of a water droplet on a flat surface, uw is the water droplet contact angle in the fully wetted state on a rough surface, and r is a roughness factor equal to the actual surface divided by the geometric surface. On a flat surface of hydrophilic material, the equilibrium contact angle is less than 90°.[48]

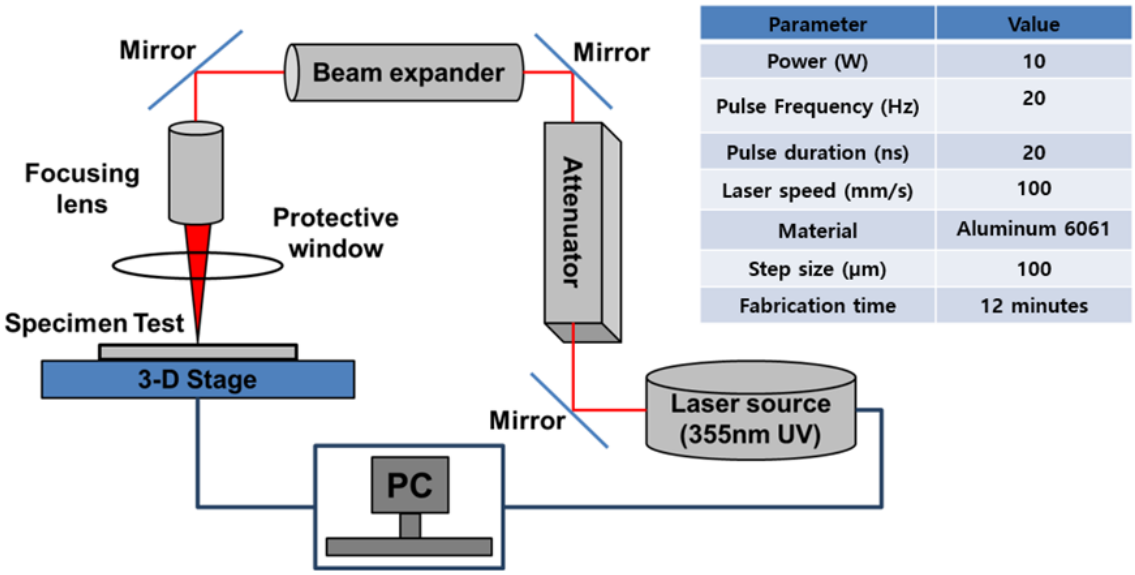

Parameter	Value
Power (W)	10
Pulse Frequency (Hz)	20
Pulse duration (ns)	20
Laser speed (mm/s)	100
Material	Aluminum 6061
Step size (μm)	100
Fabrication time	12 minutes

Figure 2.5 : An illustration of the schematic setup to making the pattern of super-hydrophobic.[47,48]

Figure 2.5 is an illustration of the schematic setup to making the pattern of super-hydrophobic. Because this type of laser is widely used in industry, and relatively large burr formation is possible for a pillar structure that can support water droplets while minimizing contact area with the water droplets, the Q-switched Nd:YAG 355-nm UV nanosecond pulsed laser was used for laser beam machining. The laser beam machining system is shown schematically in this diagram. In order to comprehend the phenomena in the absence of any extra components, a 2 mm thick material was employed as a substrate.

2.7 Summary

The diesel engine produce nitrogen oxides emissions more than other eninge, its impact on human health and environment. The current Korean goverment emission standards push the researcher to improve NOx conversion from diesel engine. The fundamental characteristics of UWS spray, urea break-up modeling, and the fundamental characteristics of ammonia generation process to the reader for a deeper understanding of the core mechanisms in this study. The relevant theories of exhaust temperature, super-hydrophobic surface and ammonia uniformity to improve NOx conversion efficiency in the SCR system; and the next chapter will explain about the study method from experimental and simulation to proved the theory was explained in this chapter.

Chapter 3

The Experimental and Simulation setup

This chapter goes through each phase of the research process in depth. The experimental setup, which includes optical access, a 3L diesel engine, and a 12L heavy-duty diesel engine, instrumentation details, measurement technique, simulation model, boundary condition, and initial value.

3.1 Experimental Apparatus for Optical access

3.1.1 Gas distribution and Urea injection setup

Due to the active presence of particulate matter (PM) in the exhaust gas and the vibration of the exhaust pipe for pressure fluctuation of exhaust gas, observation of the spray pattern in a genuine SCR system is challenging. To allow observation of the urea water solution spray, a clear optical chamber made of high-temperature resistant pyrex glass was constructed. The commercial SCR injector was attached vertically to the exhaust flow in the transparent optical chamber, which has four optical windows.

3.1.1.1 Equipment

3.1.1.1.1 The design of optical chamber

The optical chamber is a powerful instrument for researching UWS spray and wall impingement properties, and it may also be used to test alternative injector types in SCR systems. The use of an optical chamber in spray process study for a more comprehensive review of UWS spray and wall impingement. The optical access allows you to look inside the chamber, which makes it easier to employ a high-speed camera and image analysis software to gain a better knowledge of the injection and wall impingement processes, both of which are critical to the system's performance. The chamber is cylindrical in shape and has four optical windows constructed of high-temperature resistant pyrex glass to allow observation of the urea water solution spray. The inlet and exhaust ports are located on opposite sides of the chamber. Figure 3.1 is a schematic representation of the optical chamber :

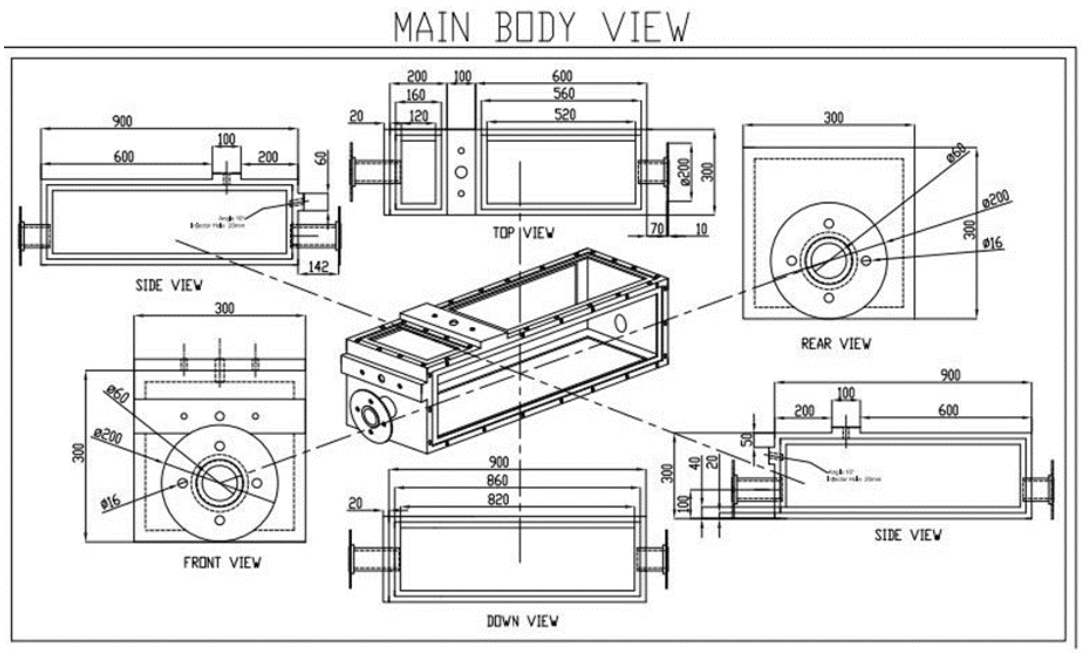

Figure 3.1: Schematic of the optical chamber. [49–51]

Inside the optical chamber, the injector is positioned in a specially built injector holder. The injector holder enables for the height and location of the injector to be adjusted according to the requirements of the experiment.

3.1.1.1.2 Thermal distribution test

Figure 3.2 shows the Pictorial layout of the experimental testbench. Figure 3.3 shows the schematic of experimental line and schematic of the experimental setup.

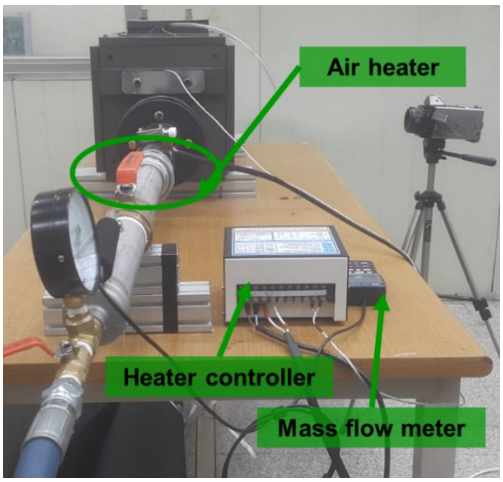

Figure 3.2: Pictorial layout of the experimental testbench [49]

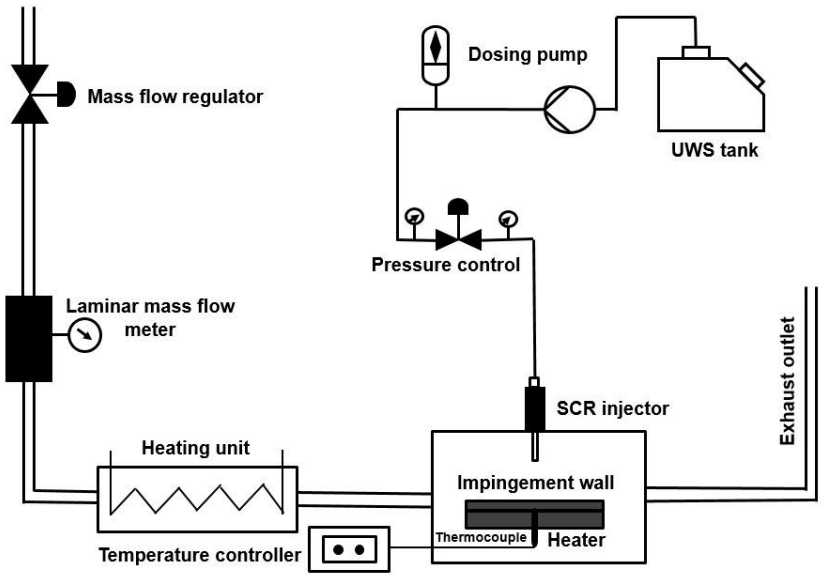

Figure 3.3: Schematic of the experimental setup [50]

3.1.1.1.3 Urea Injector and Supply System

The injector utilized in this experiment is a commercial SCR injector with a 3-hole injection nozzle with a 0.12 mm orifice diameter. The injection system is set up with supply lines that can handle UWS characteristics. To evaluate the injection mass flow rate at a given injection pressure, the injection amount of UWS was monitored at various injection rpm. The supply system pressurizes UWS as it travels from the storage tank to the injector through supply lines. The injection driver controller was used to control the injection time. The initial couple of hundred injections following the UWS refill were done in a canister, and this quantity was withdrawn before the start of the experiment to ensure that there was no air in the supply line. The experimental SCR injector is shown schematically in figure 3.4, and the experimental SCR injector is photographed in figure 3.5.

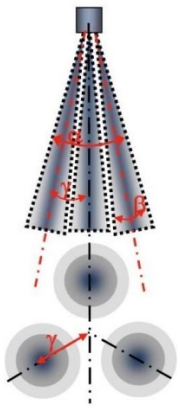

Figure 3.4: Schematic view of the experimental SCR injector.[50]

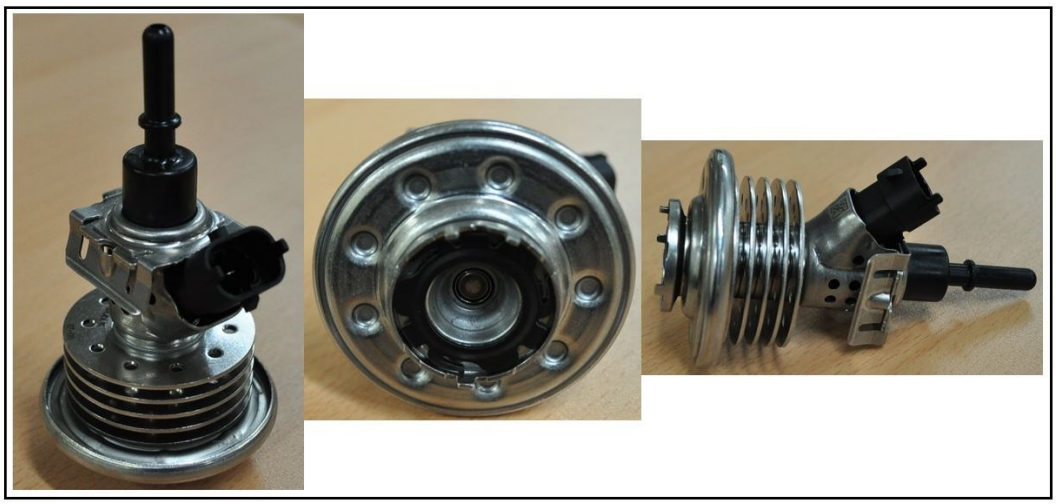

Figure 3.5: Photograph of the experimental SCR injector

3.1.1.2 Analysis Procedure

3.1.1.2.1 Injection Rate Measurement

The SCR injector utilized in the investigation was a 3-hole pressure-driven injector with a nozzle hole diameter of 0.12 mm and an equilateral triangular shape of 1.9 mm side length. Spray was formed in a triple stream due to atomization. The injection rate was evaluated by comparing the injection amount of the experimental injector. At 5 bar injection pressure, UWS was injected 100 times at 1000 rpm and 2000 rpm. A precise electronic scale was used to weigh the collected adblue. To prevent the inaccuracy, the average was calculated using 20 measurements. Figure 3.6 depicts the results of injection quantity measurements for various injection rpm and duration. The injection amount grew linearly as the injection duration increased. The measurement value was unaffected by changes in injection rpm. The injection rate was found to be 4.824 kg/h using the average of the gradient, as shown in the figure:

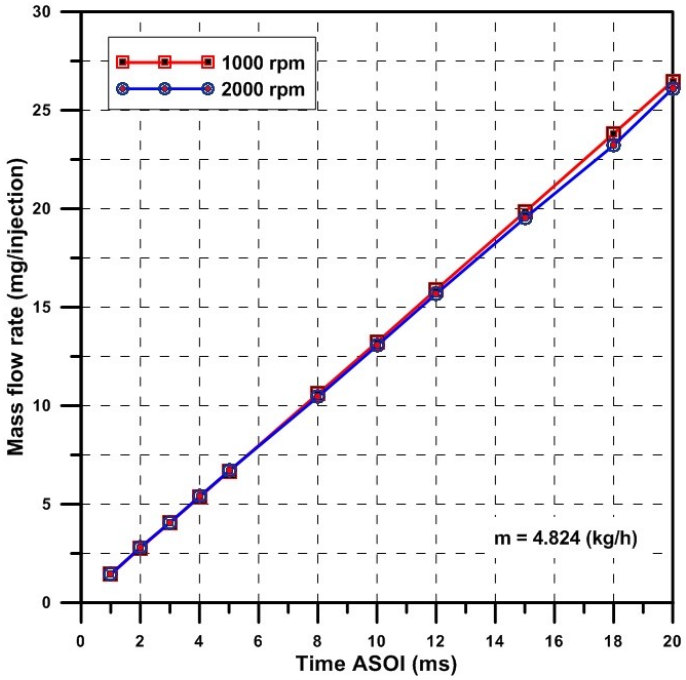

Figure 3.6: Injection quantity based on injection duration and rpm.[50]

3.1.1.2.2 Imaging Technique

The shadowgraph technique is the most basic density visualization approach, and it relies on light deflection to create a picture with variable brightness. As a result of the deflection of some light, certain regions of the picture may look black, while others will get twice the light intensity and appear bright. The areas of higher density are seen as black shadows with a brighter field adjacent to them in this fashion. The picture intensity is sensitive to the second derivative of the density distribution perpendicular to the light propagation direction, and the shadowgraph approach records light ray movement owing to refraction. The Z-type shadowgraph imaging technique was used in this work to visualize spray and wall impingement. The schematic layout of a Z-type shadowgraph arrangement for spray and wall impingement visualization is shown in Figure 3.7. The high-speed camera caught solid deposits development owing to spray wall impingement and incomplete urea breakdown at 60 frames per second with a resolution of 768x512 pixels. The camera was positioned vertically upward to the impinging wall, with a halogen light source providing illumination.

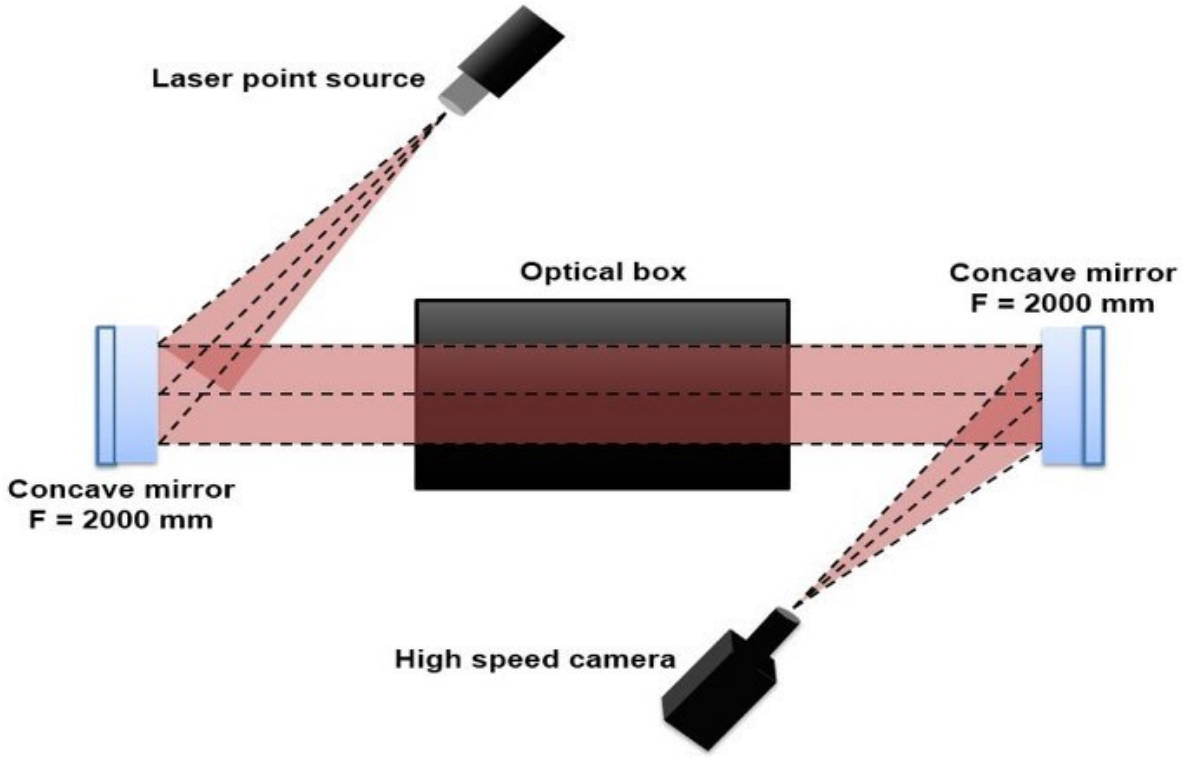

Figure 3.7: Schematic diagram of Z-type shadowgraph setup for spray visualization.[50]

3.1.2 Solid deposit formation and urea evaporation test

It might be difficult to see the gas temperature distribution in an actual SCR system. As a result, a clear optical chamber made of pyrex glass was built to allow temperature viewing.

3.1.2.1 Equipment

3.1.2.1.1 Solid deposit in the wall surface setup

Figure 3.8 (a) (b) (c) shows the Pictorial layout of the experimental testbench for impingement wall.

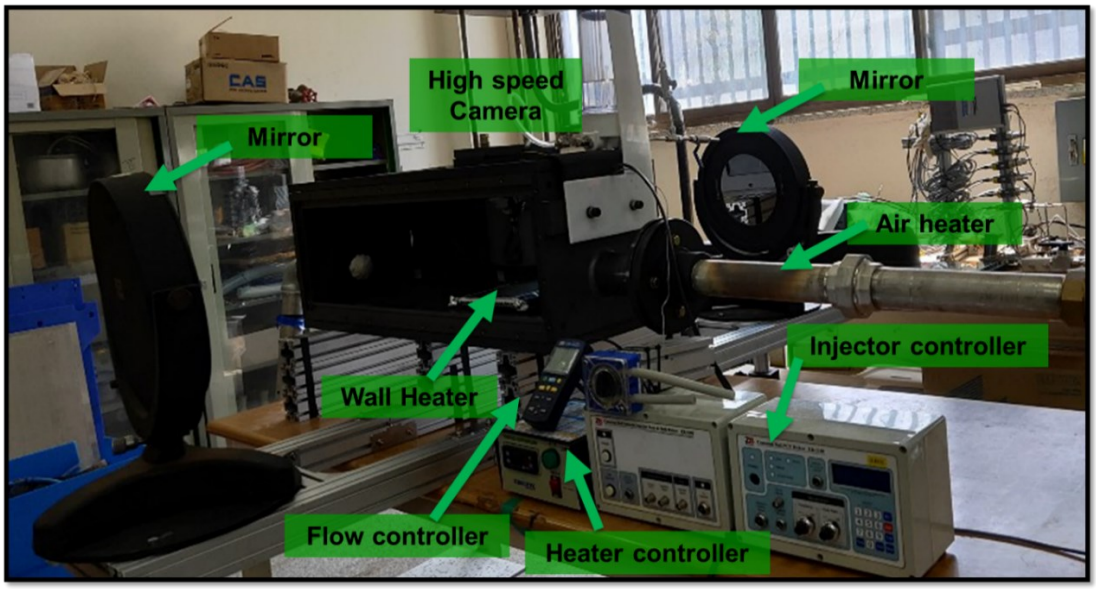

(a)

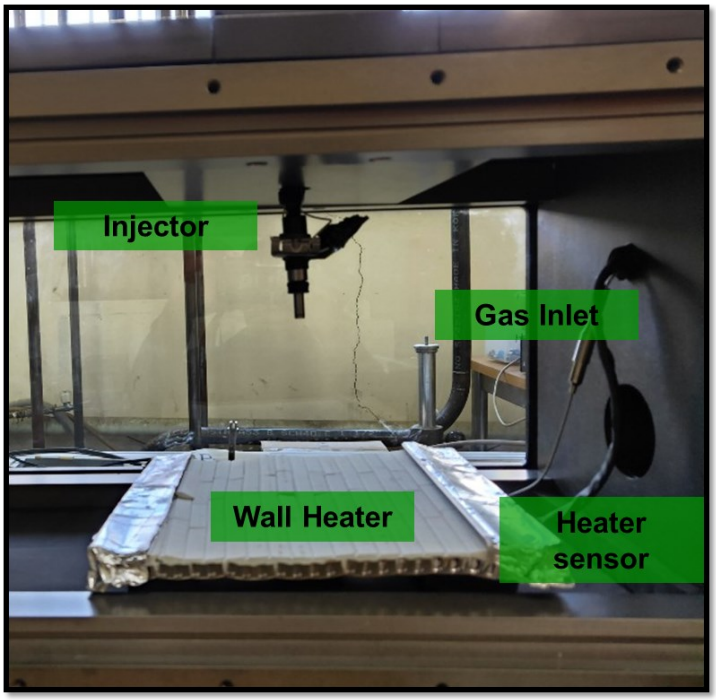

(b)

Figure 3.8: Pictorial layout of the experimental testbench for impingement wall

3.1.2.1.2 Laminar Flow Meter

A laminar flow meter was used to measure the mass flow rate of air as a representation of exhaust flow. The TES-1340 hot-wire anemometer can monitor liquid level, density, and pressure as

well as gas or stream flow. Table 3.1 shows the technical specifications of the laminar flow meter utilized in the experiment.

Figure 3.9: Laminar flow meter

Table 3.1: Laminar flow meter specification

Manufacturer	TES Electrical Electronic Corp
Model no	TES-1340
Response time	<2 second
Manual Memory Capacity	5x99 sets.
Auto Memory Capacity	5x99 sets.
Operating Condition	0°C~50°C
Power Source	6 (AAA Battery)
Battery life	10 hours
Size	150(L) x 72(W) x 35(H) mm
Accuracy	97~100% reading and FS

3.1.2.1.3 Wall Heating Unit

Wall heating unit is implemented to maintain the wall temperature for spray wall impingement experiment. The system consists of an Omega MSH00066 strip heater, solid state relay, temperature controller and thermocouple. A 150*150 mm stainless still plate was placed on the upper surface of the heater which works as the heated wall. The thermocouple is placed 1 mm up to the heated wall to control

and monitor the wall temperature during the experiment. The heater is connected to the temperature controller through the SSR.

(a)

(b)

Figure 3.10: Wall heater and controller

Table 3.2: Shows the wall heater specification:

Manufacturer	Omega engineering
Model	MSH00066 STRIP HEATER
Maximum Sheath Temperature	480º C
Nominal Watt Density	5 to 45 Watt/in^2
Voltage	220 V
Maximum Amperage	10 A
Resistance Tolerance	10%-5%
Dimensions	120*140 mm

3.1.2.1.4 Air Heating Unit

Air heating unit is used to supply the hot air for the experiment. The system consists of an Omega AHF-14240 max flow air heater, solid state relay, temperature controller and thermocouple. The thermocouple is connected inside the heater to control and monitor the air temperature during the experiment. The heater is connected to the temperature controller through the SSR.

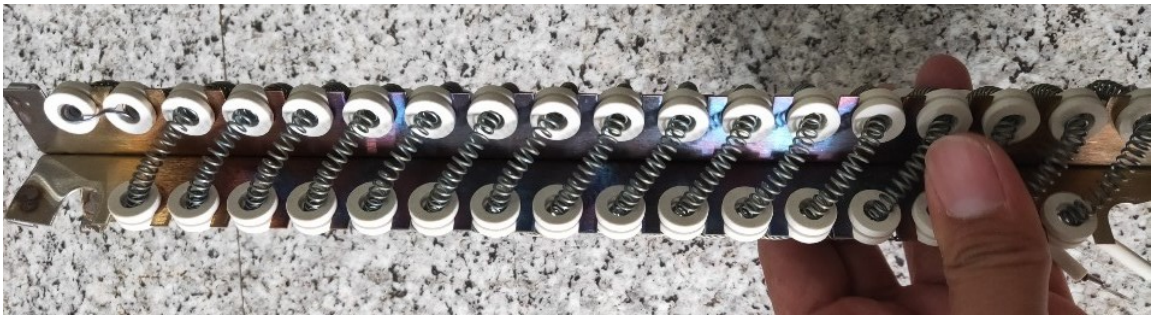

Figure 3.11: Air heater and the pipe location

Table 3.3: Shows the air heater specification:

Manufacturer	Omega engineering
Model	AHF-14240 MAX FLOW AIR HEATER
Heated Length	305 mm
Nominal Watt Density	166 Watt/in^2
Voltage	220 V
Maximum CFM	200
Resistance Tolerance	10%-5%
length	356 mm

3.1.2.1.5 High Speed Imaging

A Photron Fastcam SA3 high-speed camera with a Nikon lens with a minimum aperture of f/2.8 was used. When utilizing photos for comparison, it's critical to maintain all of the picture acquisition parameters constant. The camera settings are shown in Table 3.4.

Figure 3.12: High speed camera

Table 3.4: High speed camera settings

Setting	Value	Unit
Frame Rate	7500 Pictures/second	Pictures/second
Resolution	512x512 Pixels	Pixels
Aperture	f/2.8	[-]
Shutter Speed for z type shadowgraph	1/300000	seconds

3.1.2.2 Analysis Procedure

3.1.2.2.1 Urea Decomposition

Due to the high exhaust temperature, urea breakdown occurs after the UWS injection. For optimal mixing with exhaust gas, ammonia distribution in the exhaust pipe is critical. In SCR operation, the mass proportion of ammonia created might be an indication of urea breakdown. Incomplete urea breakdown results in the production of solid urea deposits, which can create major NOx reduction issues. Numerical simulation is used to determine urea breakdown and ammonia decomposition.

3.1.2.2.2 Temperature Distribution

Before entering the optical access, air flow of 223 kg/h was pumped from an air compressor and heated to 362°C by an air heater. A thermal camera was used to measure the temperature gas distribution in the system. When hot gas temperatures are introduced to the system, these temperatures are unable to rapidly heat the whole system. Khristamto [49] described the thermal and hydrolytic

degradation of urea in the system was detailed in the temperature range of 150 to 500 °C. As a result, a temperature rise was required to obtain a temperature acceptable for urea injection in the SCR system. We can forecast the ideal moment to introduce urea into the system based on our research, and so reduce the creation of solid deposits.

3.2 Experimental Apparatus for Diesel engine

3.2.1 3L Diesel engine

A six-cylinder, water-cooled, naturally aspirated, four-cycle diesel engine with a six-valve SOHC layout was used in this investigation. This methodological approach can demonstrate gas distribution in a commercial SCR system as well as ammonia uniformity in a 3L diesel engine. Figure 3.13 shows the torque and power parameters for the engine.

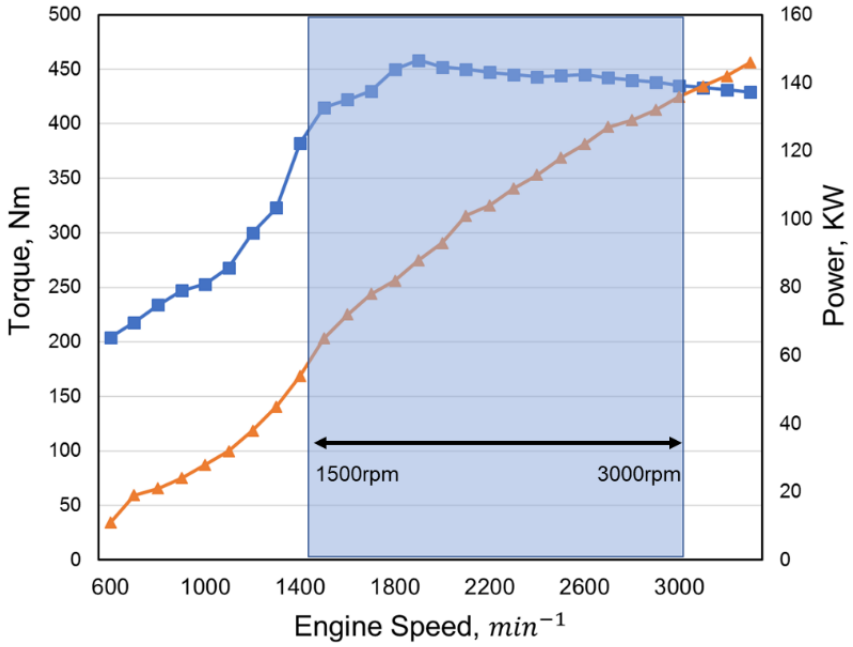

Figure 3.13: Engine torque and power specifications.[51]

3.2.1.1 Commercial SCR system for 3L Diesel Engine

Figure 3.14. shows the SCR system in the 3L Diesel Engine. That figure clearly shows the position of exhaust inlet, urea injector position, SCR catalyst position and gas sensors.

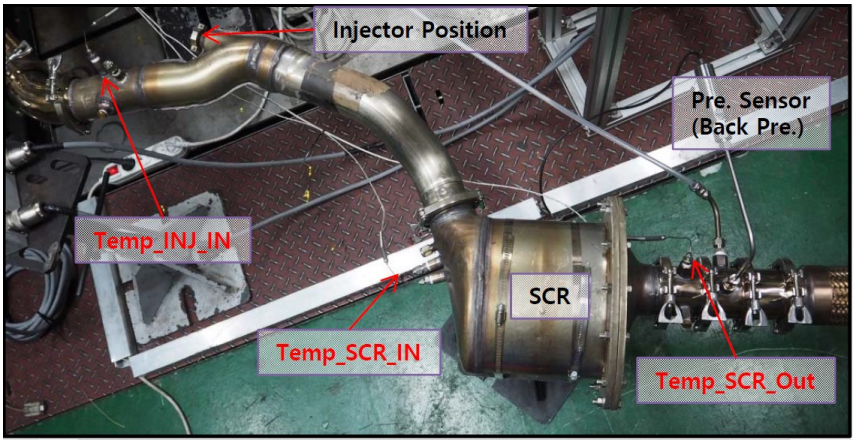

Figure 3.14: SCR system for 3L Diesel Engine.

3.2.1.2 Mixer fan

Figure 3.15 depicts a 16-bladed mixer for increasing flow in the SCR system. With the gas flow direction, each blade has a 35° inclination angle. To aid in the mixing of NH3 and gas in the system, the mixer was placed in front of the urea injector. Based on the trial configuration of the commercial muffler 3L Diesel Engine, the mixer was positioned 630 mm from the exhaust entrance.

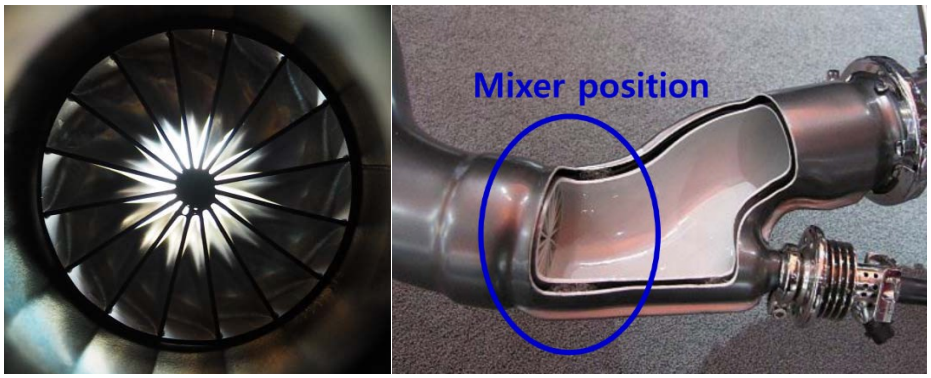

Figure 3.15: Mixer fan position.

3.2.2 12L Heavy duty diesel engine

The heavy-duty diesel engine has six cylinders in line, a displacement of 12.000cc, and a compression ratio of 17.2:1. From 1.000 to 1.700 engine speeds, this engine can create maximum power. The current study investigated ammonia homogenization with two injector shapes at 1.000 and 1.700 engine speeds. The 1.000 engine speed condition produced a 513 kg/h exhaust mass flow rate and a 1,330 ppm NOx concentration value; and 1.700 engine speed condition produced a 1.100 kg/h exhaust

mass flow rate and a 204 ppm NOx concentration value. The NOx concentration value for the 1.700 engine speed condition is lower than that for the 1.000 engine speed condition because the 1.700 engine speed conditions produce less oxygen (O_2) for combustion, resulting in lower NOx concentration.

3.2.2.1 Commercial SCR system for 12L Heavy-duty Diesel engine

Figure 3.16. shows the SCR system in 12L Heavy-duty Diesel engine. That figure clearly shows the position of exhaust inlet, urea injector position, SCR catalyst position and gas sensors.

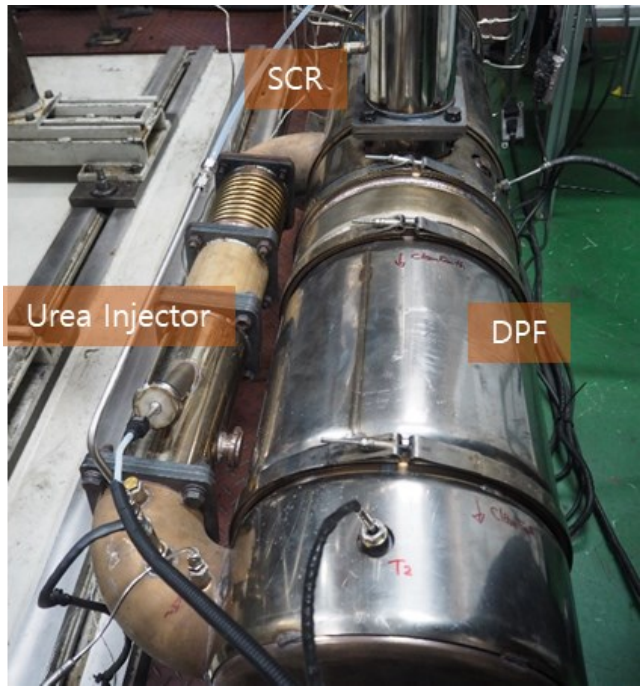

Figure 3.16: SCR system for 12L Heavy-duty Diesel engine.

3.2.2.2 12L Heavy-duty Diesel engine urea injector system

The urea injection in this current study used 2 different shape of injector, even the model and the injection position different but the parameter value is same. The urea injector can produce 8.05-E5 kg/s of mass flow rate from 3 holes and 120 μm of holes diameter.

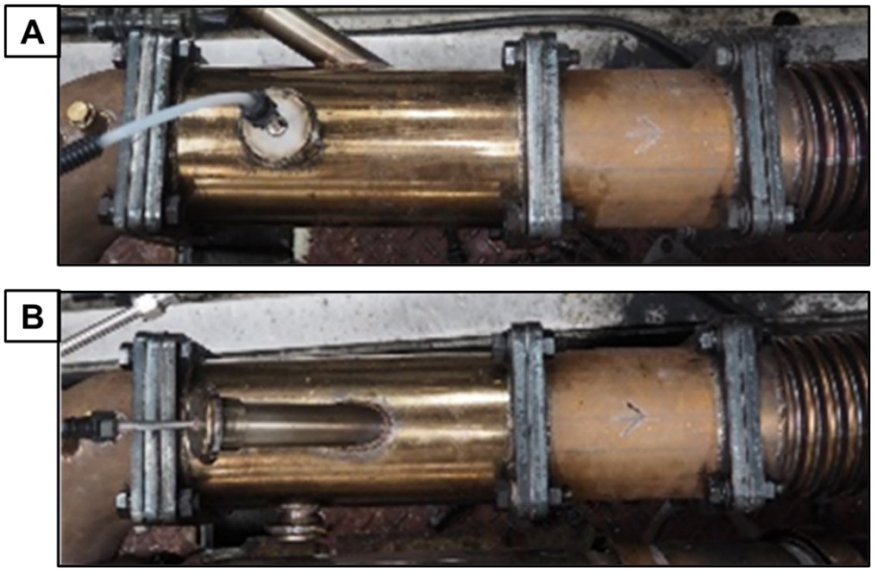

Figure 3.17: The urea injectors position: a) L-Shaped injector and b) I-Shaped injector

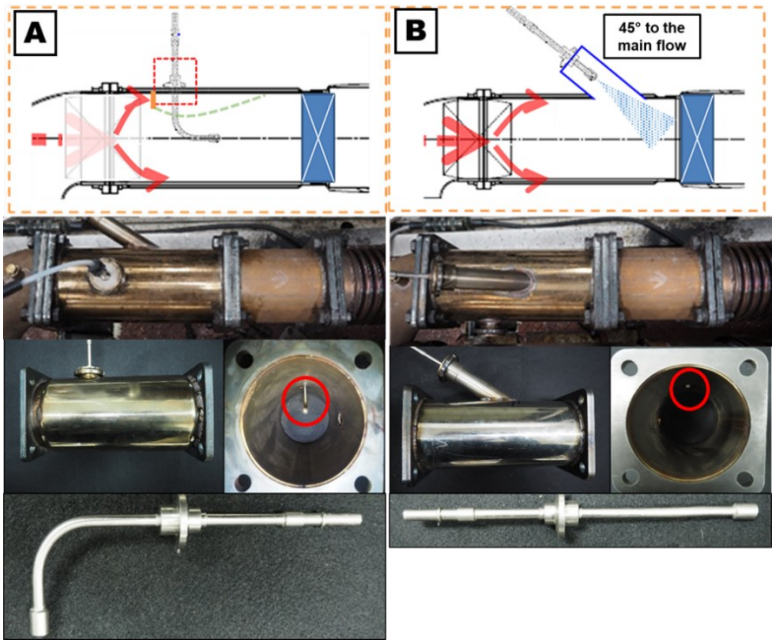

Figure 3.18: The urea injectors: a) L-Shaped injector and b) I-Shaped injector

3.2.3 NOx conversion test

3.2.3.1 NOx conversion test for 3L Diesel engine

The mixture of NOx and ammonia took place from the pipe to the catalytic converter. For monitoring at the pressure outlet and to limit emissions, the outlet catalyst was linked to the pipe gas

analyzer and the back-pressure valve (hydrocarbon and NOx). This metric was crucial in determining the quality of the research we conducted. The quantity of NOx in the result is the indicator the effectiveness of the SCR system research; lower the NOx quantity, more effective the SCR system study; however, more high NOx quantity in the result, more ineffective the SCR system study. The gas analyzer utilized in this investigation is shown in Figure 3.19. The quantity of gas in the study may be calculated using a gas analyzer, and the pattern color may be used to show the result.

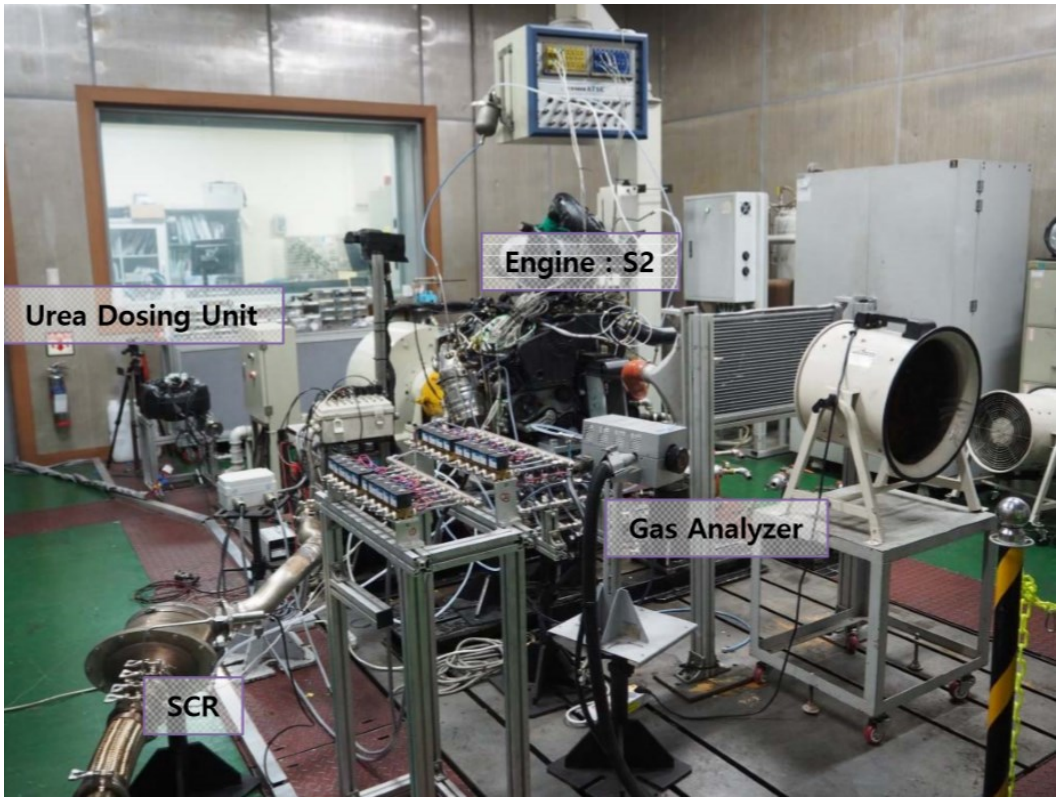

Figure 3.19: The experiment setup for 3L Diesel Engine (KATECH)

3.2.3.2 NOx conversion test for 12L Heavy-duty diesel engine

The amount of gas used to evaluate the quality of an SCR system for reducing NOx emissions from a diesel engine is the most important component. The current study investigated NOx emission quantity using a gas analyzer (MEXA-7100; Horiba, Japan). The gas analyser is attached to the SCR system's output; with that position, the gas analyzer can easily investigate the SCR system performance to reduce NOx emission; the chemical process between ammonia and NOx emission also can analyze based on the NOx quantity.

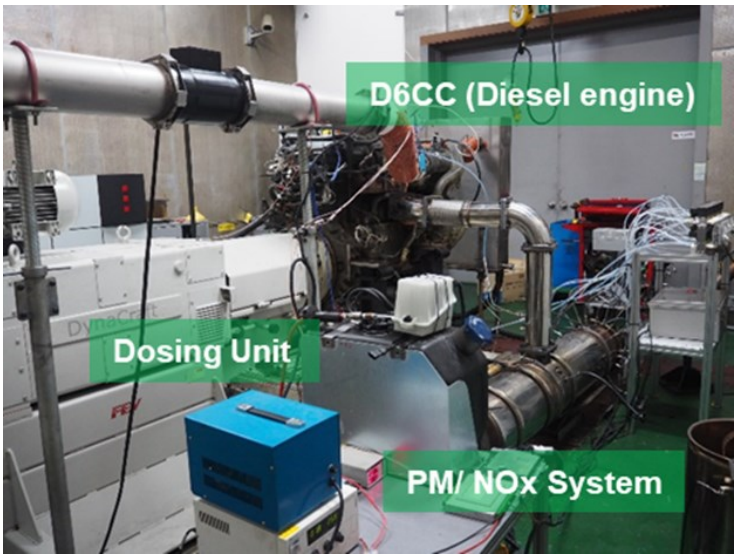

Figure 3.20: The experiment setup for 12L Heavy-duty Diesel engine (KATECH)

3.2.4 Ammonia uniformity test

3.2.4.1 Ammonia uniformity test for 3L Diesel engine

The experiment with 19 sensors in the SCR catalyst is shown in Figure 3.21. The sensor data was analyzed in a gas analyzer to determine which gas was present in the catalyst. As illustrated in figure 3.22, the sample data from the 19 sensors was translated into a hexagram pattern, which was colored according to the amount of gas detected.

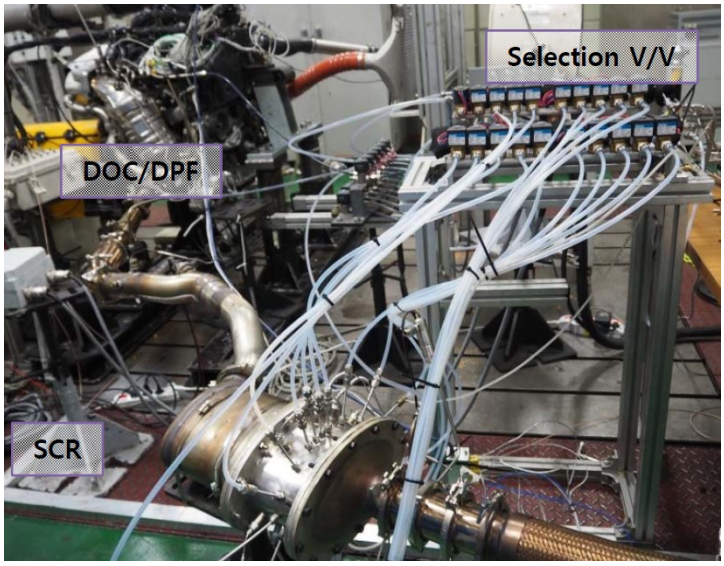

Figure 3.21: Gas analyzer for 3L Diesel Engine

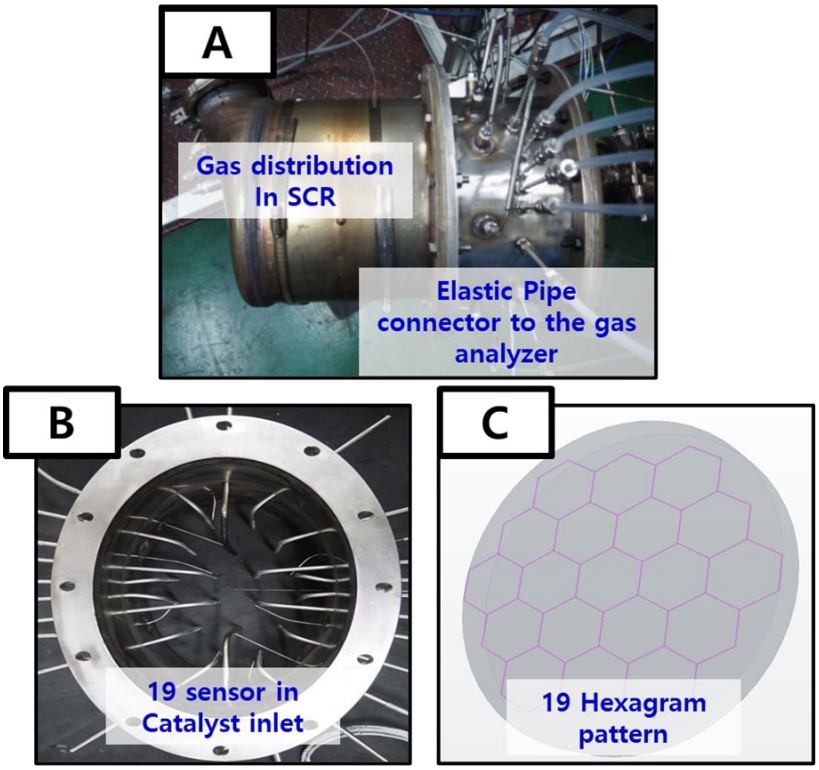

Figure 3.22: Gas analyzer sensors for 3L Diesel Engine

3.2.4.1 Ammonia uniformity test for 12L Heavy-duty diesel engine

The gas analyzer is limited to identify the exact value of ammonia homogenization at the surface catalyst. Thus, 19 sensors were inserted at the catalyst to investigate ammonia homogenization. The information about 19 sensors and ammonia homogenization gaseous analyzer was show in the Figure 3.23. The value of ammonia gas was computed by every sensor and transferred to the gas analyzer. The value from the sensors can described by the color in the catalyst figure. The contrast color in the figure can decide the ammonia homogenization quality in this study.

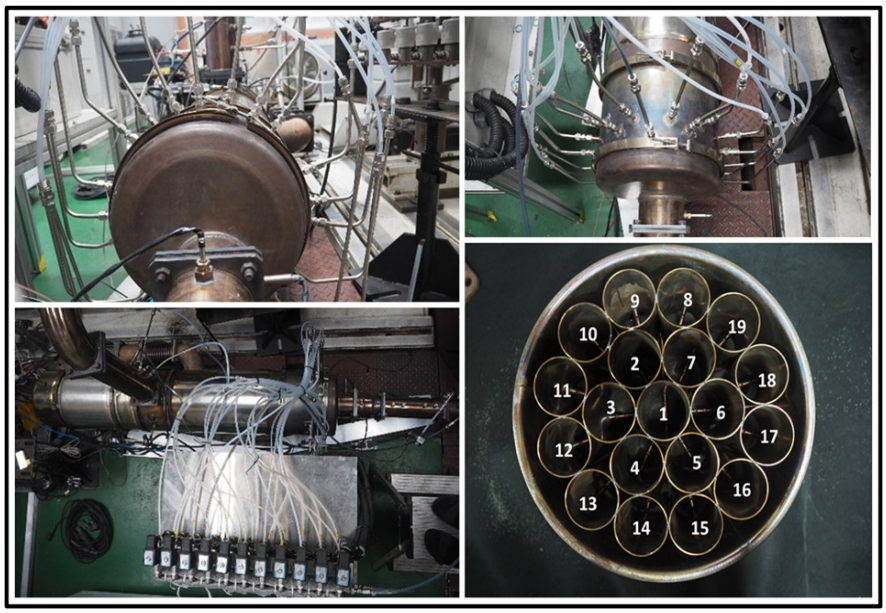

Figure 3.23 : Gas analyzer sensors for 12L Heavy-duty Diesel engine

3.3 Simulation and modeling

3.3.1 Governing Equations

Direct numerical simulation (DNS), the Eulerian-Eulerian model, and the Eulerian-Lagrangian model are the most frequent methodologies for multiphase flow modeling with superior accuracy among the different extant methods. Only the DNS technique models the interphase that exists between the continuous and scattered phases. Although DNS predicts near-perfect results, it is a computationally intensive procedure. DNS computation can take many weeks to complete, hence it is not recommended for commercial application due to the high computational cost [38]. The benefits of Eulerian-Lagrangian modeling over Eulerian-Eulerian modeling include more specific information on discrete particle behavior rather than continuous dynamics, and Eulerian-Eulerian modeling becomes computationally costly when numerous sets of equations are utilized. The Eulerian-Lagrangian framework works in two ways: the particles are described as individual droplets or as a bundle in the Eulerian-Lagrangian framework. Individual particle modeling is more accurate than bundle or parcel modeling, although it is more computationally intensive. Within the same parcel, the particle's dynamic attributes (such as size and velocity) are identical. The interaction between each particle or parcel and the continuous phases is described using the incompressible and unsteady Reynolds-averaged NavierStokes (RANS) equations for energy, mass, momentum, and species in an Eulerian-Lagrangian method. The realizable k-model is used to simulate turbulent flow since it outperforms the traditional k-model when it comes to estimating turbulence quantities.

The Linearized Instability Sheet Atomization (LISA) model is used to represent the main spray atomization for the thin liquid sheet formed at the nozzle tip by the pressure-swirl atomizer [52]. The centrifugal motion and sheet breakdown of the injected liquid generate a liquid film surrounded by an air core, and the LISA model can compute the thickness and velocity of the fluid film generated. An empirical function known as the Rosin-Rammler distribution is used to model the droplet size distribution, and it is represented as:

$$1-Q=\exp(-(\frac{D_p}{X})^q) \qquad (1)$$

The percentage of total holding drop volume with a diameter smaller than D_p is denoted by Q. The spread is measured by the exponent value q, and a greater value indicates a more uniform spray. The reference droplet diameter is denoted by the letter X. The NTC (No Time Counter) collision detection technique estimates the collision between the droplets [52].

The probable number of collisions in a cell with N droplets over a time interval is calculated by adding the probability of all conceivable collisions:

$$M_{col}=\frac{1}{2}\sum_{i=1}^{N_p}q_i\sum_{j=1}^{N_p}q_j\frac{v_{i,j}\sigma_{i,j}\Delta t}{v} \qquad (2)$$

Where $v_{i,j}$ is the relative velocity of two colliding particles, σ_{ij} is the collision cross section of the two drops, and,

$$\sigma_{i,j}=\pi(r_i+r_j)^2 \qquad (3)$$

The time-step size is Δt, the cell volume is V, the number of parcels in a cell is N_p, and the number of droplets in parcel I is qi. The Reitz-Diwakar droplet breakup model is used to model secondary breakdown. Newton's second law of motion, which stipulates that the momentum rate change is equal to the total of forces acting on the particle, is used to estimate the atomized droplet trajectories.

$$F_i=m_p\frac{dv_{p,i}}{dt} \qquad (4)$$

The mass of the particle is mp, and the velocity of the particle is $v_{p,i}$. Body forces, which act on the particle mass, and surface forces, which are created by shear stresses and pressure forces acting on the particle surface, are the two types of forces acting on the particle. These active forces can be subdivided further,

$$\begin{aligned}F_i &= F_{i,\mathrm{D}rag}+F_{i,\mathrm{Pr}essureandShear}+F_{i,Addedmass}+F_{i,History}\\ &+F_{i,Buoyancy}+F_{i,Lift}+F_{i,Thermophoretic}+F_{i,Turbulent}+F_{i,Brownian}\end{aligned} \qquad (5)$$

All of the forces mentioned above have an influence on particles, but forces with significant impacts are modeled to decrease processing costs. The drag force is included since it is the most significant force acting on the particle [53]. Pressure and shear gradient forces have little influence on particle motion since the density ratio between the dispersed and continuous phases is minimal, hence these forces are ignored [29]. When the size and density of the particles grow, the historical forces impact decreases. It works in the same direction but with a considerably stronger drag force, reducing its impact; as a result, it gets overlooked [53]. The difference in density between the phases determines buoyancy force, which is taken into consideration. The lift force works perpendicular to the drag force, i.e. in the radial spray direction, which means it has an influence on the spray cone and is thus included in the modeling. Brownian and thermophoretic forces have minimal impact, thus they are ruled out. If particle relative velocity drop or turbulent kinetic energy rises, turbulence intensity is increased. Turbulence affects particles having a high kinetic energy at the nozzle tip and a low relative velocity downstream. Spray particles with a high Stokes number are less impacted by turbulence, whereas a large number of tiny particles with a low Stokes number are strongly influenced by turbulence. As a result, the turbulence impact is accounted for in the simulation. The spray droplet evaporation rates are modeled using a multicomponent droplet evaporation model. The model assumes that all of the spray droplets are in a homogenous multi-component liquid mixture. Each component's quasi-steady evaporation rate is given by

$$m_{pi} = -\zeta_i g^* A_S \ln(1+B) \qquad (6)$$

B stands for Spalding transfer number, AS stands for droplet surface area, g* stands for mass transfer conductance, and I stands for fractional mass transfer rate, which is defined as

$$\sum_T \zeta_i = 1 \qquad (7)$$

The transfer number is T in this case. When UWS spray droplets collide with the catalyst wall, the momentum force perpendicular to the wall is considered to be zero. The wall film model provides for maintained quantity transfers inside the fluid film as well as interactions with the environment. Energy conservation, mass conservation, and momentum conservation are all part of it. The film thickness is so tiny that it sticks to the boundary, and the velocity profile along the film is parabolic. These are the general assumptions for film model implementation. The normal direction flow is regarded minimal since the film thickness is so thin. On the wall film, three separate forces are at work. The film moves in the same direction as the gas flow. The viscous friction force seeks to prevent movement of the wall film. Another force is at work as a result of the increased mass impingement. The force operating on the wall film as a whole is,

$$\rho g \delta \frac{du_{film}}{dt} = \tau_g + \tau_w + \tau_{imp} \qquad (8)$$

Here, τ_g denotes the force acting on per unit area of film on the gas side, τ_w denotes the force acting on per unit area of film on the wall side, and imp denotes the force acting on per unit area of wall film owing to impingement momentum.

Mass conservation equation is,

$$\frac{d}{dt}\int_v \rho_f dv + \int_A \rho_f (v_f - v_g).da = \int_v \frac{s_m}{\delta} dv \qquad (9)$$

V is volume, and A is area, all of which are functions of the thickness of the fluid film and its partial distribution, ρ_f is fluid film density, V_f and V_g are film and grid velocity, and Sm is the mass source per unit wall area.

Momentum conservation equation is,

$$\frac{d}{dt}\int_v \rho_f v_f dv + \int_A \rho_f \, v_f (v_f - v_g).da = \int_A \tau_f da - \int_A \rho_f da + \int_v (p_f f_b + \frac{s_m}{h_f}) dv \qquad (10)$$

S_m denotes the momentum source in relation to the mass source. The viscous stress is τ_f, and the pressure force is p_f.

Energy conservation equation is,

$$\frac{d}{dt}\int_v \rho_f E_f dv + \int_A (\rho_f H_f (v_f - v_g) + v_g \, p_f) da = \int_A q''_f da \int_A \tau_f v_f .da + \int_v f_b v_f dv + \int_v \frac{S_u}{h_f} dv \qquad (11)$$

The total energy of the film is E_f, the energy sink/source for unit film area is S_u, and the body force is f_b.

3.3.2 Numerical Formulation

The governing equations are solved using the commercial simulation program STAR CCM+. For multiphase simulations, the second order upwind technique is used because it is more accurate than the first order method. The implicit technique, which is bounded unconditionally and has a longer time step, was chosen as the temporal discretization scheme. The two-way couplings with droplet particles simulate the effects of droplet particles on continuous phases and phase interactions. Under the influence of the relaxation factor of 0.7. The UWS spray droplets are represented as a nonreacting

dispersed Lagrangian phase with discrete computational parcels, with the force acting on each droplet parcel compressed over time to update velocity and spatial location. In the continuum phase, each droplet parcel is considered as a point source in the governing equations for momentum, energy, and mass. The Leidenfrost temperature effect is implemented in droplet wall contact modeling utilizing a specifically created user specified function (UDF) subroutine. To address the wall film thickness and droplet size distribution, two additional UDFs are used. All y+ treatments were used, as well as a two-layer strategy that used a high y+ wall treatment for coarse mesh and a low y+ wall treatment for fine mesh. To track the convergence, the residuals for energy, turbulent kinetic energy, turbulent dissipation rate, momentum, temperature, continuity, and each species were examined until they stabilized.

3.3.3 Mesh Computation

The proper study of urea-water spray, good meshing is required; however, traditional CFD modeling uses sophisticated meshing that necessitates sophisticated techniques and increases solution time. In this work, automatic meshing technique [54] was used with a base size of 5 mm. For correctly resolving the near wall area flow, two prism layers with a thickness of 2 mm were utilized. Prism layers have a crucial role in determining heat transmission and pressures on walls, as well as flow separation along the wall. It also prevents numerical diffusion, resulting in a faultless outcome [55]. The fundamental curvature size was raised to 72 to provide the geometry a smoother surface curvature. The sensitivity study was carried out using a mesh base size of 4 mm and three prism layers, while the other variables remained same.

3.3.4 Multiple Flow Regimes

The Multiple Flow Regime Phase Interaction model is used for cases where both segregated and dispersed two-phase flows exist in the same domain. An example scenario is a flow of a liquid and gas under undulating motion. In the example flow of liquid and gas, it is possible to have three concurrent regions of two-phase flow:

- The first regime: A region where the gas is dispersed in the liquid.
- The intermediate regime: A region where, of the two phases, neither phase is dispersed in the other phase.
- The second regime: A region where the liquid is dispersed in the gas.

In the intermediate regime, the interface between the two phases can be modeled as separated or blended. If the two phases are clearly separated by a sharp interface, the Large-Scale Interface

Detection model is used to determine the interface. If there is no clear separation of the two phases in the intermediate regime, a blended interface is modeled.

3.3.4.1 Modeling Multiphase Segregated Flow

The Multiphase Segregated Flow model can used when the phases are expected to be mixed on length scales smaller than the length scales to resolve and coexist everywhere in the flow domain. In this model, each distinct phase has its own set of conservation equations. It is assumed the time averaged behavior of the flow, rather than the instantaneous behavior. The phases in a multiphase segregated flow can be gas, liquid, or solid particles. Each phase has its own velocity, energy, and other variables, and its own physical properties. This definition includes the models for the interfacial area, and for the rates of interphase transfer of mass, momentum, and energy.

3.3.4.1 Modeling Turbulent Flow

The STAR-CCM+ software can show the effects of turbulence on continuous and dispersed phases in several ways:

- Continuous and dispersed phases can each be modeled with their own set of equations for the turbulence energy and dissipation. The model phases independently as laminar, turbulent or with different turbulence models. The turbulence equations are identical to the single-phase formulation, except each phase is scaled with a factor of the volume fraction of that phase. The same phase volume fraction also modifies convection and diffusion fluxes of phase-turbulence quantities.
- The turbulence of the dispersed phase can be calculated from the turbulence of the continuous phase using the Turbulence Response Model. This algebraic model reduces the computations that are required as only the continuous phase equations are solved. However, the model couples the turbulence of dispersed phases to the continuous ones.
- The phases can also be coupled through bubble/particle induced turbulence of the dispersed phase which adds more source terms to the continuous phase turbulence energy and dissipation equations.
- In addition to its contribution to the model turbulence, particle-generated turbulence can also be dissipated locally at the particle scale. This effect can be thought as a local enhancement of the mixing and is accounted for by the Particle Induced Mixing Model.

- The transfer of turbulence from one phase to another is accounted for by the Interphase Turbulence Transfer Model.

The STAR-CCM+ software supports Large Eddy Simulation (LES) turbulence in multiphase flows. Large Eddy Simulation is a technique intermediate between the direct numerical simulation of turbulent flows and the solution of the Reynolds-Averaged Navier-Stokes (RANS) equations. In LES the contribution of the large, energy-carrying structures to momentum and energy transfer is computed exactly, and only the effect of the smallest scales of turbulence is modeled. Since the small scales tend to be more homogeneous, isotropic, and universal, and less affected by the boundary conditions than the large scales, the LES models can be simpler and require fewer adjustments when applied to different flows than similar models for the RANS equations. A good application for LES in a multiphase flow is a bubbly flow. The dispersed phase can use the Laminar model instead of a turbulence model. However, the dispersed phase to carry a significant proportion of the wall stress or wall heat transfer, do not use the Laminar model.

3.4 Summary

This chapter goes through each phase of the research process in depth. The experimental setup, apparatus details, measurement technique, simulation model, boundary condition, and start value have all been described in detail. The initial step in performing this study was to do numerical simulations and experiments to see how the urea injection timing strategy may improve NOx conversion efficiency in SCR systems. The second step was investigate the solid deposit formation in the SCR system by the super-hydrophobic surface. Both of this step used optical access chamber. The study in this step 1 and 2 was used 3L diesel engine parameter with exhaust mass flow rate of 93 kg/h and NOx quantity of 130 ppm in 1500rpm engine operation condition. The third step was investigate the ammonia uniformity to predict NOx conversion efficiency in SCR system. In this step, the experiment and simulation was used optical access and 3L diesel engine. The variation of engine speed (1500, 2000 and 3000rpm) and mixer was used to analyze the ammonia uniformity quantity in this study. The mass flow rate, NOx amount, and other parameters were similar to those measured at 1500 rpm. 1500 rpm, 2000 rpm, and 3000 rpm were determined to be reflective of the whole variance predicted based on this observation. The mass flow rate and NOx amount of the engine operation circumstances at 2000 rpm and 3000 rpm revealed a significant difference, making it easy to compare NH3 uniformity of the engine operating circumstances. The fourth phase involved testing several types of urea injectors in heavy-duty diesel engines in order to improve NOx conversion in the SCR system. In this step, the experiment and simulation study used 12L heavy-duty diesel engine with 1.000 to 1.700 engine speed conditions. The 1.000 engine speed condition produced a 513 kg/h exhaust mass flow rate and a 1,330 ppm NOx con-

centration value; and 1.700 engine speed condition produced a 1.100 kg/h exhaust mass flow rate and a 204 ppm NOx concentration value. The NOx concentration value for the 1.700 engine speed condition is lower than that for the 1.000 engine speed condition because the 1.700 engine speed conditions produce less oxygen (O2) for combustion, resulting in lower NOx concentration. The result from this experimentas and simulation setup will shows in chapter 4 to chapter 7, when the chapter 4 explain the effects of urea injection time on NOx conversion prediction in an SCR system; chapter 5 explain the effects of urea injection strategy on solid deposit formation; chapter 6 explain the ammonia uniformity to predict NOx conversion efficiency; and chapter 7 explain the investigation of different types of urea injectors in an SCR system.

Chapter 4

Effects of urea injection time on NOx conversion prediction in an SCR systems

This chapter presents the numerical modeling and experiments used to study how the urea injection timing strategy might improve NOx conversion efficiency in SCR systems. The NOx conversion efficiency value may be improved by considering the urea characteristic, the impacts of exhaust gas temperature, gas distribution value, and ammonia homogeneity.

4.1 Urea Spray Characteristics

The basic spray features of the SCR injector were determined by capturing atmospheric spray parameters. The SCR injector utilized in the investigation was a 3-hole pressure-driven injector with a nozzle hole diameter of 0.12 mm and an equilateral triangular form with 1.9 mm side length. Spray was formed in a triple stream due to atomization. Figure 4.1 depicts the whole length experimental and numerical spray producing operations.

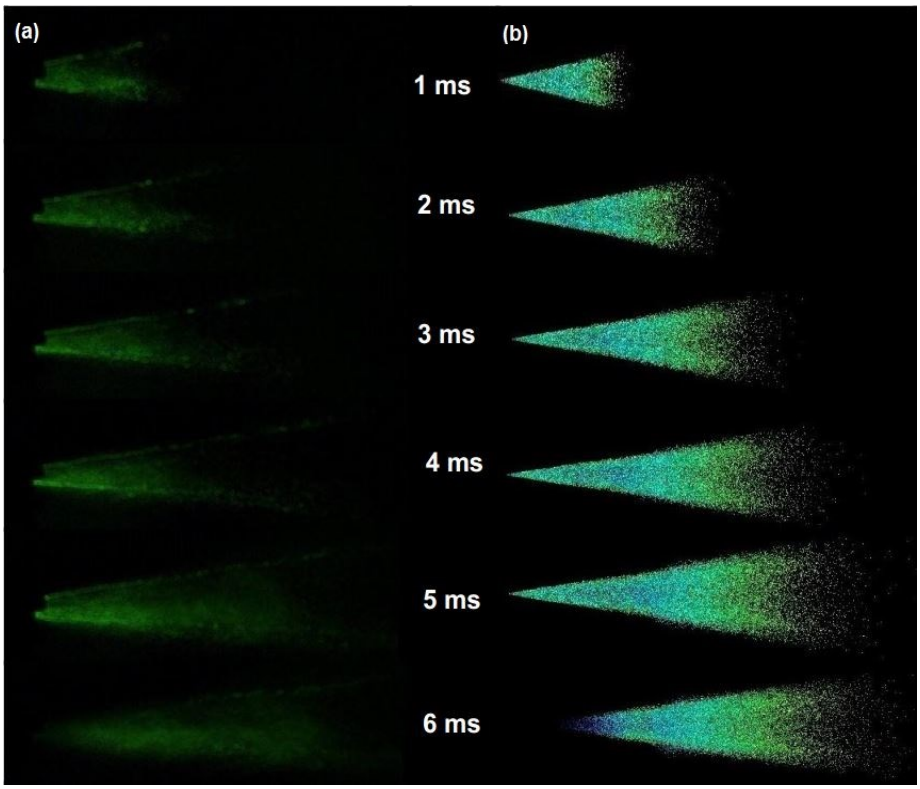

Figure 4.1: Spray developing process at injection pressure 5 bar (a) Experiment; (b) Simulation

With each disintegration of the droplets, the diameter of the UWS droplet decreases, and it now measures between 100 and 40 microns. When the distance between the injector nozzle tip and the droplet diameter is raised, the droplet diameter grows larger at the nozzle tip and shrinks as the distance between the nozzle tip and the droplet diameter is narrower. Because of the effects of temperature and pressure on droplet viscosity and surface tension, the size of the droplets shrank. Figure 4.2 depicts a comparison of the droplet width of UWS spray as estimated by numerical modeling, with values for 3 bar and 5 bar injection pressures and 373 K and 573 K exhaust gas temperatures, respectively. Injection pressure has a big impact on spray development; as you can see in the graph, the spray was fully formed and atomized after 2 ms at 5 bar injection pressure, while it just started after 3 ms at 3 bar injection pressure. The temperature of the exhaust gas has a little impact on spray formation and droplet breakup. For mixing and droplet evaporation, early atomization and breakdown are quite beneficial. Smaller droplets evaporate quicker during spray injection and droplet impingement on the exhaust pipe wall, resulting in the production of more active components. Because the exhaust gas and SCR reductant mix evenly, the possibility of deposit formation is reduced. The study found that as injection pressure is increased, the size of the droplets shrinks. Another thing to note is that high temperatures result in smaller droplets, as seen by the 3 bar and 573 K conditions.

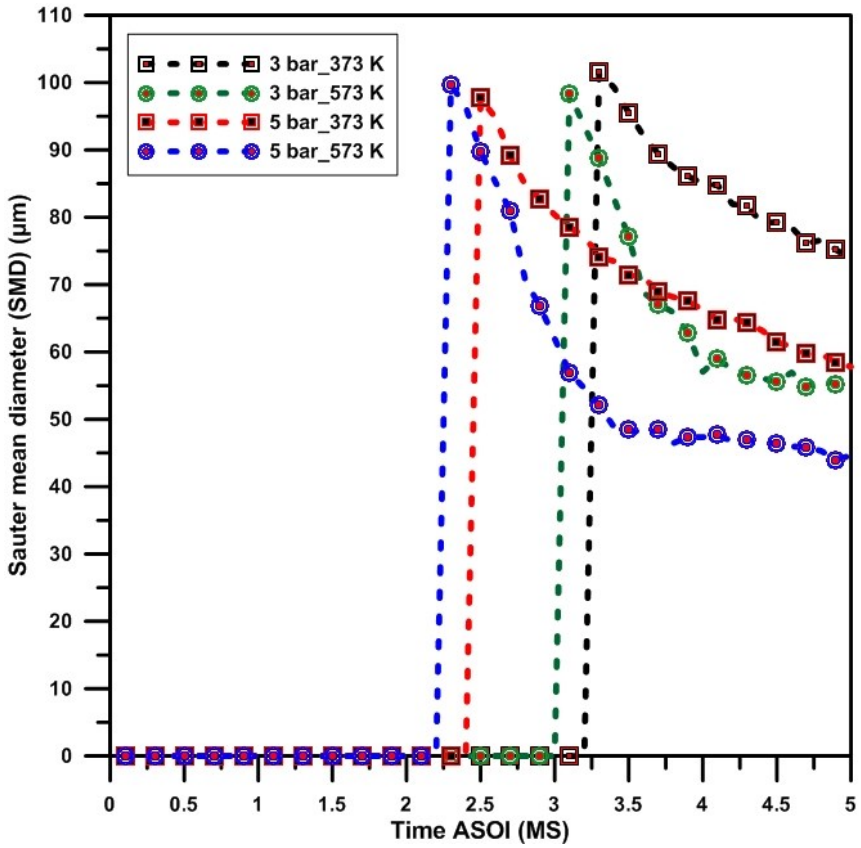

Figure 4.2: Comparison of the UWS droplet size at 3 bar and 5 bar injection pressure; 373 K and 573 K exhaust gas temperature.

Figure 4.3 depicts the droplet size distribution of UWS after a single injection at 5 bar injection pressure. UWS droplets range in size from 5 to 85 microns, with the bulk of particles falling between 30 and 60 microns.

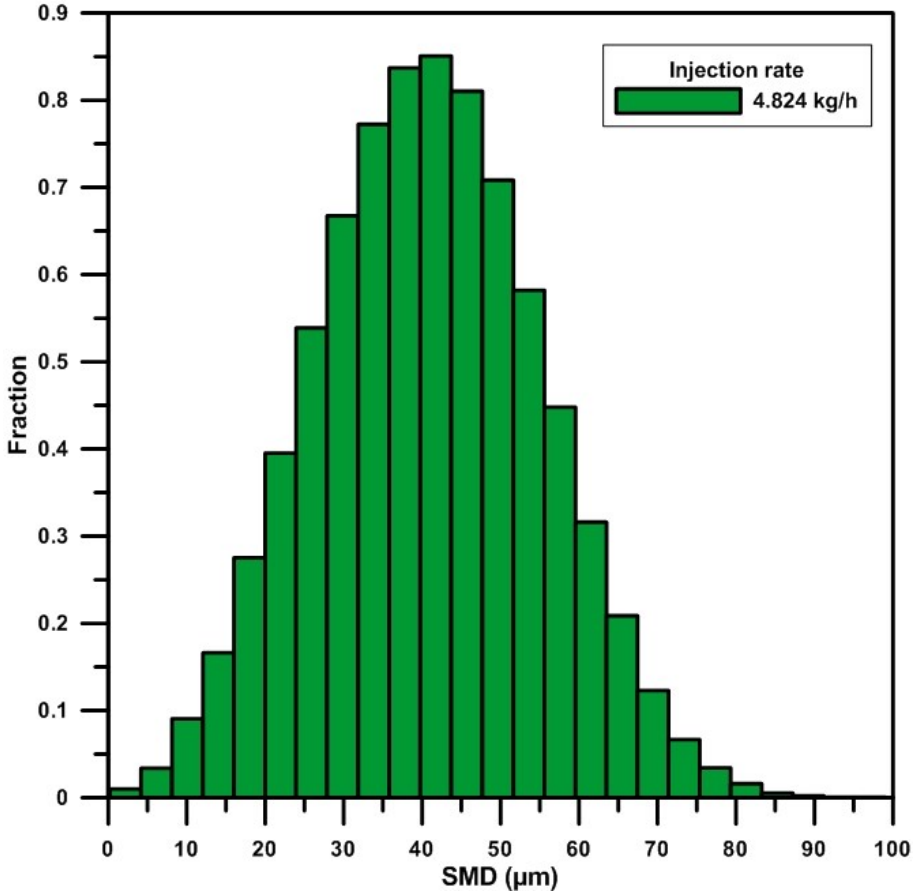

Figure 4.3: UWS droplet distribution at 5 bar injection pressure and 4.824 kg/h injection rate.

The exhaust gas temperature causes the UWS droplets to evaporate, resulting in NH_3, which interacts with the NOx components to form N_2 and H_2O. Urea turns to ammonia when the temperature is higher than the decomposition temperature. However, partial urea breakdown happens at low temperatures, causing UWS droplets to stick to the exhaust pipe wall and form a solid deposit. This occurrence has a significant negative influence on system performance. Because of the short residence time in the exhaust pipe, faster droplet evaporation produces more active components and is suggested.

4.2 CFD modeling for Optical access

CFD (computational fluid dynamics) is a field of fluid mechanics that employs numerical analysis to solve problems. The three-dimensional CFD model was effective in observing the urea injection shape, gas distribution, ammonia pattern, and system temperature value. This simulation study

used three dimensional model of CFD results for clearly showing the flow distribution model, temperature value distribution and other information clearly. That information will show with flow pattern, color value, graphic, and other information in the simulation. This study used the simulation with the commercial software from STAR CCM+ version 11.04. The simulation in this study used the parameter and dimension of system same on the real value in the experiment study. Initial validation of simulation is typically performed using experimental with the real systems. Figure 4.4 depicts the SCR system geometry, including the position of the UWS injector. The geometry of the CFD for optical access is 30x30x60cm. The UWS injector was positioned 10 cm from the entrance at the top of the optical access, at a 90° angle to the main flow. The urea decomposition events and exhaust gas temperature distribution in the system will be readily visible with this optical access.

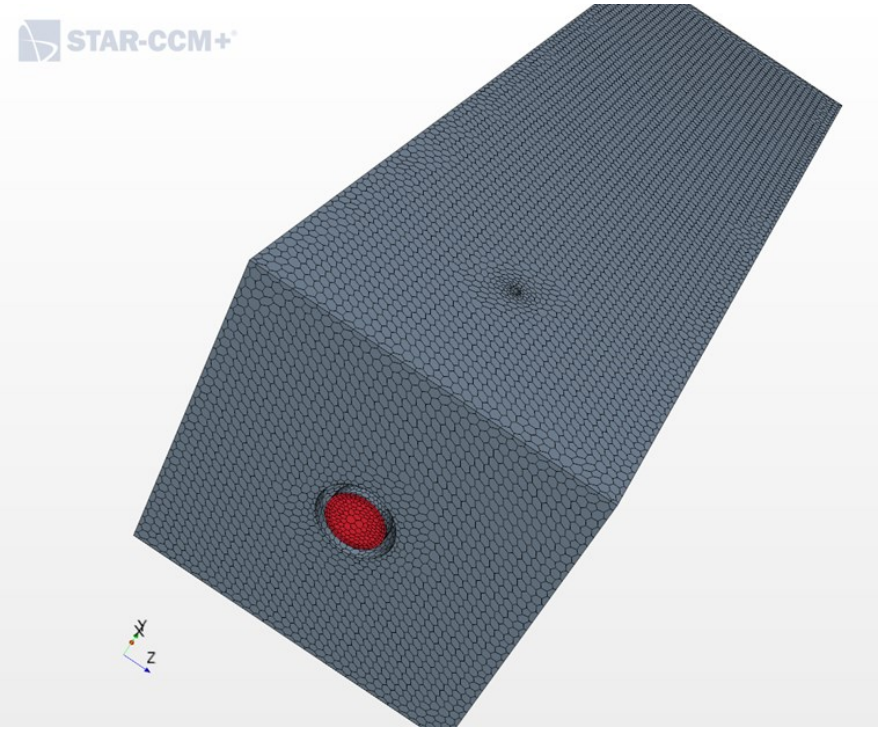

Figure 4.4: The CFD of optical access

4.3 Effects of Exhaust Gas Temperature

One technique to vividly display the phenomena in the SCR system is to use optical access. Figure 4.5 depicts a simulation of the distribution exhaust gas phenomena in the optical access at a temperature of 686 K and a flow rate of 223 kg/h. When it came to combining ammonia and NOx, the most crucial indications were gas flow and exhaust pressure. Zhang et al [56] analyzed the effects of gas flow on ammonia homogenization in straight exhaust pipe systems were investigated. The influences of air flow and exhaust pressure also contribute to the SCR system's temperature rise. Engine

running conditions of 2000 rpm might result in excessive temperatures in the system. These temperatures, however, cannot rapidly heat up the entire system. Koebel and Strutz [27] described the thermal and hydrolytic degradation of urea in the system was detailed in the temperature range of 150 to 500 °C. As a result, a temperature rise was required to obtain a temperature acceptable for urea injection in the SCR system. According to Figure 4.5, the optical access was reached in an acceptable situation 20 seconds after the engine started up. The temperature in the system reached 326°C, with the velocity magnitude, pressure, and mass flow rate remaining constant, and the flow pattern forming a shape. This study discovered that 20 seconds after engine start-up was the best time to feed urea into the system, based on Koebel and Strutz hypothesis. The temperature simulation result was also supported by the experiment outcome in Figure 4.5.

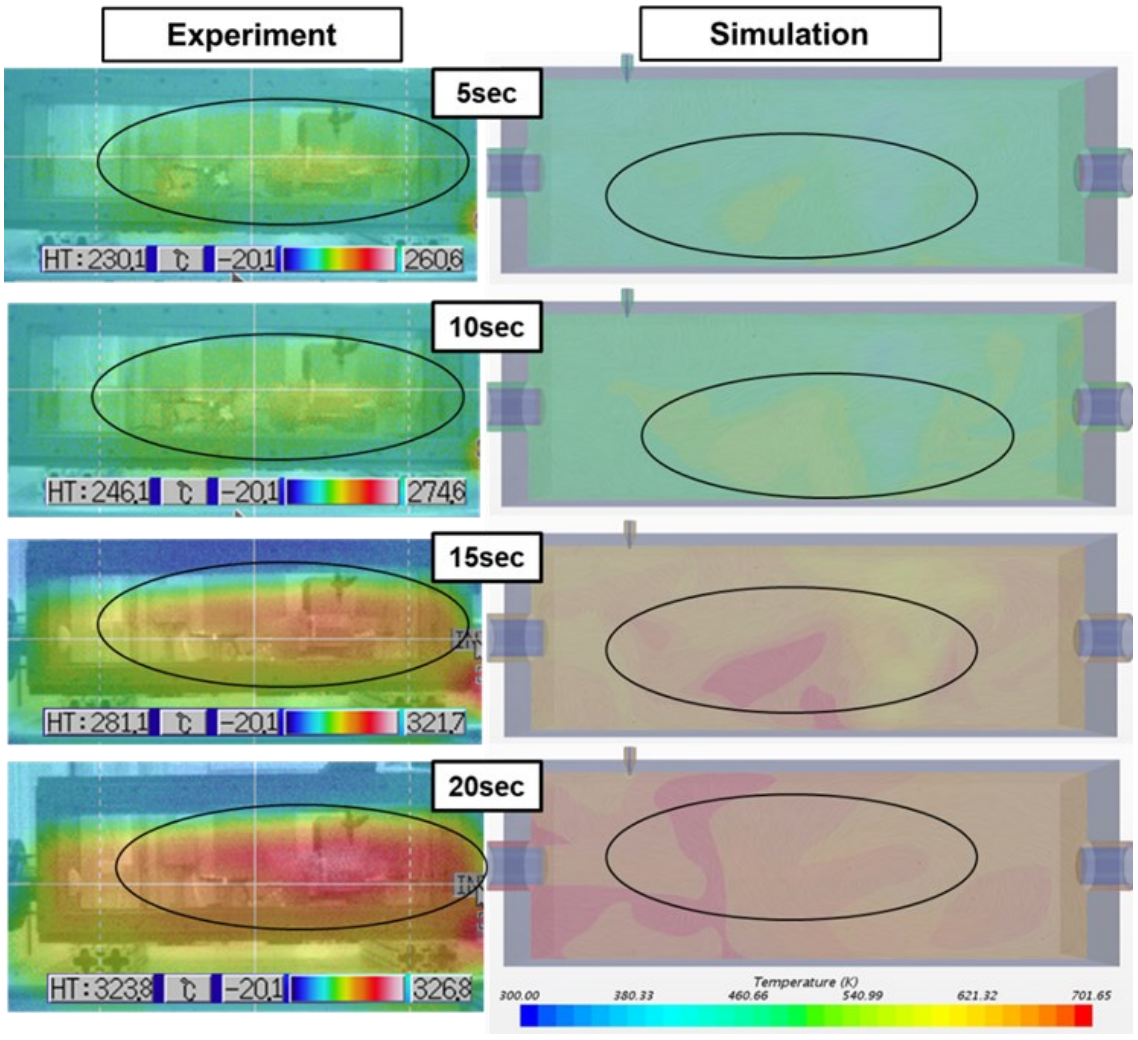

Figure 4.5: The comparison of temperature condition inside the optical access between simulation and experiment

In the experiment, Figure 4.5 depicted the optical access temperature distribution phenomena 20 seconds after engine start-up using a thermal camera. The 326°C optical access temperature can help to speed up the urea breakdown process and avoid solid accumulation in the SCR system. The gas flow and adequate temperature can impact the urea breakdown and evaporation process in the SCR system, according to simulation and experiment findings from the optical access. In order to characterize the influence of proper conditions in the system, information on mass flow amount and pressure was required.

Figure 4.6 depicts the magnitude of velocity and mass flow rate in the simulation as a function of time. In the optical access, the highest flow mass was 3.13 x 102 kg/s and the minimum flow mass was -2.08 x 102 kg/s, as shown in the diagram. These findings suggest that the gas reaction distribution in the simulation was unstable for less than 20 seconds of the period. That phenomenon happened in real life as well. The temperature and gas flow in the system were affected by the unstable circumstances. In the SCR system, the urea was trapped at the wall and unable to dissipate. The trapped urea collected and obstructing gas air movement, and the extended reactions caused a major issue in the SCR system.

Figure 4.7 depicts the time-dependent reaction of pressure and force in the simulation. After 20 seconds of engine start-up, the pressure remained unchanged. In the simulation, however, the pressure and force did not attain constant levels for more than 20 seconds. In the simulation, the initial pressure condition and optical access size impacted the lowering pressure till it reached -39.15 bars in 3 seconds. In addition, the pressure rose dramatically in 12 seconds, reaching 13.2 bars. Because the simulation was run using pressure and velocity parameters that were identical to those in the experiment, this response also happened under real-world optical access circumstances. This was in contrast to the exhaust gas force measurements, which showed that as the exhaust gas pressure dropped, the exhaust gas forces grew until reaching 17.78 kN with a minimum value of -2.63 kN before stabilizing at a constant value. In the optical approach utilized in the simulation and experiment, this huge pressure was measured with relation to time.

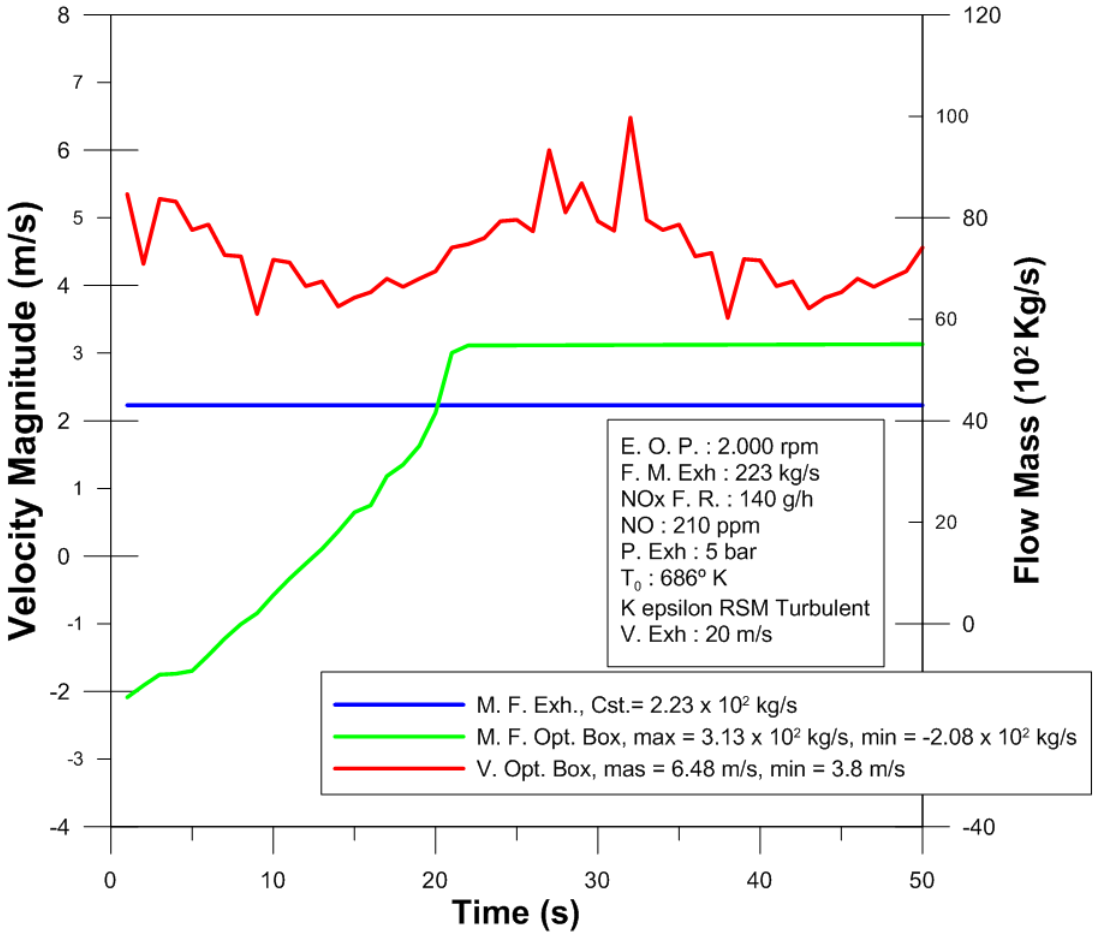

Figure 4.6: Velocity and mass flow rate effects in simulation of the optical access

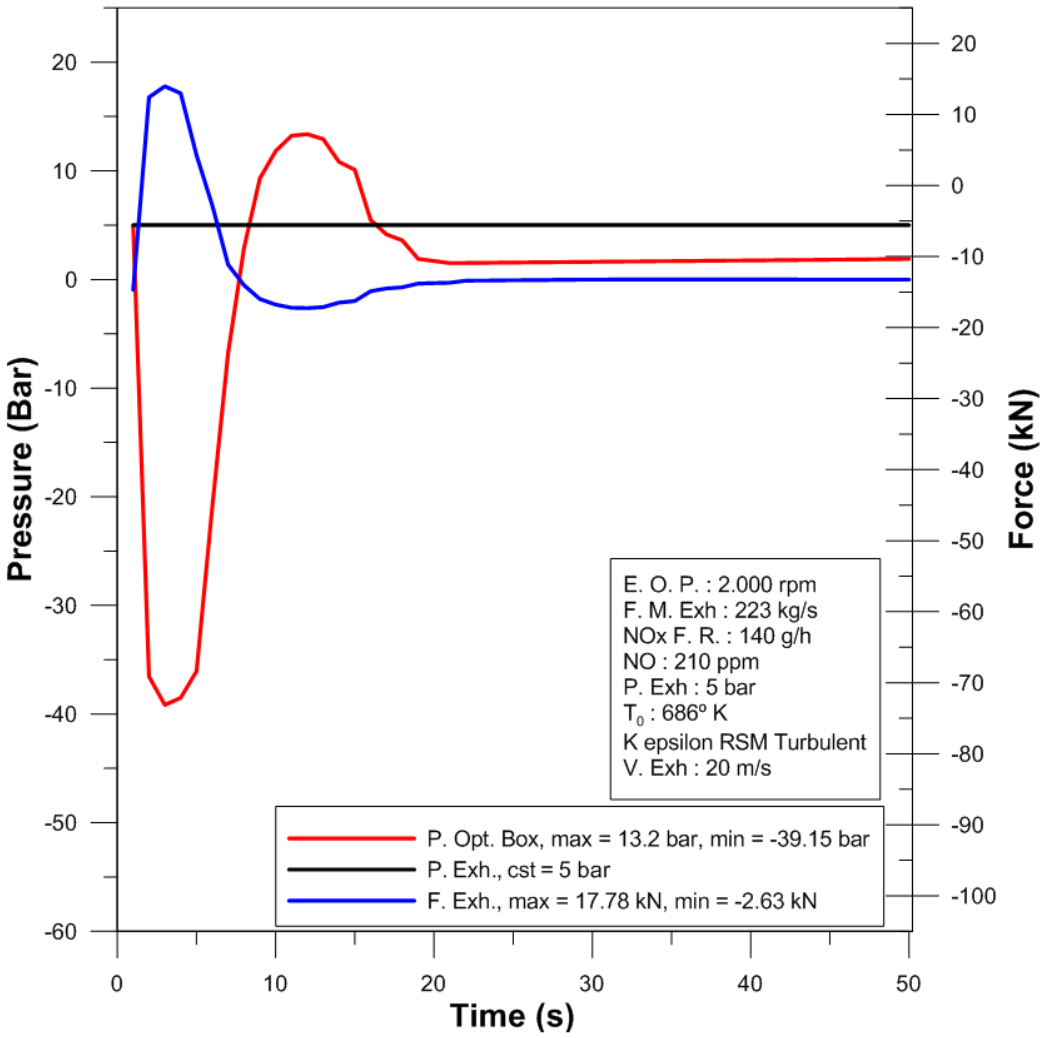

Figure 4.7: Pressure and force effects in simulation of the optical access

4.4 Effects of Urea Injection Timing to Distribution Gas

The distribution of exhaust pressure might be used to anticipate when urea should be injected into the catalytic converter to maximize NOx reduction efficiency. After 20 seconds of engine start-up, the SCR system had the best quantity of mass flow and the best temperature. Those were the ideal circumstances for injecting urea into the SCR system. The urea distributed quickly to all corners of the optical access, and the high temperature conditions in the SCR system aided urea evaporation. Figure 4.8 depicts the distribution of urea and exhaust gas phenomena in an optical access simulation. The breakdown of urea to create ammonia was aided by the exhaust gas velocity and temperature. As a result, when the flow mass, pressure, and temperature reached the correct levels, the urea was injected into the simulation. The procedure aided the mixing of ammonia and NOx to create steam and nitrogen at the SCR system's output, lowering NOx levels in the diesel engine.

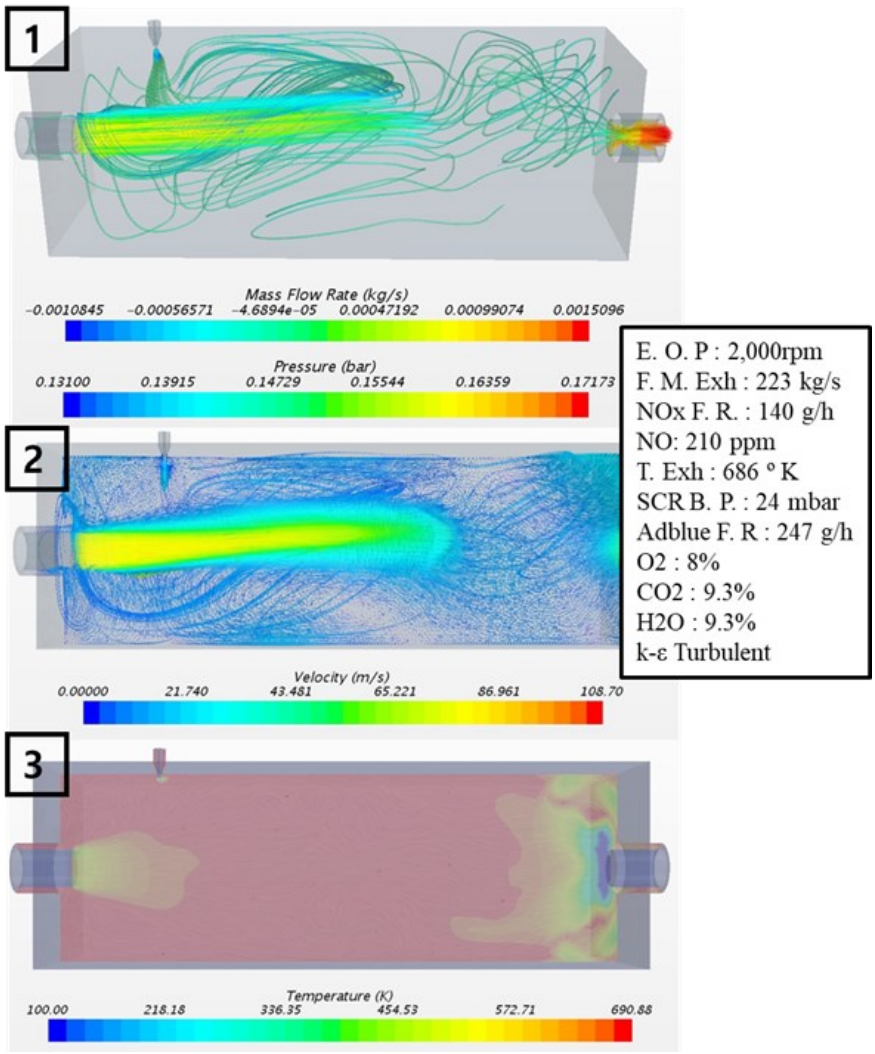

Figure 4.8: Distribution of urea and the exhaust gas phenomena in the simulation of optical access

4.5 Effect of Injection Timing strategy to 3L Diesel Engine SCR system

The optical access distribution of urea and exhaust gas phenomena were essential parameters for ammonia optimization. The optical access simulation can identify the appropriate temperature and flow condition for the urea injection process in the SCR system, which can then be verified using the thermal camera in the experiment setup. However, additional testing of this work in a commercial SCR system utilizing a genuine diesel engine is required. As a consequence, using simulation, the influence of optical access on the commercial SCR system was analyzed in this part. Figure 4.9 depicts the urea distribution and exhaust gas phenomena in the SCR system in this simulation. The velocity magnitude of urea and exhaust gas colors the air flow. Inside the SCR systems, the blue color signifies low velocity while the red color symbolizes high velocity. The ammonia particles in the catalyst were aided in mixing with NOx by the multi-component gas distribution from the exhaust intake and urea injection. Excessive ammonia particles on the injection and isocyanic acid slips, on the other hand, might degrade the

catalyst quality in the SCR system. The goal should be to keep the amount of liquid within the catalyst as low as possible. This strategy might be performed by adjusting injection and temperature in the SCR system to generate perfect urea evaporation.

The optimal urea evaporation and mixture quality in the SCR system may be predicted by the pattern of ammonia homogeneity in the catalyst intake. Figure 4.10 depicts the ammonia mass fraction and multicomponent gas distribution on the catalyst intake. The distribution gas on the catalyst input is depicted in this diagram. The pressure and velocity numbers in this simulation, however, were far too low. As demonstrated in Figure 4.10, this reaction might be displayed at a low mass fraction value. The ammonia ratio revealed that the catalyst was underutilized. As a result, information on quantitative measurements of mixture quality must be provided. The examination of ammonia homogeneity in the catalyst inlet is detailed in the next section.

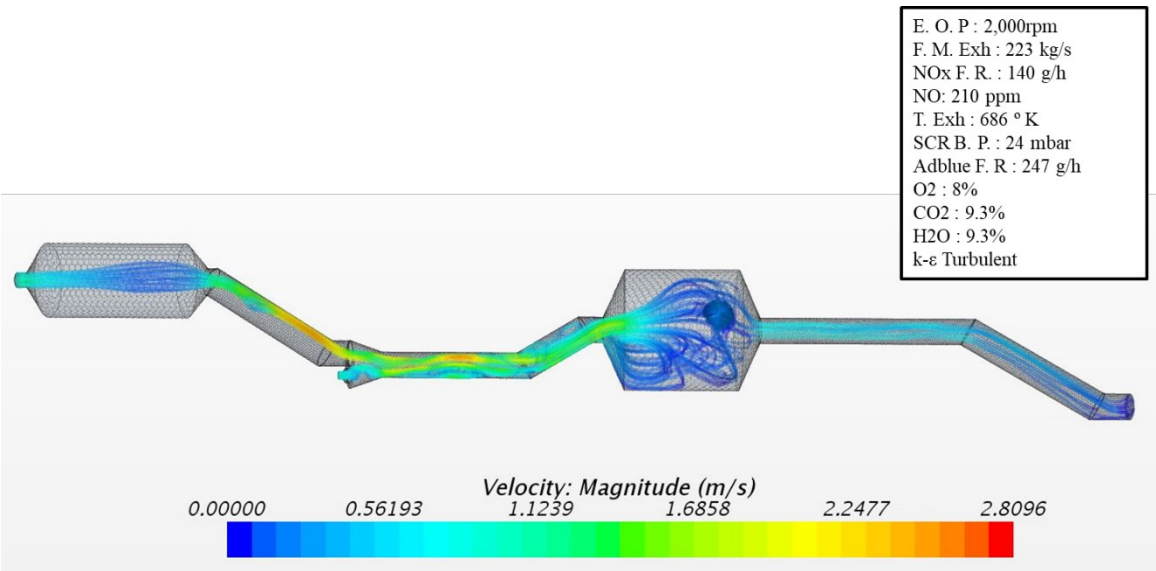

Figure 4.9: Distribution of urea and the exhaust gas phenomena in the simulation of the SCR system.

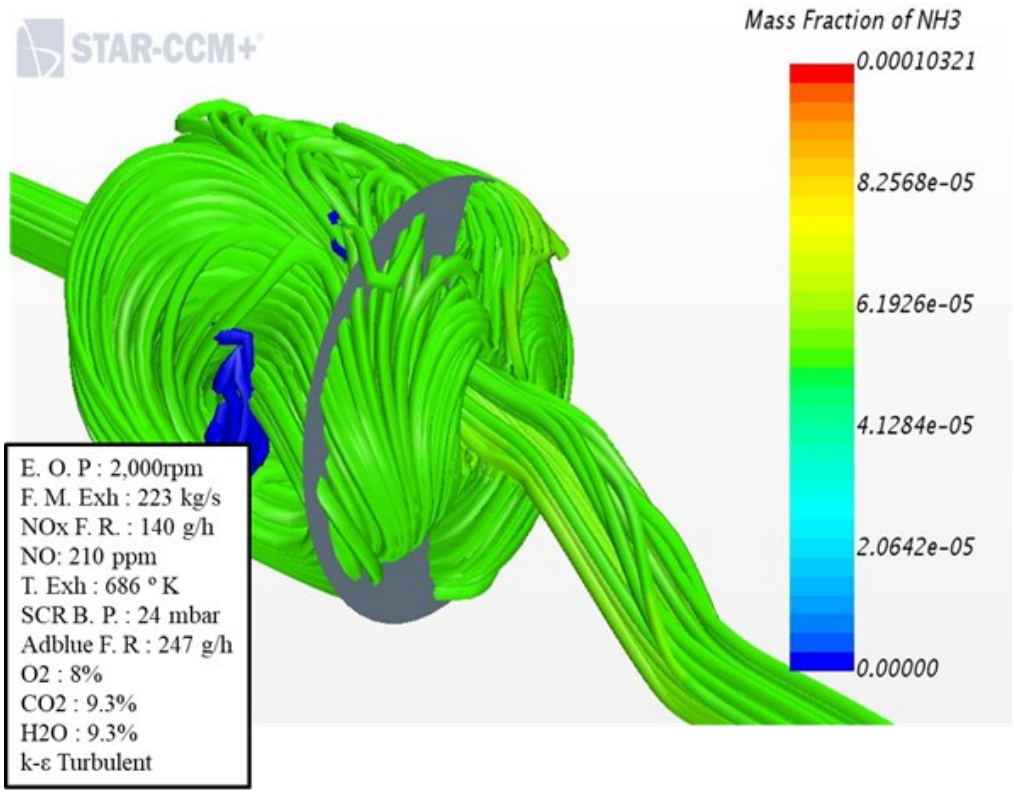

Figure 4.10: Distribution of mass fraction ammonia at the catalyst inlet.

4.6 Effect Injection Timing strategy to Ammonia uniformity

The study of ammonia uniformity is the parameter to predict the quality of urea evaporation process. Urea will evaporate and will generate become ammonia in the system. The distribution of ammonia will compute the quantity of ammonia in the catalyst surface. In order to get a uniform ammonia distribution at the SCR input face, the urea dosed must be mixed uniformly with the exhaust gas stream in order to achieve a high NOx reduction efficiency in an SCR system. The mixing uniformity problem must be solved throughout a large and continually variable range of exhaust flow rate and temperature, resulting in variability in injected urea spray dispersion and interaction with mixing devices. This links the effectiveness of the catalyst to the degree of ammonia homogeneity. As a result of the inadequate ammonia distribution, the SCR system will be more prone to urea consumption, NOx reduction, and NH3 production. Since SCR technology is widely used in light duty cars, the consistency of ammonia entering the SCR reactor has become even more crucial. This vehicle normally has a close-coupled aftertreatment system, which means there's less volume and time to mix in the ammonia.

A high-density grid of measurement spots at the SCR outlet was used in the approach provided below to maximize the accuracy of the ammonia dispersion evaluation at the SCR front face. A special test stand with an autonomously operated gas sampling probe was designed to enable for efficient and flexible testing of various SCR system configurations. The test technique was developed to assist Euro 6 emission-compliant SCR applications that require a NOx conversion efficiency of over 95% while also requiring low ammonia slip and UWS usage. The goal is to calculate the ammonia distribution at the SCR front face with precision. The real measurement is impossible at this place since a sample probe cannot be inserted into such a small space. The homogeneity level of NH3 and NOx on both sides of the reactor is the same if the exhaust gas flows linearly throughout the SCR brick. As a result, it was determined to monitor the amounts of gaseous chemicals at the SCR rear face. The moving probe may reach this site, and the findings are post-processed to compute ammonia dispersion at the SCR reactor front face.

The ammonia distribution over the exhaust pipe or the catalyst cross-section is often described using a uniformity index (UI). It's based on a formula that takes into account local and mean NH3 concentrations in relation to the catalyst surface. For light-duty and heavy-duty applications, well-optimized Euro 6/VI mixing systems may reach UI values greater than 0.98. System performance can be hampered by improper mixing element integration, which can lead to urea deposit development difficulties. The priority of three major SCR catalyst chemical processes is determined by the NO_2/NO_x ratio. The following is the typical reaction, which solely decreases NO:

$$\mathbf{NH_3 + NO + \frac{1}{4}O_2 \rightarrow N_2 + \frac{3}{2}H_2O} \qquad (4)$$

At this temperature, the urea generated is unstable and decomposes further into HNCO and NH3. Isocyanic acid production continues to rise as the temperature rises. As a result of the interaction between water vapor and HNCO, CO_2 is produced as well. Koebel and Strutz [27] describe in the temperature range of 150 to 500°C, the thermal and hydrolytic degradation of urea was characterized. They discovered that when urea is heated rapidly, it decomposes mostly into ammonia and isocyanic acid..

$$\boldsymbol{NH_2 - CO - NH_2 \rightarrow HNCO + NH_3} \qquad (5)$$

The following process might hydrolyze isocyanic acid with water to create carbon dioxide and ammonia:

$$\boldsymbol{HNCO + H_2O \rightarrow CO_2 + NH_3} \qquad (6)$$

The quantities of ammonia and isocyanic acid supplied into the catalyst were found to be identical, and the quantity of Urea injected into the catalyst may also undergo a hydrolysis reaction with water to produce carbon dioxide and ammonia:

$$\boldsymbol{NH_2 - CO - NH_2 + H_2O \rightarrow 2NH_3 + CO_2} \quad (7)$$

The quantities of ammonia and isocyanic acid put into the catalyst were determined to be comparable, and the quantity of urea was detected under their experimental circumstances [27]. The UWS is sprayed in this paper with three holes forming a 7-degree angle in the spray. The evaporation of liquid water is slowed by an injector droplet connected to the wall. Each hole has a width of 120 micrometers, and the droplets produced by the injection have a smaller diameter, as indicated. The number of droplets varies according to the atomization and evaporation processes in the system, and the screen diameter is unrelated to the liquid mass. The UWS is characterized as a two-component liquid with an evaporative approach to water and urea in this work; fluid mass concentrations are set in each computational cell to reflect the liquid's mass distribution:

$$C_{liquid} = \sum m_{droplet} \Big/ V_{cell} \quad (8)$$

where $\sum m_{droplet}$ is the total mass of all droplets in a computational cell, and V_{cell} is the volume of this computational cell. A consistent distribution of liquids offers key parameters for the system's evaporation process. In monoliths, the evaporation of these droplets and urea degradation will continue, and excessive particles in the catalyst might limit de-NOx performance dramatically. [57]. Under some circumstances, the urea particles pouring into the catalyst intake can also prevent monoliths from entering. As a result, it's critical to optimize the injection to reduce the amount of fluid entering the catalyst. This study applies a previous study method [27,58] to evaluate the ammonia mixture's correct purity in the SCR system The mass-weighted value for each component is used to calculate the liquid characteristics:

$$\rho_p = \sum_i Y_i \rho_i \quad (9)$$

The density is computed by the volume weighted value of the densities of each component:

$$\emptyset_p = \sum_i X_i \emptyset_i \quad (10)$$

where ρ_p represents the liquid characteristics, Y_i represents the volume fraction of component *i* in the liquid mixture, and X_i represents the mass fraction of component *i* in the liquid mixture. $\emptyset_p$ as the temperature rises, the vapor pressure rises with it:

$$P_{sat} = A \exp\left(\frac{-\Delta H_{vap}}{R\,T}\right) \quad (11)$$

where P_{sat} is the saturation vapor pressure, ΔH_{vap} is the enthalpy of vaporization, T is the temperature, R is the gas constant (= 8.3145 J mol-1 K-1), and A is the vapor pressure constant. Because the water component of the liquid combination is released first via vaporization, the variable A is a constant value for water vapor pressure that is controlled by SCR temperature. The vapor pressure of an aqueous

solution of urea is controlled by the mole fraction of urea, hence the variable A is a constant value for the vapor pressure of an aqueous solution of urea. Vaporization is used to extract the H2O component from the liquid mixture. The current study employs Raoult's equation for multi-component mixture systems to forecast the UWS drop's water evaporation rate. [57]:

$$\frac{dm_p}{dt} = MW_{water} k_c \left(\frac{X_{water} P_{sat,water}}{R\ T_p} - C_{water,\infty} \right) \quad (12)$$

where MW_{water} is the mass transfer coefficient is k_c, the saturation vapor pressure of water on the droplet surface is $P_{sat,water}$, R is the universal gas constant, T_p is the droplet temperature, and $C_{water,\infty}$ is the molar concentration of water vapor in the ambient gas. The urea particle loses mass as a result of the urea thermolysis processes, which produce gas species such as ammonia, isocyanic acid, and carbon dioxide. The mass change rate is computed as

$$\frac{dm_p}{dt} = MW_i \sum_{r=1}^{N_R} R_{i,r} \quad (13)$$

where,

$$R_{i,r} = \left(V''_{i,r} - V'_{i,r}\right) \left(k_r \left[C_{j,r}\right]^{n'_{j,r}}\right) \quad (14)$$

where MW_i is the molecular weight of species *i*, $R_{i,r}$ is the molar rate of destruction of species *i* in reaction *r,* and N_R is the number of reactions. $V''_{i,r}$ and $V'_{i,r}$ are the stoichiometric coefficients for reactant i and product i in reaction r, respectively, $\left[C_{j,r}\right]^{n'_{j,r}}$ is the molar concentration of species i , $n'_{j,r}$ is the rate exponent for reactant i in reaction r , and k_r is the rate constant for reaction r, which can be computed by the Arrhenius rate equation as

$$k_r = AT^{\beta} \exp\left(\frac{E_A}{RT}\right) \quad (15)$$

where A is the pre-exponent factor, β is the temperature exponent, and E_A is the activation energy. The values for the pre-exponent factor and activation energy for equation (16) were 1.27-E4 kmol-J-m-K unit and 15540 kmol-J-m-K unit, respectively, while for Eq. (17), the same values were 6.13-E4 kmol-J-m-K unit and 20,980 kmol-J-m-K unit. Gas species such as ammonia, carbon dioxide, and isocyanic acid were produced from the decomposition reaction, while water vapor is generated by evaporation and dissipates by hydrolysis reactions. The changes of ammonia, carbon dioxide, and isocyanic acid by the reaction are accounted for by the source terms of the continuity and species transport equations:

$$\frac{\partial (\rho Y_i)}{\partial t} + \nabla (\rho \bar{v} Y_i) = -\nabla . J_i + S_i + R_i \quad (16)$$

and

$$\frac{\partial \rho}{\partial t} + \nabla (\rho \bar{v}) = S_m \quad (17)$$

where ρ is the gas density, Y_i is the mass fraction of species i in the gas phase, $\bar{v}$ is the gas velocity vector, J_i is the diffusion flux of species I, R_i and S_i are the source terms of the rate of production of species i by evaporation and chemical reaction, respectively, and S_m is the total mass addition to the gas phase from reactions and evaporation

The ammonia mole fraction and ammonia mass flux distributions at the catalyst were used to calculate the uniformity index. The pattern of ammonia mass flux might be used to calculate the uniformity index, which may be used to assess the system's NOx reduction efficiency and catalyst use. A uniformity index of 1 implies that the system's mixture is perfectly uniform. Other scalars, such as HNCO and temperature, might be used to define the homogeneity index. In this simulation, we employed four forms of ammonia homogeneity to characterize it. An underused mixer fan and unpredictable urea injection circumstances were the first. The second factor was an underutilized mixer fan and consistent urea injection temperatures. The third experiment employed a mixer fan and urea injection circumstances that were unstable. The most recent experiment employed a mixer fan and constant urea infusion settings. Table 4.1 lists the four categories employed in this investigation.

Table 4.1. Types of studies used to describe the ammonia uniformity.

Type	The urea injection conditions	Mixer
1	Unstable	Without
2	Stable	Without
3	Unstable	With
4	Stable	With

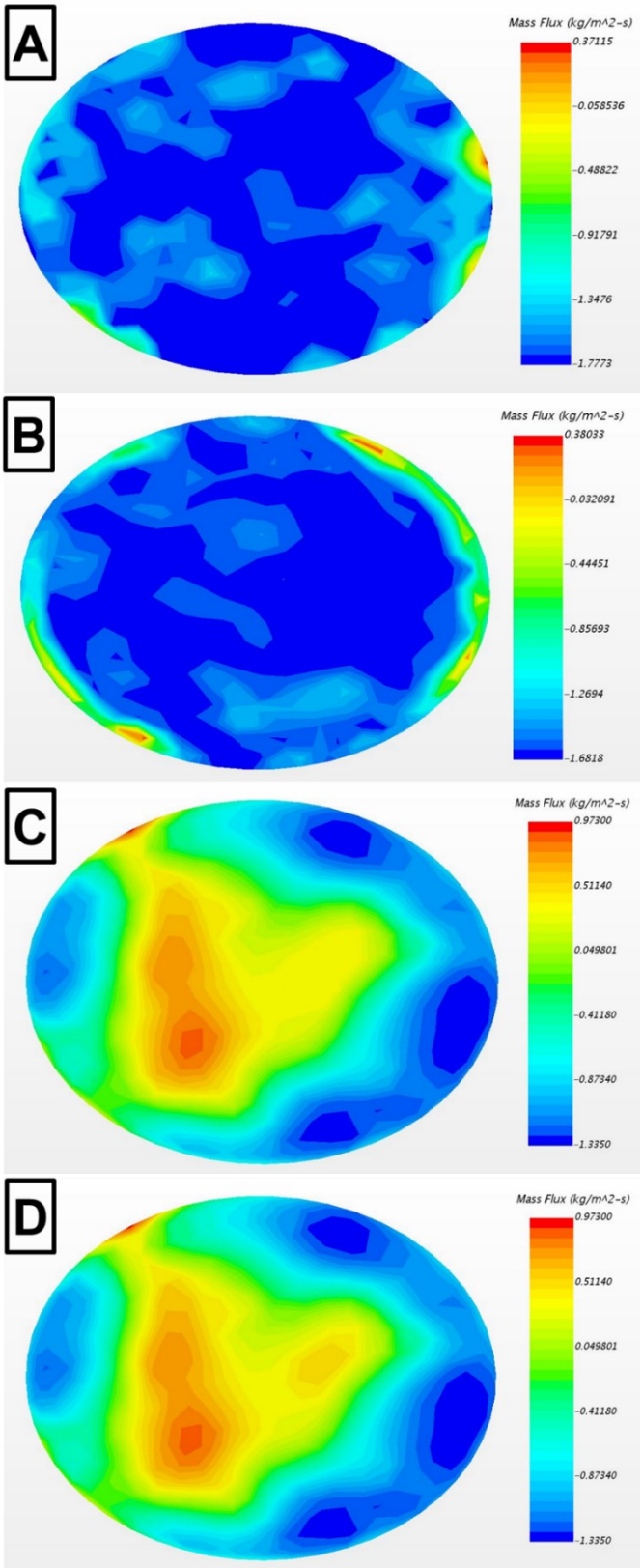

Figure 4.11: Ammonia uniformity pattern at the catalyst inlet: (a) Type I; (b) Type II; (c) Type III; (d) Type IV.

Figure 4.11 depicts the pattern of mass flux-based ammonia uniformity indices for the four examples. Type-I and type-II ammonia uniformity distributions on the catalyst input were low uniform, and the extremely lean mixture was practically dispersed throughout the catalyst. As a result, the ammonia gas ratio in the SCR system used the catalyst inefficiently. The ammonia was unable to reach the catalyst inlet, resulting in this reaction.

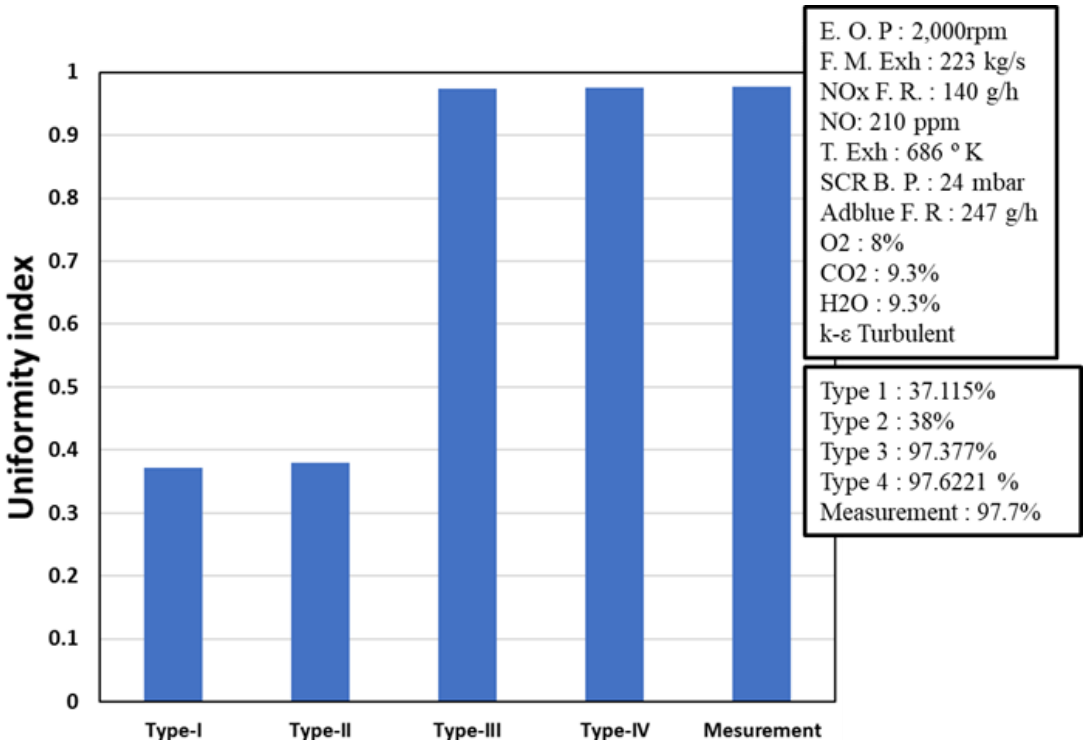

Figure 4.12: Ammonia uniformity index values at catalyst inlets Type I, Type II, Type III, Type IV, and from measurement.

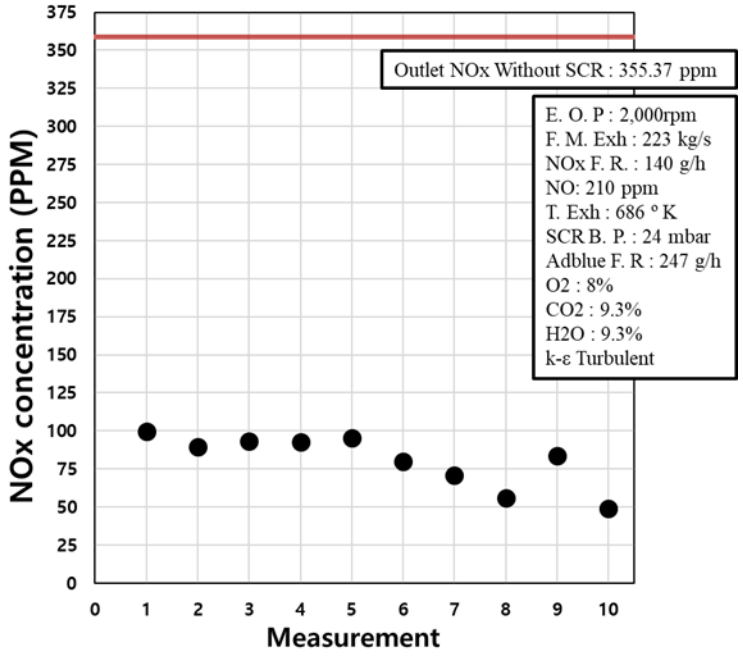

Figure 4.13: NOx concentration value in the outlet (after the SCR system).

Type-III and type-IV ammonia homogeneity on the catalyst input showed distinct patterns than type-I and type-II. The ammonia dispersion pattern had a high value of ammonia. Mixers were shown to increase mixture quality, allowing more ammonia to flow into the catalyst and lowering NOx in the SCR system. Figure 4.12 shows the validation and ammonia uniformity index values at the catalyst input. The values of ammonia uniformity at the catalyst input from the four scenario simulations and experiment are more clearly explained in the figure. The modeling and experiment findings for the ammonia uniformity index in type-IV were 97.62% and 97.7% , respectively. Dust or other particle concentrations had no effect on the process in the simulation. That is, the reaction was simply caused by the injection of urea and the qualities of the exhaust gas. However, in the experiment, those circumstances were difficult to achieve. Unknown quantities and temperatures were occasionally present in this process. As a consequence, even though the ammonia homogeneity was different from the experimental result, the simulation findings were plausible. This study used 10 consecutive time data gathered based on NOx conversion results in a diesel engine to explain the influence of urea injection timing on the quality of urea decomposition process. The experiment's 3000cc diesel engine was turned on for 20 seconds to produce the necessary flow and temperature for optimizing the urea breakdown process. When the flow and temperature were at their optimum, the urea waster solution was introduced into the system. The quantity of NOx concentration in the output catalyst with emission analyser will indicate the quality of the urea breakdown process (Horiba MEXA- 7100DEGR). Figure 4.13 displays the NOx levels in the output. The NOx concentration value without the SCR system is

indicated by the red line in this diagram, and the value obtained at 2,000 rpm engine speed was 355.37 ppm. In this diagram, the black dots represent 10 NOx concentrations after employing the SCR system. With the urea injection timing parameters optimized, the SCR system might cut NOx emissions from the diesel engine by up to 75%.

4.7 Summary

At 20 seconds after engine start-up, the study with optical access and a 3L diesel engine spinning at 2000rpm can create 223 kg/h of flow mass and 362°C of exhaust temperature, achieving the ideal conditions for urea injection. The ammonia uniformity value was investigated using four different designs based on 2,000 rpm engine speed settings. The stable situation occurred after a 20-second engine start-up, whereas the unstable situation was when the temperature in the system was ignored. The ammonia pattern in Type I and Type II was reasonably consistent, however the ammonia gas ratio in the SCR system exhibited low catalyst usage. Ammonia levels were high in Types III and IV. In type-IV, optimizing the urea injection schedule resulted in an ammonia uniformity value of 97.6%, which was similar to the experiment's ammonia uniformity value of 97.7%. However, the improving ammonia uniformity value can be found by the investigation of urea injection strategy in order to increase ammonia gas value and prevent the solid deposit formation in the next chapter.

Chapter 5

Effects of Urea Injection Strategy on Solid Deposit Phenomenon

This chapter describes the investigation of solid deposit formation in the SCR system by the super-hydrophobic surface. This chapter can inform the urea injection phenomenon in low and high wall temperature condition, ammonia evaporation process and solid deposit effected to improving NOx conversion efficiency value in SCR system.

5.1 Urea Injection Phenomenon in Low Wall Temperature (313K)

The comparison of experimental and simulated UWS spray wall impingement is shown in Figure 5.1. In terms of urea dispersion and solid deposit development, droplet spray impingement is critical. The critical criteria in forecasting droplet impingement behavior are droplet velocity, spray injection angle, and wall surface temperature. Figure 5.2 shows the numerical and experimental UWS spray production after impinging on a heated wall at a temperature of 313 K. Spray photos are shown here at times ranging from 4 ms to 12 ms, with a 2 ms time gap.

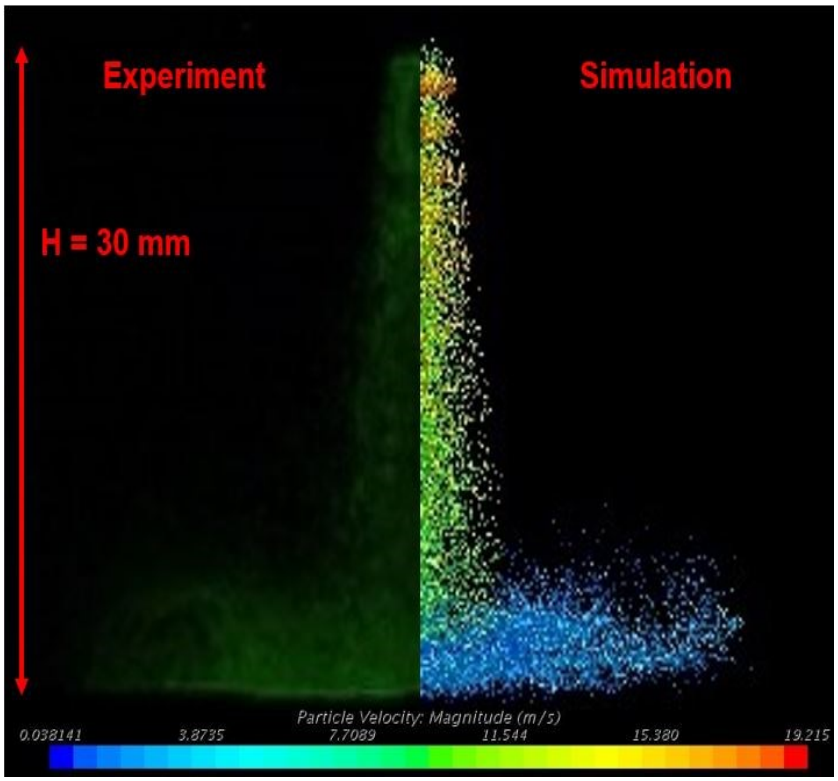

Figure 5.1: Comparison of experimental and simulated UWS spray wall impingement

The injection angle is 90º and the injection height is 30 mm from the heated wall. The velocities of the droplets in the numerical pictures are used to color images. The axial and radial propagation of the spray front in the spray impinging process can indirectly expose the droplet atomization rate after impinging on the hot surface, thereby presenting the contact surface between SCR reductant and exhaust gas, as seen in the spray pictures. The extensive propagation following impingement produces increased wall wetting, which leads to the production of a wall film, which acts as a prelude to the creation of solid deposits. The acting wall temperature (313 K) is substantially lower than the temperature at which urea decomposes, and the UWS spray cools the impingement region locally, As a result of the impingement, urea-SCR reductant droplets cling to the wall surface, and urea crystallization occurs following water evaporation, as shown in the picture. Figure 5.3 shows a closer look at the axial and radial distance measurements of UWS spray after impinging on the heated wall. The graph clearly shows that both values are substantially higher, and the numerical forecast matches the experimental measurement.

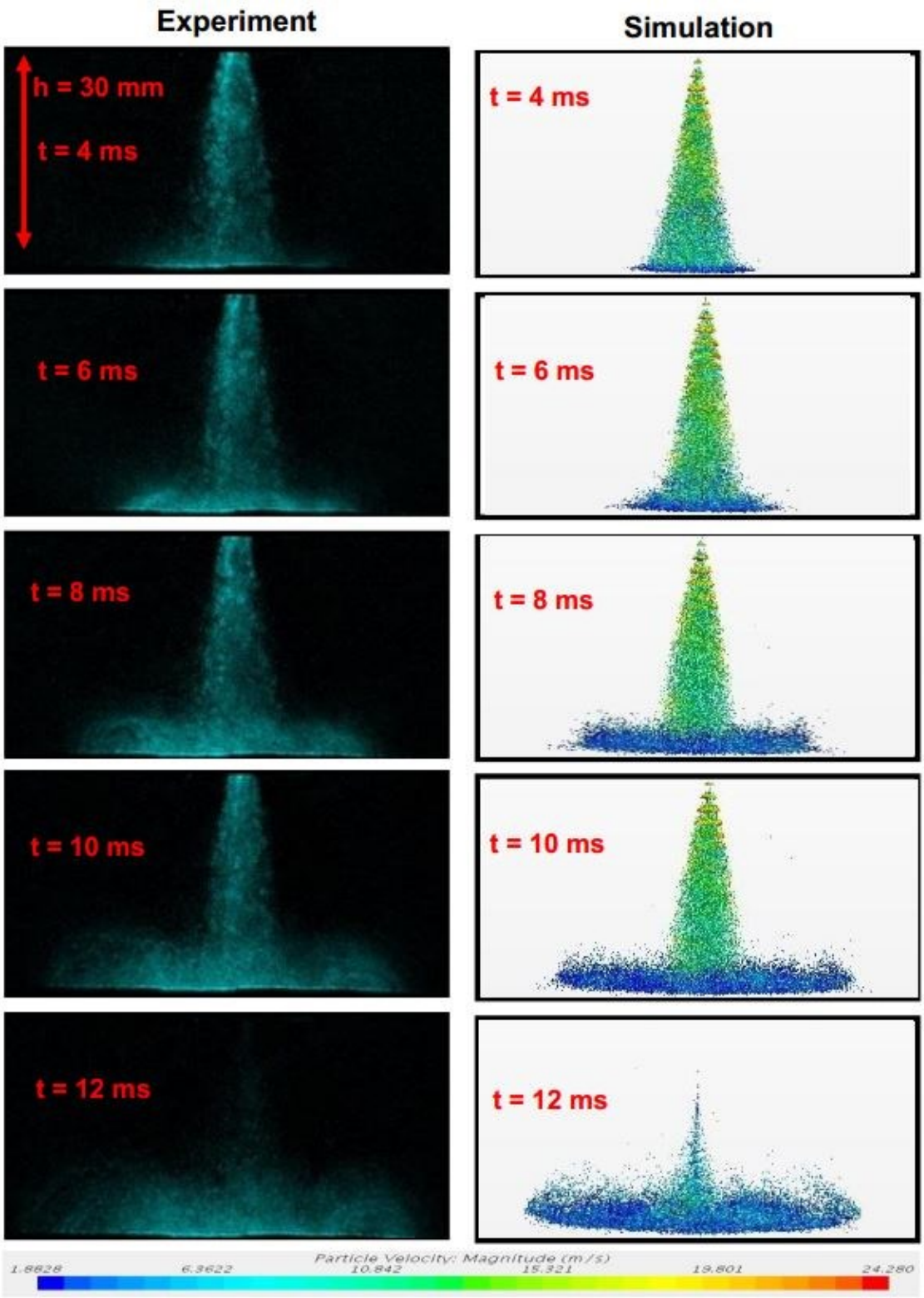

Figure 5.2: UWS spray development after impinging on the heated wall, at Tw = 313 K

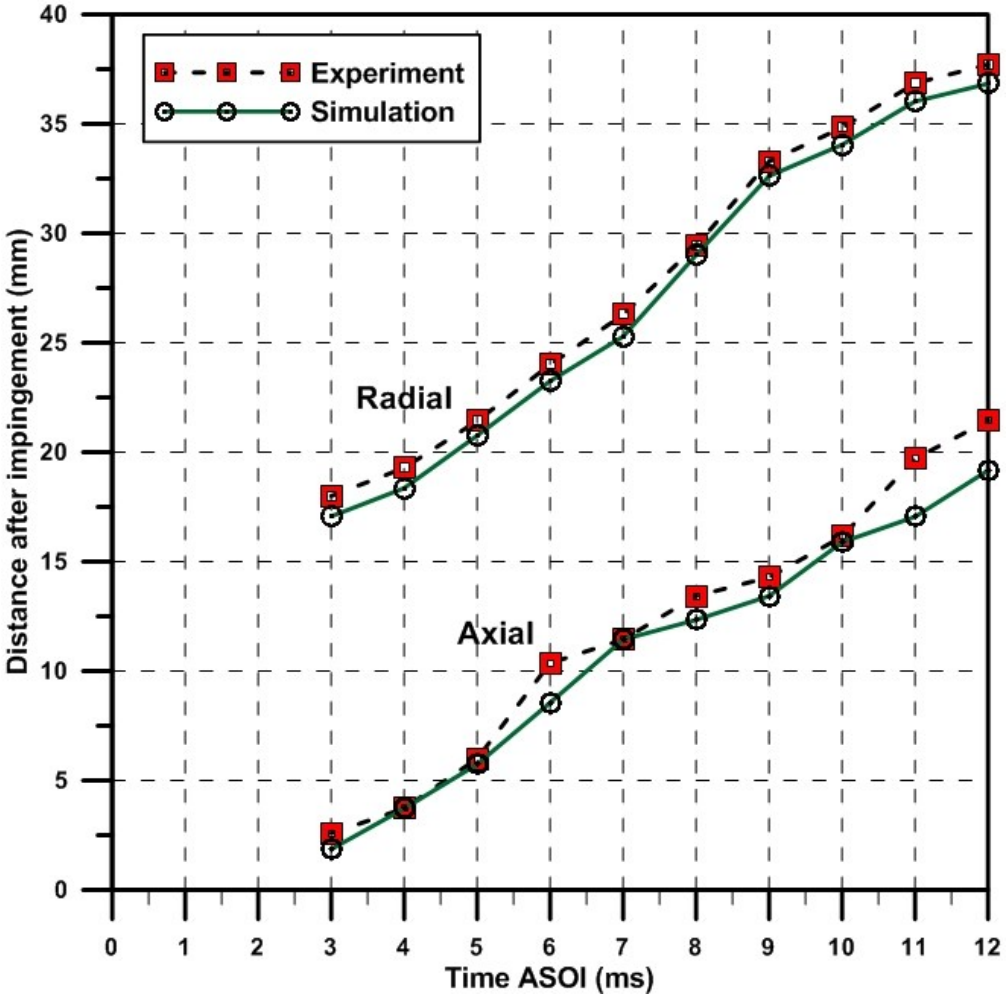

Figure 5.3: Comparison between the experimental and simulation measurement of axial and radial distance after impingement, at Tw = 313 K.

5.2 Urea Injection Phenomenon in High Wall Temperature (573K)

Figure 5.4. shows a wall temperature of 573 K, the spray impingement phenomenon after impinging on it. Images of spray events are shown here for the time range 4 ms to 12 ms, with a 2 ms gap. The injection angle is 90o and the injection height is 30 mm from the heated wall. The momentum of impinged spray droplets is considered to shift into three components during the droplet spray impingement event. These include momentum associated with secondary droplets generated following impingement, momentum related with spray front movement along the impingement surface, and momentum loss due to rebounding and thermal disintegration. The spray wall contact behavior is governed by wall temperature and droplet Weber number, and impinging droplet rebound and thermal breakage occur as a result of these variables. It is obvious from an examination of droplet rebounding and thermal breakage on a hot surface impingement that the rebounding phenomenon is beneficial for

the evaporation and mixing of SCR reductant with exhaust gas within the pipe. Rebounding droplets flow in the opposite direction of the exhaust pipe wall, giving SCR reductants more time to mix and evaporate, speeding up the synthesis of active chemicals. Figure shows a comparison of simulated and experimental UWS spray visibility for 573 K wall temperature and various time intervals after injection start. The impingement is better for homogeneous mixing and thermolysis of SCR reductant when the wall surface temperature is high enough, as shown in figure 5.4. Due to UWS spray impingement, a significant volume of gas is created at high wall temperatures (> 453 K) [59]. Because the rate of heat transmission from the wall to the droplets is particularly high at high temperatures, droplet evaporation increases dramatically. Urea also degraded into NH_3 and HNCO at high wall temperatures. Curls and bouncing in the spray are caused by evaporated droplets and these gases lifting and compressing the spray droplets. The majority of the droplets impact on and mix with the vapor phase droplets and gases when the next spray injection occurs. As a result, the quantity of droplets impinging on the wall decreases dramatically with continuous injection, and wall wetness decreases. As a result, measurements of the axial and radial distance of UWS spray after impinging on the heated wall are shown in figure 5.5. Due to the high temperature, droplet evaporation is accelerated, and both axial and radial distances for rebounding droplets decrease, which is good for mixing SCR reductant with exhaust gas.

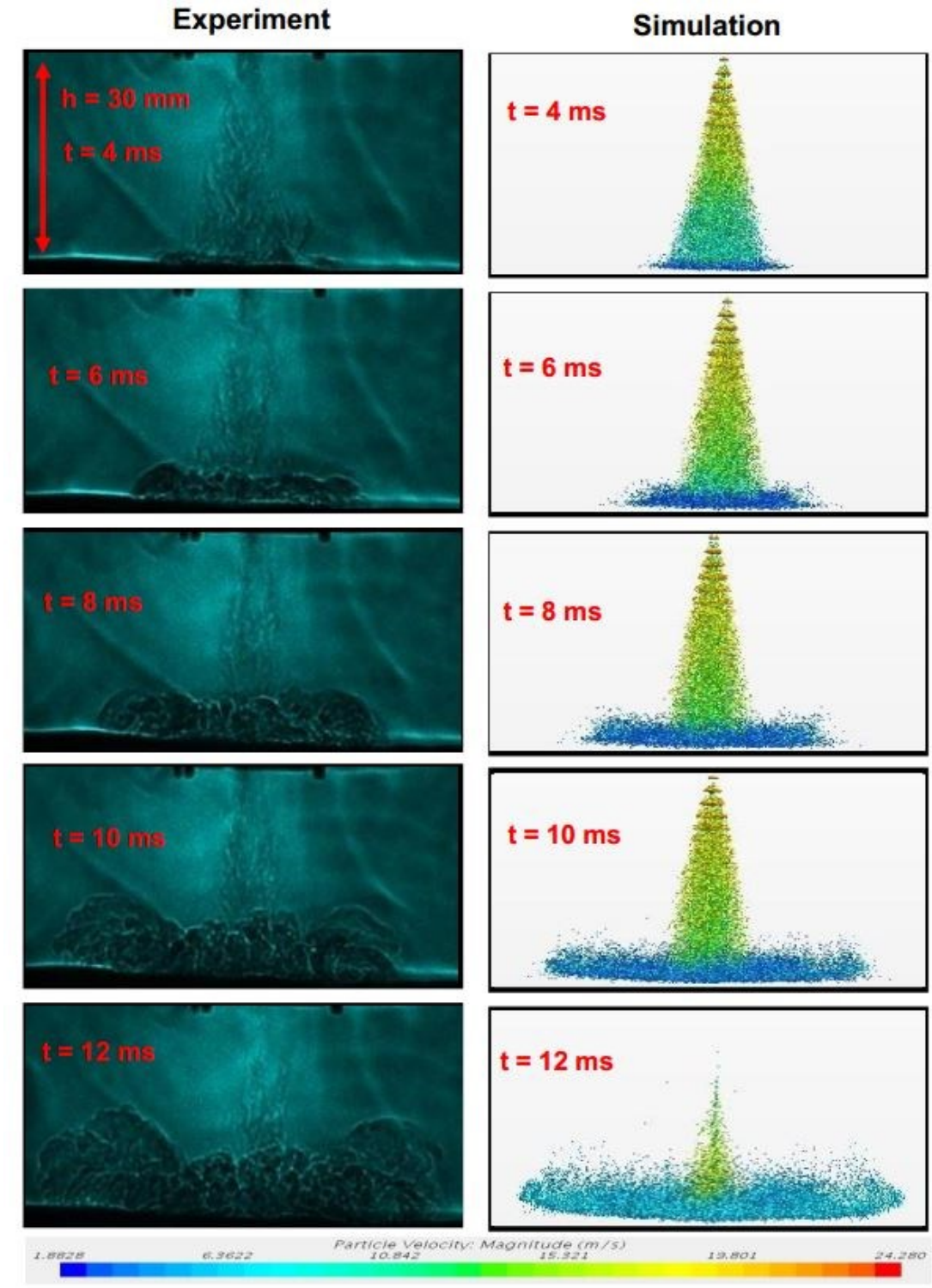

Figure 5.4: UWS spray development after impinging on the heated wall, at Tw = 573 K

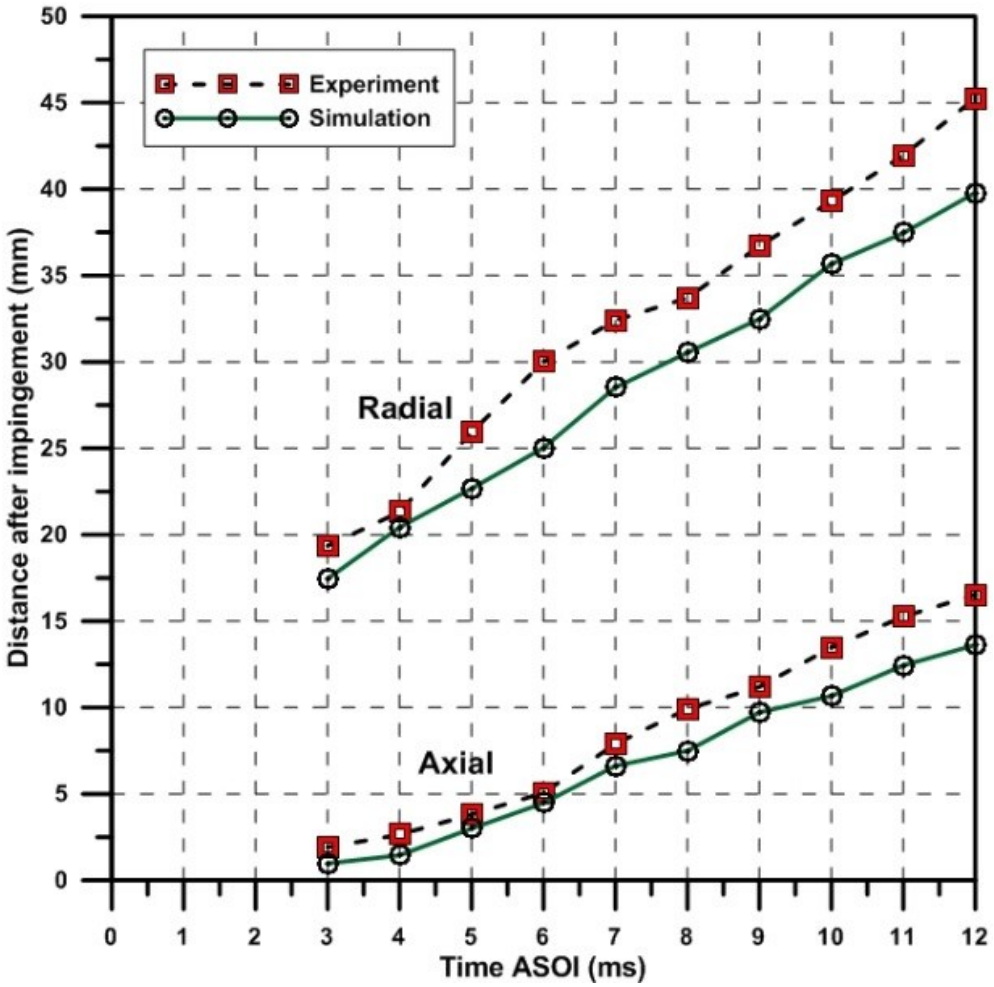

Figure 5.5: Comparison between the experimental and simulation measurement of axial and radial distance after impingement, at Tw = 573 K.

5.3 Solid Deposit Formation

When the last injection occurs, water begins to evaporate from the wall film, revealing the first footprint of solid urea, and urea begins to crystalize from the urea enriched wall film, as seen in figure 5.6. (a). Figure 5.6 depicts the greatest quantity of solid deposit generated for the injection event at 12 sec (b). After then, solid deposits begin to melt owing to the heated plate's temperature recovery, since there is no longer any spray impingement and no longer any local cooling. Figure 5.6 demonstrates how the deposits practically vanish after 40 sec (d). One thing to note is that the rate of solid deposit creation is significantly larger than the rate of deposit melting, and the melting process is greatly influenced by the plate's heat transmission rate, as shown in figure 5.7.

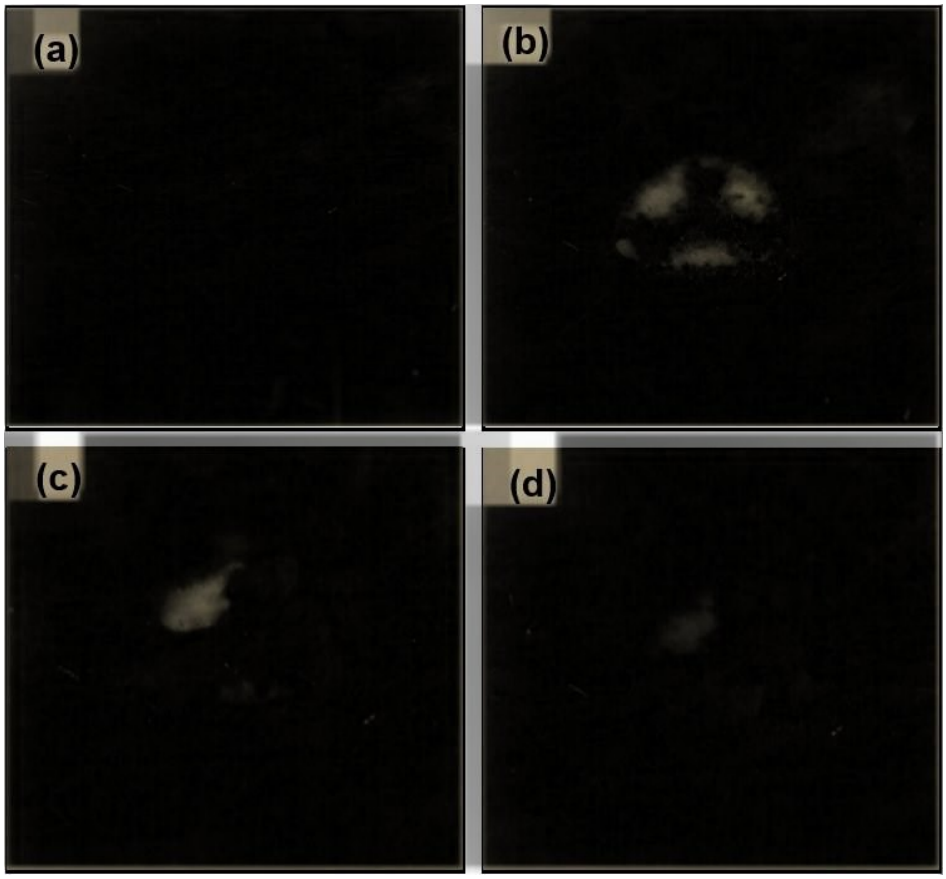

Figure 5.6: Solid deposit formation (a) AEOI, (b) AEOI + 12 s, (c) AEOI + 27 s, AEOI + 40 s

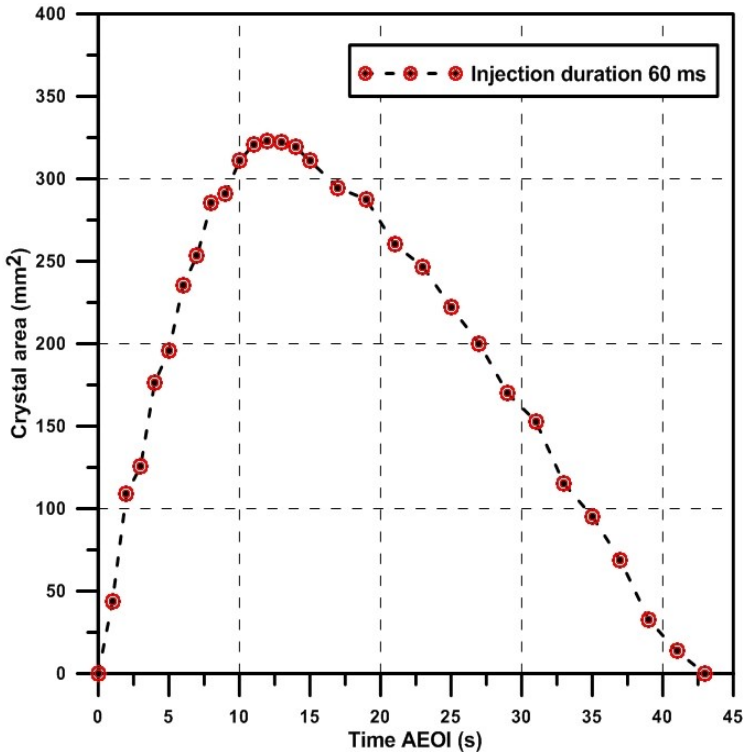

Figure 5.7: Evalution of solid deposit

5.3.1 Deposit Composition Analysis

Figure 5.8: Solid deposit formed on the injector tip during experiment

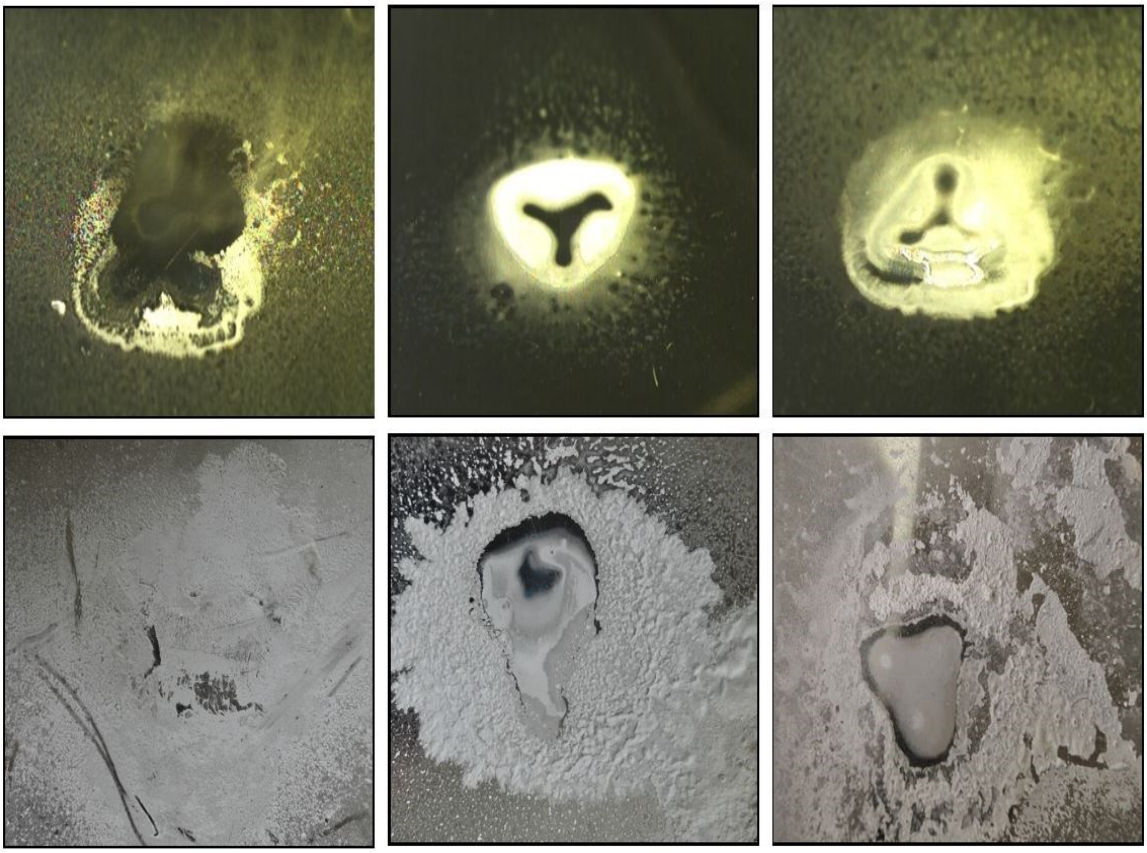

Figure 5.9: Solid deposit formed during the experiment at different conditions

5.3.2 Super-Hydrophobic surface to reduce solid deposit

Figure 5.10 is the urea solid deposit in plate without super-hydrophobic pattern. To showing this figure we do the experiment with flat plate without any pattern. That plate inserted at the bottom of urea injector. The injection angle was 90 degrees with 40mm of high between injector hole and plate wall. The urea will inject to the plate with 5 bar of injection pressure and 4.824kg/h of injection rate. Based on the experiment we found that solid deposit easily occurred in plate without super-hydrophobic pattern. That reaction happens because the urea difficult to break-up after hit the plate and easily to attach. The attached urea will transform become solid after heating by the ceramic heater. The urea water solution has composition of 40% of urea and 60% of water. After UWS got the temperature the water will be evaporate and urea will stick on the plate. That reaction happens in low or high temperature of the experiment. In figure 5.10 (a) shown the solid deposit in low temperature and figure 5.10 (b) shown the solid deposit in high temperature.

Figure 5.11 is the urea solid deposit in plate with super-hydrophobic pattern. To showing this figure we do the experiment with aluminum plate with micro pattern. That pattern produces the super-hydrophobic reaction in the plate and that plate was inserted at the bottom of urea injector. The injection angle was 90 degrees with 40mm of high between injector hole and plate wall. The urea will inject to the plate with 5 bar of injection pressure and 4.824kg/h of injection rate. The sample of plate was heated with ceramic heater to get the varies of temperature in the experiment. In this case we used low temperature and high temperature figure to identify the solid deposit formation in urea.

Based on the experiment we found that solid deposit reduces significantly if we compare with the plate without super-hydrophobic pattern. That reaction happens because the urea easy to break-up after hit the plate and difficult to attach in the material. The urea break-up produces smaller size of urea particle. That particle easily to evaporate and produce high quality of ammonia in the system. Even though urea water solution has composition of 40% of urea and 60% of water. The smaller particle UWS droplet can effected easily after getting temperature from the plate. That reaction also happens in low or high temperature of the experiment. In figure 5.10 (a) shown the solid deposit in low temperature and figure 5.10 (b) shown the solid deposit in high temperature. Based on that result, the quality ammonia generation process significantly improves with the super-hydrophobic surface. The quantity of urea solid deposit also reduces significantly in the system. And finally, the performance of SCR system will improve and can adopt to multiple varies of diesel engine. That result also can assist the automotive industry to achieve the world emission standard from their diesel engine.

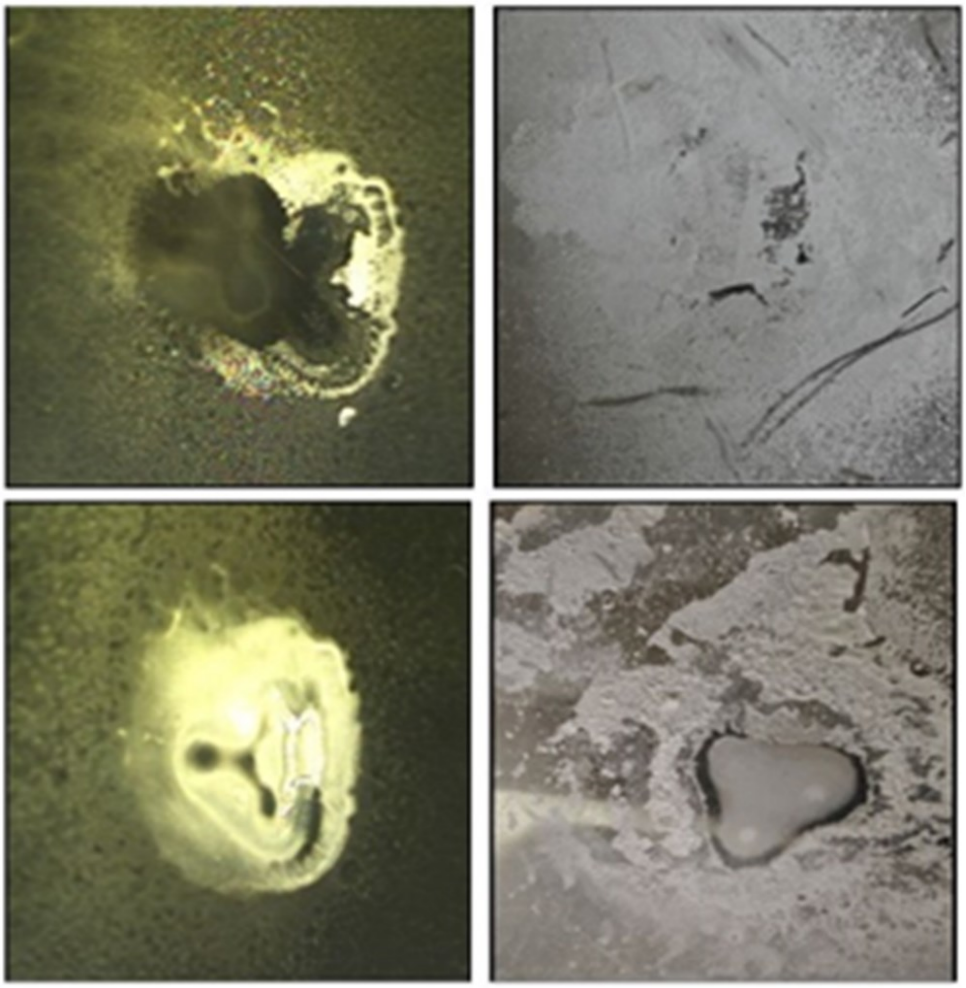

Figure 5.10: Urea solid deposit in plate without super-hydrophobic pattern

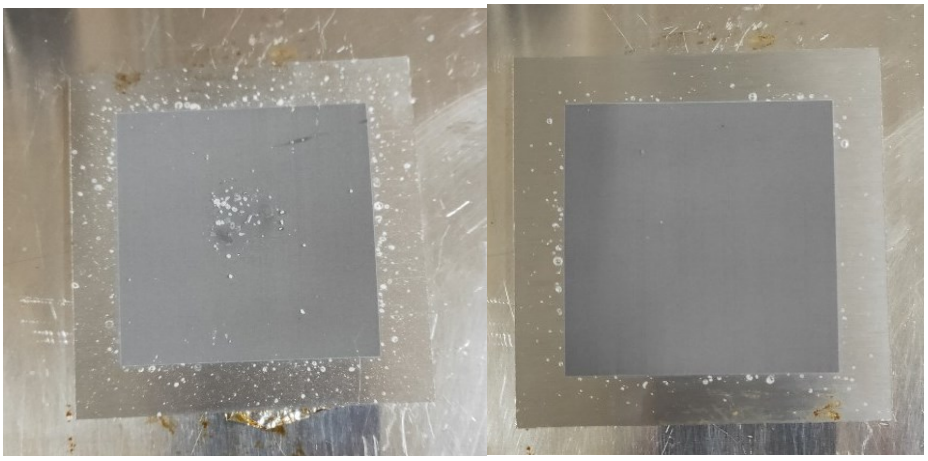

Figure 5.11: Urea solid deposit in plate with super-hydrophobic pattern

5.4 Summary

The investigation of urea injection phenomenon in low and high wall temperature condition, ammonia evaporation process and super-hydrophobic surface in order to prevent the solid deposit formation in the SCR system was described in this study. The experimental and computational results for UWS spray in low and high wall impingement reveal that droplet spray impingement has a significant influence in urea dispersion and solid deposit development. The critical criteria in forecasting droplet impingement behavior are droplet velocity, spray injection angle, and wall surface temperature. Because the low wall temperature (313 K) is below the criterion for urea breakdown, urea-SCR reductant droplets cling to the wall surface after impingement, and urea crystallization occurs after water evaporation. Impingement is preferable for homogeneous mixing and thermolysis of SCR reductant when the wall surface temperature is high; and ammonia gas is easily created at high wall temperatures (> 453 K). Because the rate of heat transmission from the wall to the droplets is particularly high at high temperatures, droplet evaporation increases dramatically. The improvement for urea droplet evaporation also can found by adding the super-hydrophobic surface. Based on the experiment, urea particle is easy to break-up after hit the plate with super-hydrophobic pattern and difficult to attach in that material. The urea break-up can produce smaller size of urea particle and easily to evaporate; that particle can produce high quality of ammonia in the system. That result will be applied in the next chapter with 3L diesel engine to increase ammonia uniformity value in order to predict NOx conversion efficiency in SCR system.

Chapter 6

Ammonia Uniformity To Predict NOx Reduction Efficiency In 3L Diesel Engine SCR System

This chapter describes the investigation of ammonia uniformity value in 3L diesel engine to predict NOx conversion efficiency in SCR system. This chapter inform the distribution of gas value, the concentration of mass fraction and multi-component gas distribution, ammonia uniformity value and engine speed operation and mixer fan strategy in order to improve NOx conversion efficiency in SCR system.

6.1 The distribution of gas in SCR system

6.1.1 CFD for SCR system 3L Diesel Engine

The second CFD analysis used pipes with a winding form, which were based on the experimental configuration of a commercial BENZ ML350 SCR system. The UWS injector was installed on the pipe's side, and the UWS spray was discharged at a 15-degree angle to the main flow. The connection optical access and commercial SCR system 3L Diesel Engine (figure 6.1) were crucial in this study in order to promote urea decomposition and optimize ammonia homogenization in the system. The optical access can identify the system's gas temperature and flow distribution, which may then be used in a commercial SCR system. The quality of the urea breakdown process will increase, and solid deposits in the system will be avoided. For these CFD models, the injector hole diameters and pressure in were identical to the experiment configuration. This injector has three holes with a diameter of 120 micrometers for spraying urea into the system. To distribute urea into the system, each hole had a cone angle of 7° and could provide a urea mass flow rate of 8.05-E5 kg/s with a velocity magnitude of 24 m/s.

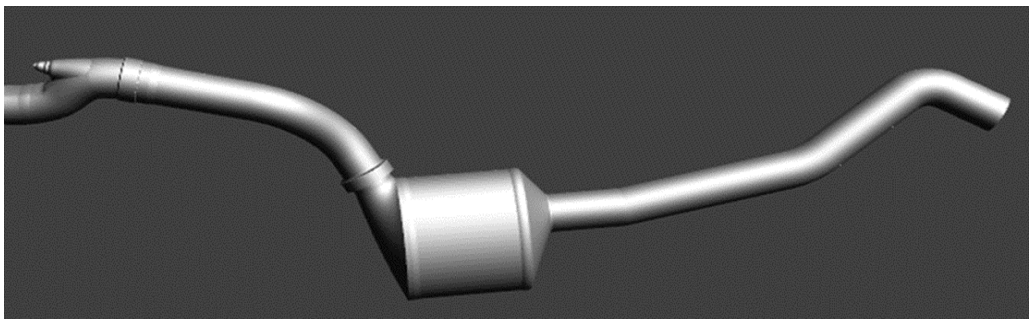

(a)

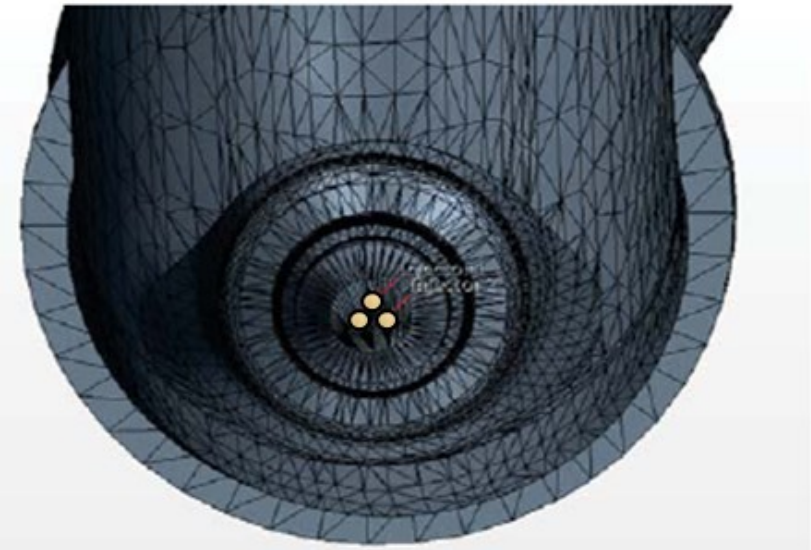

(b)

Figure 6.1 : The CFD of commercial SCR system 3L Diesel Engine

The optical access distribution of urea and exhaust gas phenomena were essential parameters for ammonia optimization. The optical access simulation can identify the best temperature and flow conditions for the urea injection process in the SCR system, which can then be verified using the thermal camera in the experiment setup. However, additional testing of this work in a commercial SCR system utilizing a genuine diesel engine is required. As a consequence, using simulation, the influence of optical access on the commercial SCR system was analyzed in this part. Figure 6.2 depicts the velocity distribution in the exhaust pipes. The magnitude of the exhaust velocity and the mass fractions of N_2, H_2O, CO_2, and O_2 color the particles. In the SCR system, blue symbolizes low velocity and red signifies high velocity. Following the screening process in the DPF catalyst, the exhaust velocity reduces. The amount of gas coming into the system is affected by this reaction. At this system, the highest velocity is 5.5 m/s in the exhaust inlet, which drops to 2 m/s after filtration.

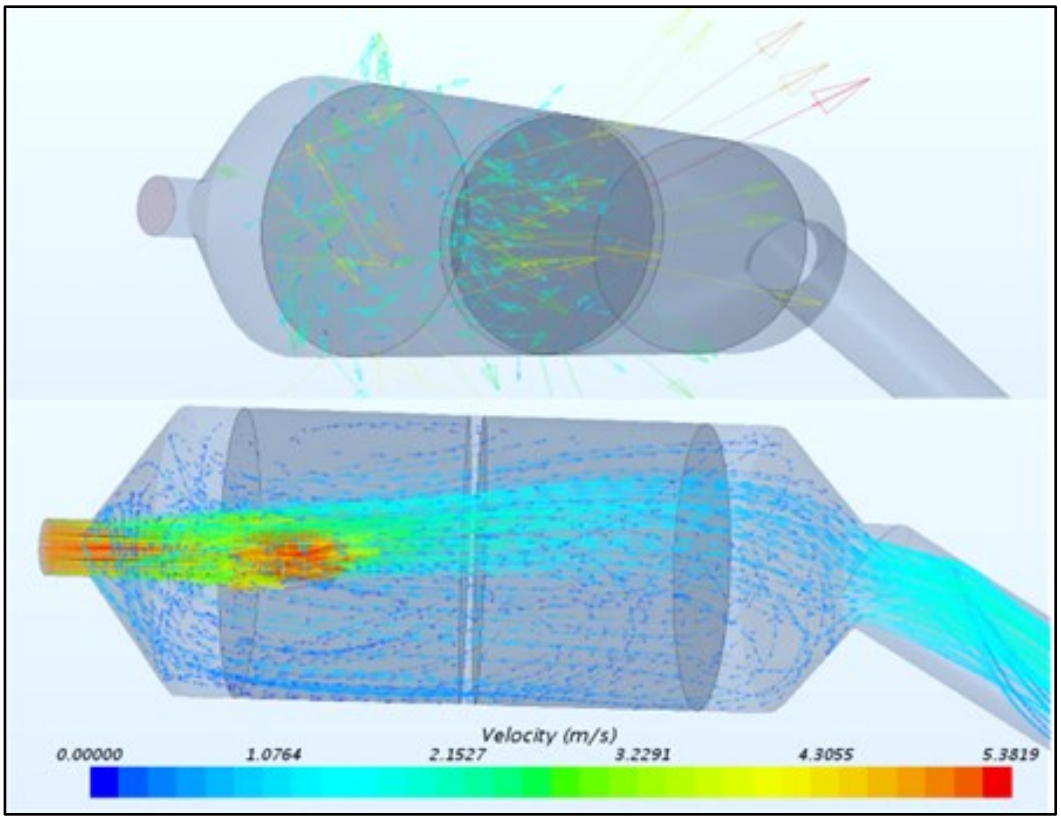

Figure 6.2: The velocity distribution in the DPF catalyst

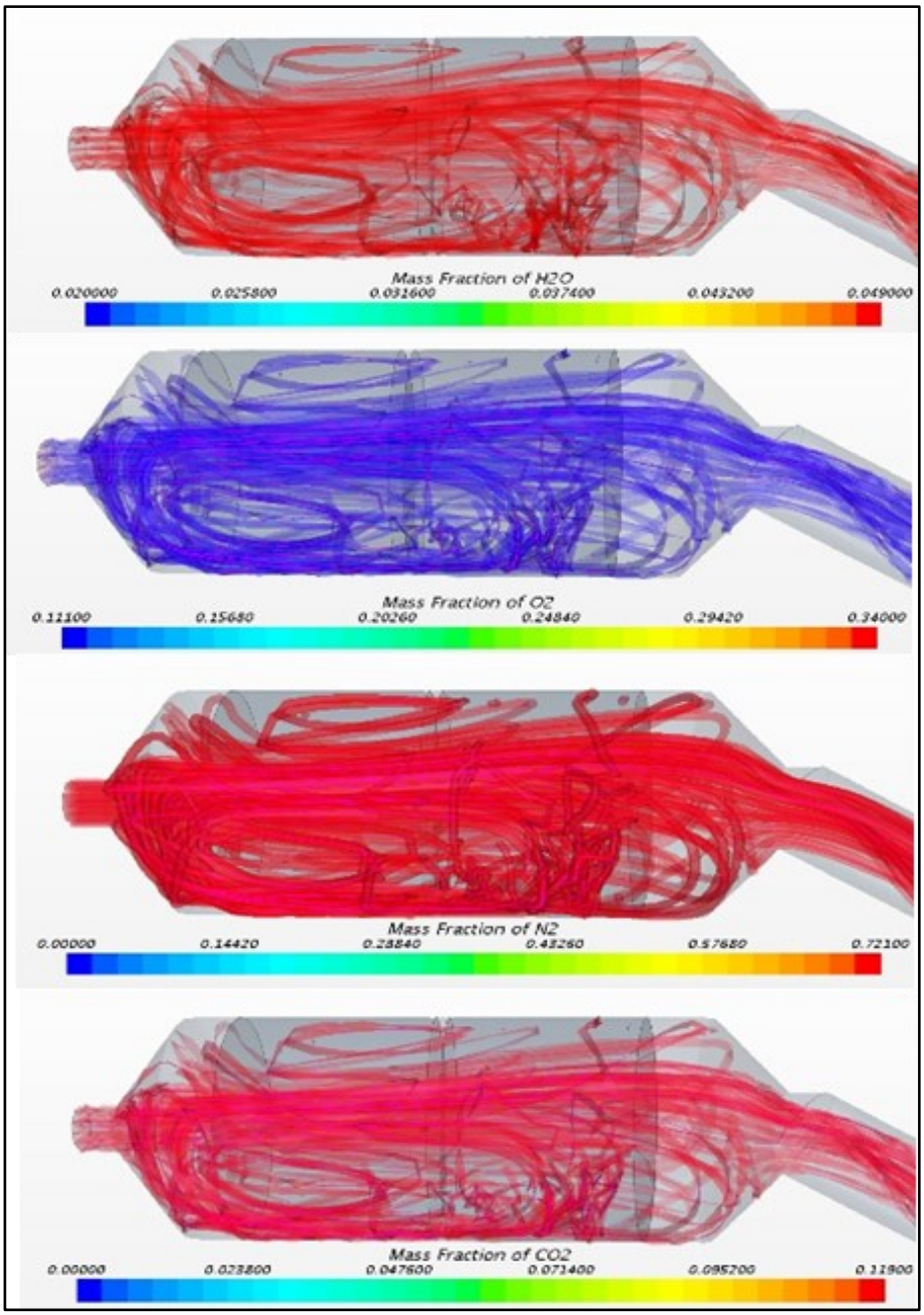

Figure 6.3: The mass fractions of N2, H2O, CO2, and O2 distribution in the DPF catalyst

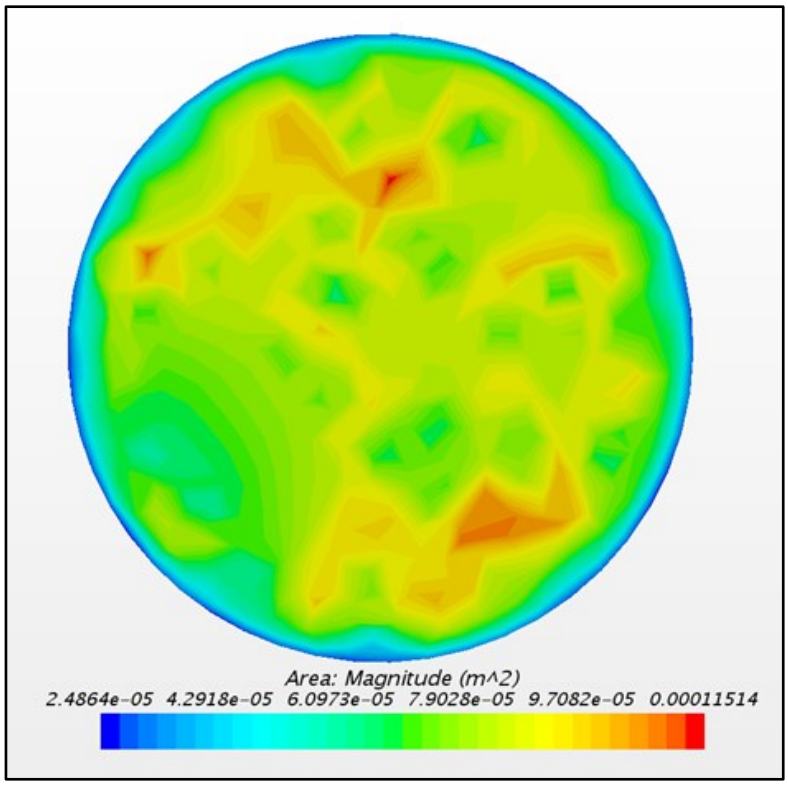

Figure 6.4: The mixing reaction of NH3 and multi-component gas in the pipe.

Figure 6.3 shows the mass fraction amounts of N_2, H_2O, CO_2, and O_2. In this system, the mass percentage of N_2 is larger than the other gases. However, following the screening process in the DPF catalyst, the amount of N_2 dropped. The mass fraction of N_2 from the exhaust line was 0.72 kg/kg, with a molecular weight of 28.1 kg/kmol, but the mass fraction of H_2O was lower than that of the other gases in this system. At the exhaust line, H_2O has a tiny mass fraction of 0.049 kg/kg and a molecular weight of 18 kg/kmol. The multi-component gas distribution was a critical requirement in the SCR system's design.

As previously stated, ammonia will persist in the monolith, and excessive particles in the catalyst might limit the de-NOx performance greatly. Under some conditions, the urea particles pouring into the catalyst intake can also prevent monoliths from entering. As a result, it was critical to reduce the amount of fluid entering the catalyst by improving injection time and pressure. Figure 6.4 depicts the NH_3 and gas combination reaction in the pipe, as shown by the amount of gas filling a certain region [60]. The reactivity of a gas mixture is measured in area (m^2). In the diagram, the blue color represents the least value, while the red color represents the highest value. The smallest value indicates that mixing NH_3 and other gases is difficult near the pipe wall, whilst the highest value indicates that mixing NH_3 and other gases becomes more difficult towards the center of the pipe. Without a mixer, the gas pressure in the pipe is relatively low, resulting in uneven response mixing. Because heat and mass transmission

are normally restricted by the surface area of the SCR wall, another crucial parameter to analyze is the multi-component gas flow from the exhaust pipe. As a result, it was necessary to reduce UWS deposition on the wall in order to improve the evaporation process.

6.2 The Concentration Mass Fraction and Multi-Component Gas Distribution

The ammonia homogeneity at the catalyst input was another significant criterion for maximizing NO_x reduction efficiency in the catalytic process, in addition to the multi-component gas distribution. This section will also cover ammonia distribution and multi-component gas distribution. The contour plot is perpendicular to the view angle downstream of the catalytic converter toward the intake, as shown in Figure 6.5. The velocity in m/s unit is used to measure NO_x dispersion. The distribution of ammonia mass flux into the catalyst may be measured using the NH_3 flow rate (Yi, 2007). The distribution of NH_3 to the catalyst was improved with higher velocity levels. The gas flow velocity was in the range of 0 to 0.0366 m/s, as shown in the diagram. This result showed that the flow rate of NH_3 and other gases is so low that the ammonia dispersion in the catalyst is very low. The NH_3 distribution is computed as follows:

$$\boldsymbol{m_i'' = \rho \gamma_i (V . n)}$$

where $\boldsymbol{m_i''}$ is the mass flux of species *i* that may represent NH_3, CO, CO_2, HCNO, etc.; ρ is the local density of the gas mixture; and $(\boldsymbol{\gamma_i})$ is the mass fraction of species *i*. *V* is the local velocity vector, and *n* is the unit normal vector of the post-processing plane.

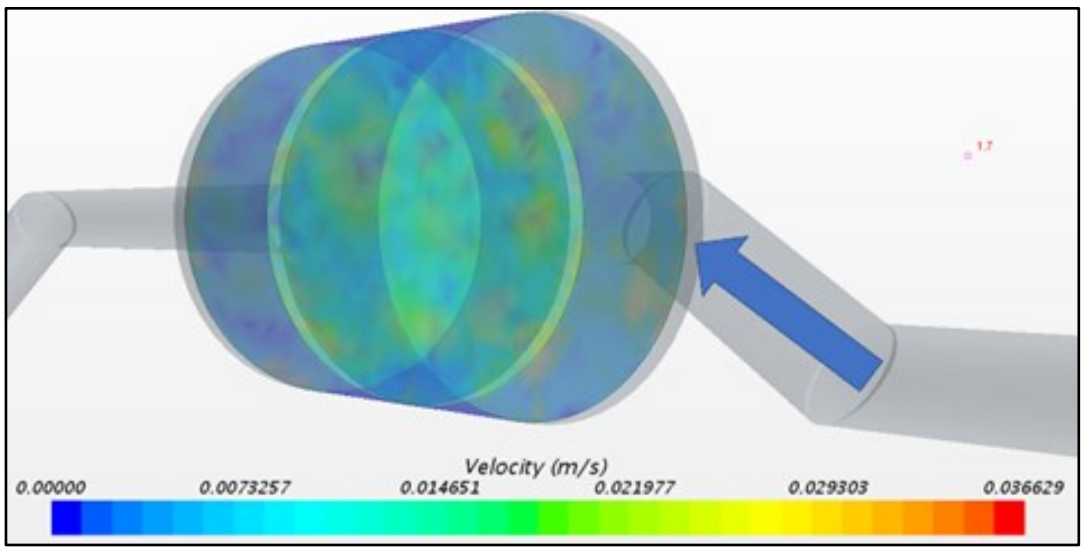

Figure 6.5: The post-processing plane and view angle of the NH_3-NO_x distribution

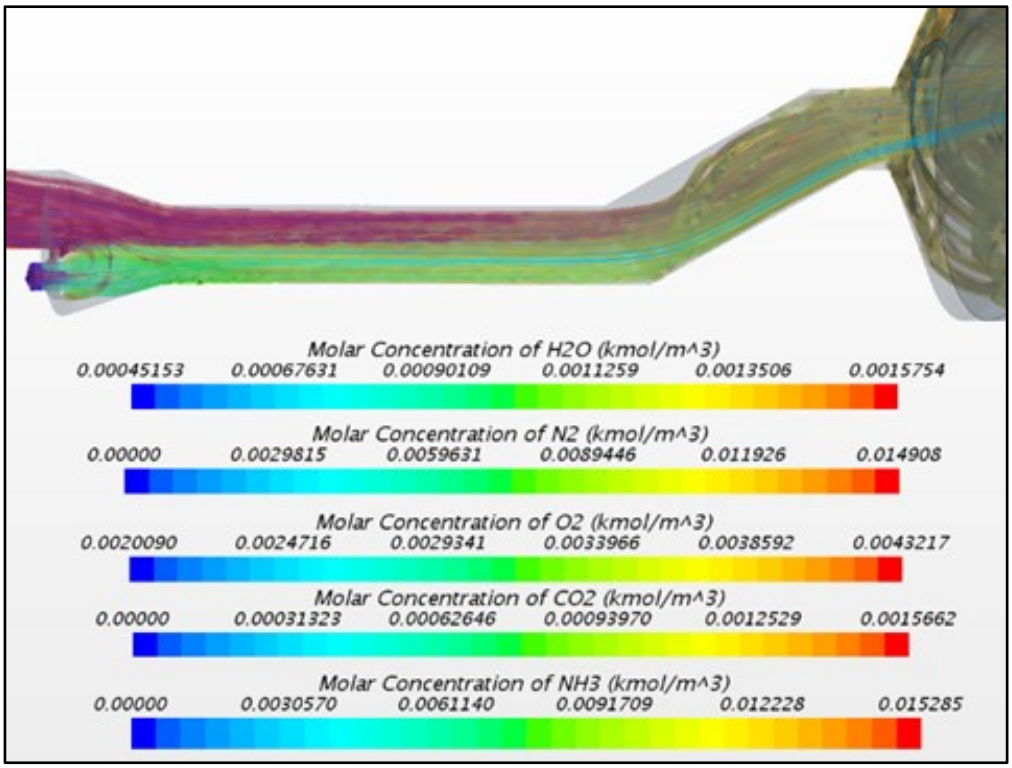

Figure 6.6: The gas distribution in the pipe

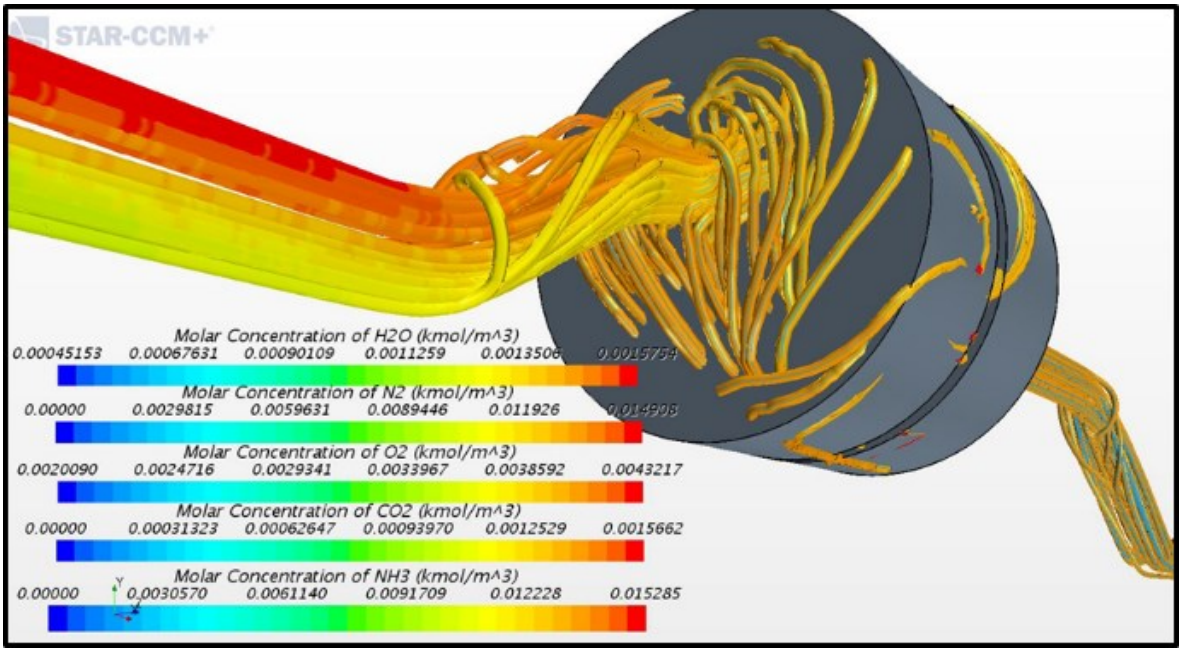

Figure 6.7 : The gas distribution in the pipe at the catalyst inlet

Figure 6.6 shows the ammonia mass fraction and multi-component gas distribution in the pipe. Figure 6.7 shows the ammonia mass fraction and multi-component gas distribution at the catalyst input.

The gas distribution from the pipe to the catalyst input is depicted in these diagrams. However, the pressure and velocity in this simulation result were determined to become too low; This reaction prevents ammonia and multi-component gas from spreading across the catalyst inlet. Only a small fraction of the catalyst is occupied by gas, which is present in varying proportions. While the overall distribution is quite consistent, the catalyst contains an exceedingly lean mixture. The high ammonia and isocyanic acid slips are caused by the NH_3 and multi-component gas ratio, which results in poor catalyst utilization, low NOx removal rate, and high ammonia and isocyanic acid slips. By examining the ammonia uniformity, information regarding quantitative measurement of mixture quality is introduced in the next part.

6.3 Ammonia Uniformity Investigation

The ammonia mole fraction and ammonia mass flux distributions at the catalyst were used to calculate the uniformity index. The pattern of ammonia mass flux might be used to calculate the uniformity index, which may be used to assess the system's NOx reduction efficiency and catalyst use:

$$\boldsymbol{\gamma_{mass\_flux} = 1 - \frac{\int_A (m''_{NH3} - \bar{m}''_{NH3}) dA}{2\bar{m}''_{NH3}}}$$

$$\boldsymbol{\gamma_{NH3\_NOx} = 1 - \frac{\int_A (r_{NH3\_NOx} - \bar{r}''_{NH3\_NOx}) dA}{2\bar{r}''_{NH3\_NOx} A}}$$

where m''_{NH3} is the local ammonia mass flux at a position on the plane, $\bar{m}''_{NH3}$ is the mean mass flux of ammonia of the plane, $\bar{r}''_{NH3\_NOx}$ and r_{NH3_NOx} are the mean NH_3-NOx ratio and the local NH_3-NOx ratio, respectively, and A is the surface area of the catalyst inlet. A uniformity index of 1 indicates that the combination is perfectly uniform. Other scalars, such as HNCO and temperature, might be used to define the homogeneity index. The distributions of uniformity indexes may also be explained as follows:

$$Ui = 1 - \sum_{i=1}^{n} \frac{|V_i - V_{avg}| A_i}{2.V_{avg}.A}$$

And

$$Ui = 1 - \frac{1}{2}\left[\sum_{i=1}^{n} \frac{A_i}{A_{total}} \frac{|NH_{3,i} - NH_{3,\ average}|}{NH_{3,\ average}}\right]$$

where $NH_{3,i}$ is the decomposition of urea velocity (m/s), and $NH_{3,\ average}$ is the average of the decomposition urea velocity in the system. The decomposition of urea velocity in the system is calculated as follows:

$$NH_{3,i} = C\ \left(2.\frac{delP}{\rho_{fluid}}\right)^{\frac{1}{2}} \qquad (25)$$

where $delP$ is the pressure that enters the catalyst (Pa), ρ is fluid density (Kg/m^3), and C is the molar concentration of water vapor in the ambient gas. The NOx reduction reaction and the NH_3 oxidation reaction are the two major processes in the SCR process. For most SCR catalysts, the bell shape of NO_x removal activity with respect to reaction temperature is prevalent. To represent the greatest conversion of NO_x and NH_3 slips, the intrinsic reaction kinetics for the SCR process must include both the NH_3 oxidation and the NO_x reduction reactions. [61]. The Eley-Rideal equation may be used to model the NH_3 oxidation process and determine the maximum conversion of NOx and NH_3 slips at different temperatures.:

$$-r_{NOx} = \frac{k_{NOx}\,K_{NH_3}\,C_{NOx}\,C_{NH_3}}{1+K_{NH_3}\,C_{NH_3}} - \frac{k_{NH_3}\,K_{NH_3}\,C_{NH_3}}{1+K_{NH_3}\,C_{NH_3}} \qquad (26)$$

$$-r_{NH_3} = \frac{k_{NOx}\,K_{NH_3}\,C_{NOx}\,C_{NH_3}}{1+K_{NH_3}\,C_{NH_3}} + \frac{k_{NH_3}\,K_{NH_3}\,C_{NH_3}}{1+K_{NH_3}\,C_{NH_3}} \qquad (27)$$

where $\boldsymbol{k_{NOx}}$ is a reaction rate constant of NOx reduction ($\boldsymbol{S^{-1}}$) , $\boldsymbol{k_{NH_3}}$ is a reaction rate constant of NH_3 oxidation (cm^3/(mol S), $\boldsymbol{K_{NH_3}}$ is an adsorption equilibrium constant for NH_3 (cm^3/mol), $\boldsymbol{C_{NH_3}}$is the concentration of NH_3 species (mol/cm^3), and $\boldsymbol{C_{NOx}}$ is the concentration of NOx species (mol/cm^3).

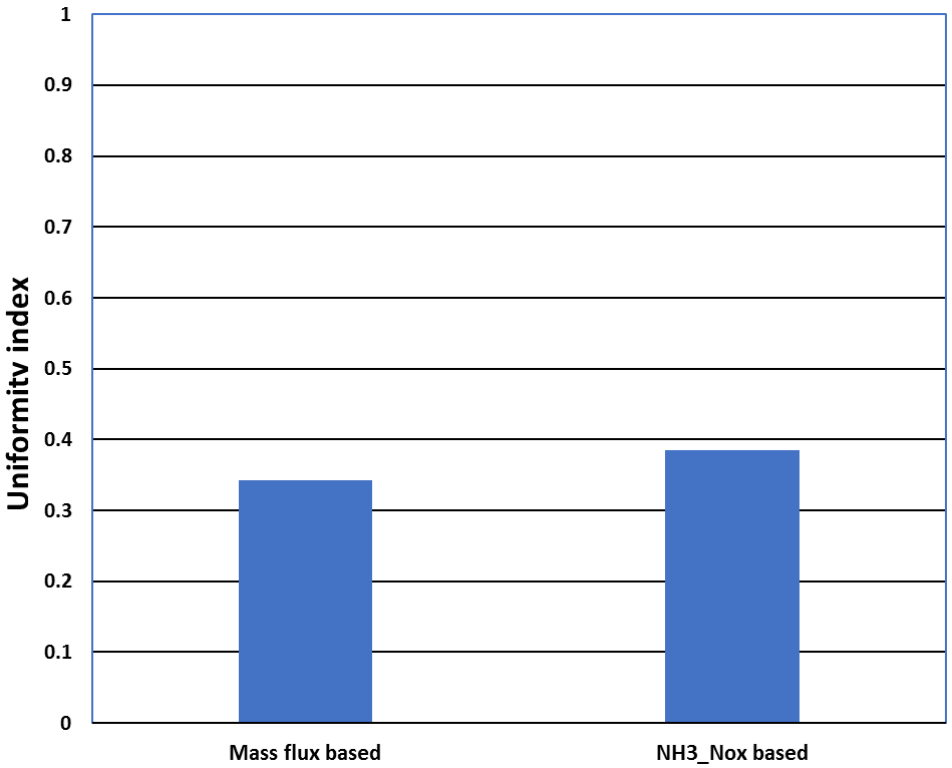

Figure 6.8: Ammonia uniformity at the catalyst entrance

As indicated in Figure 6.8, the uniformity index of ammonia mass flow on the catalyst inlet was calculated to be 0.342, whereas the uniformity index based on the NH3-NOx ratio was around 0.385. This figure suggests a non-uniform ammonia distribution, which will almost probably result in poor SCR performance.

6.4 Engine Speed and Fan Mixer Strategy

The injection pattern (defined by injector type, injection location, and direction), UWS atomization, evaporation, and breakdown all have a role in the homogeneity of the mixture. By modifying the injection settings, adjusting the exhaust flow pattern, and increasing turbulence, the mixture quality may be enhanced. The ammonia distribution homogeneity in the SCR system was calculated using a 1500 rpm operation condition in this investigation.

Table 6.1. Ammonia and exhaust injection (2000 rpm)

Engine Operation Points	Engine speed = 2000 rpm	
	Experimental condition	Unit

Engine Operating Point	2000/200	rpm/Nm
Exhaust Mass Flow Rate	223	kg/h
Injector Inlet / SCR Inlet Temperature	362/353	°C
NOx Quantity (NOx)	380 (210)	ppm
Downstream SCR Line Back Pressure	24	mbar
NOx Flow Rate	140	g/h
Adblue Flow Rate (Predicted)	247.0	g/h, NSR=1.0
Adblue Rate	68.6	mg/s, NSR=1.0
O_2, Volume	8	%
CO_2, Volume	9.3	%
H_2O, Volume	9.3	%

Table 6.2. Ammonia and exhaust injection (3000 rpm)

Engine Operation Points	Engine speed = 3000 rpm	
	Experimental condition	Unit
Engine Operating Point	3000/240	rpm/Nm
Exhaust Mass Flow Rate	478	kg/h
Injector Inlet / SCR Inlet Temperature	413/406	°C
NOx Quantity (NOx)	642(422)	ppm
Downstream SCR Line Back Pressure	131	mbar
NOx Flow rate	493	g/h

Adblue Flow Rate (Predicted)	869.5	g/h, NSR=0.85
Adblue Rate	241.5	mg/s, NSR=0.85
O_2, Volume	10	%
CO_2, Volume	7.8	%
H_2O, Volume	7.8	%

Table 6.3. Type of study to improve ammonia uniformity based on engine speed and mixer presence.

Type	Engine speed	Note
1	1500 rpm	No Mixer
2	2000 rpm	No Mixer
3	3000 rpm	No Mixer
4	1500 rpm	With Mixer
5	2000 rpm	With Mixer
6	3000 rpm	With Mixer

This study altered the engine operation condition from 1500 rpm to 2000 rpm and 3000 rpm to increase ammonia homogeneity, as indicated in Tables 6.1 and 6.2. Table 6.3 shows the engine specifications as well as the six ways for improving ammonia consistency.

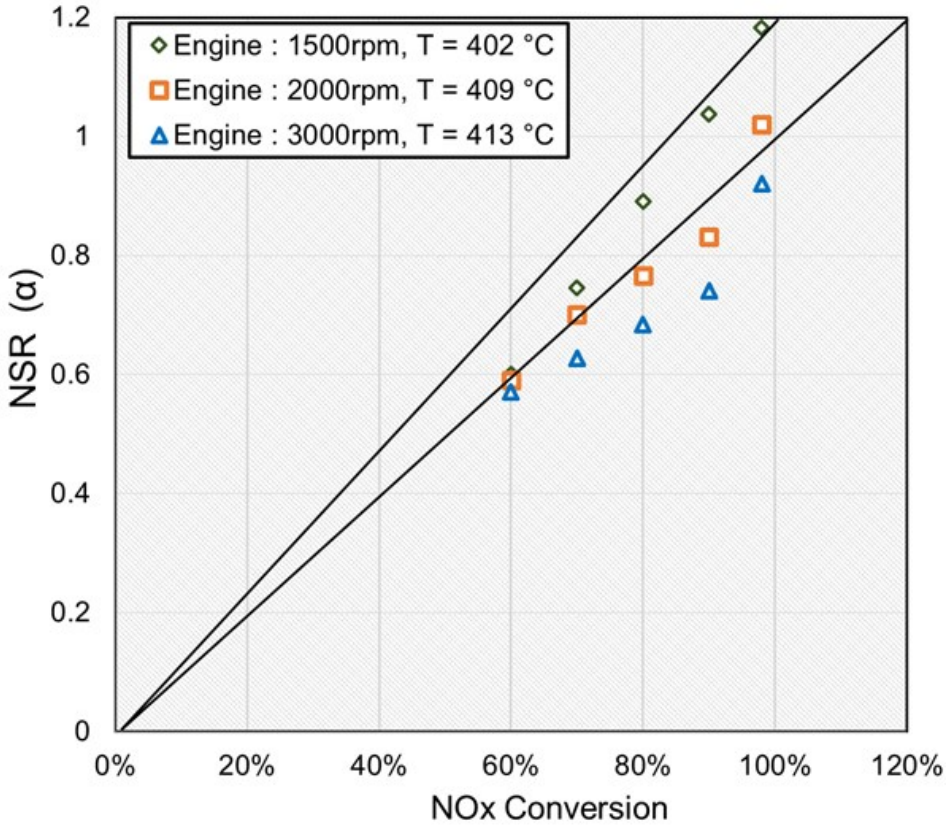

Figure 6.9: Comparison of Normalized Stoichiometric Ratio (NSR) and NOx conversion in each engine operation condition

The torque and power grow from 1500 rpm to around 3000 rpm, according to the engine specs. The mass flow rate, NOx amount, and other parameters were not substantially different from those at 1500 rpm during the simulation and experiment. 1500 rpm, 2000 rpm, and 3000 rpm were determined to be reflective of the whole variance predicted based on this observation. The mass flow rate and NOx amount of the engine operation circumstances at 2000 rpm and 3000 rpm revealed a significant difference, making it easy to compare NH3 uniformity of the engine operating circumstances.

The Normalized Stoichiometric Ratio (NSR) is a formula that determines how much reagent is required to accomplish the desired NOx reduction. The NSR employed in this study is shown in Tables 6.1, 6.2, and 6.3, and Figure 6.9 describes the NSR ratio of each engine operation state with temperature for the NOx conversion objective in detail. The engine operating type II employed 2000 rpm with the following parameters: NSR=1.0, UWS injector temperature of 262 °C, adblue flow rate (140 g/h), adblue rate (68.6 mg/s), O2 volume (8%), CO2 volume (9.3%), and H2O volume (9.3%). The engine operation type-III used 3000 rpm with the following related values: NSR=0.85, UWS injector temperature of 413 °C, adblue flow rate (869 g/h), adblue rate (241.5 mg/s), O2 volume (10%), CO2 volume (7.8%), and H2O volume (7.8%). The Increases in engine speed from 1500 rpm to 2000 rpm and 3000 rpm resulted in higher exhaust velocity and load, as well as increased pressure and temperature,

compared to the preceding kind. However, when the engine's operating condition improved, so did the exhaust flow rate, NOx amount, and other factors. As a result, the urea distribution quantity in the system should be determined as follows:

$$U_{inj.\ g/min} = \frac{K\ x\ NOx_{emission\ (g/min)}}{C_u}\ x\ De\_NOx$$

where $\boldsymbol{U_{inj.\ g/min}}$ is the urea aqueous solution injection amount in the system, *De-NOx* is reduced target value, $\boldsymbol{K}$ is the concentration of NO_2 (0.785), $\boldsymbol{NOx_{emission}\left(g/min\right)}$ is NOx quantity emission from exhaust, and $\boldsymbol{C_u}$ is the urea concentration (0.33). Thus, the NH_3 uniformity can be calculated precisely based on the actual conditions at each rpm. For engine speed conditions of 1500 rpm, 2000 rpm, and 3000 rpm, respectively, Type-IV, Type-V, and Type-VI were employed, and a mixer with 16 blades was employed to increase flow in the SCR system. With the gas flow direction, each blade has a 35° inclination angle. Figure 6.10 depicts the mixer's shape. To aid in the mixing of NH3 and gas in the system, the mixer was placed in front of the urea injector. Based on the testing setting of the commercial muffler by BENZ ML350, Figure 6.11 reveals that the mixer was 630 mm from the exhaust entrance.

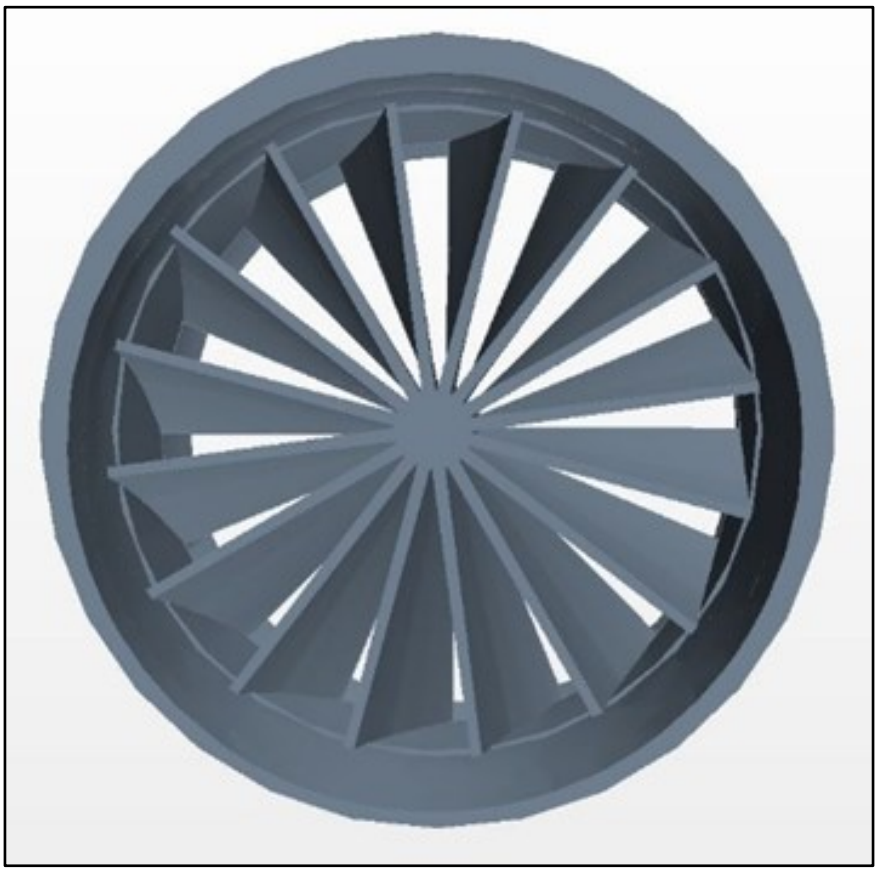

Figure 6.10: Mixer design and geometry

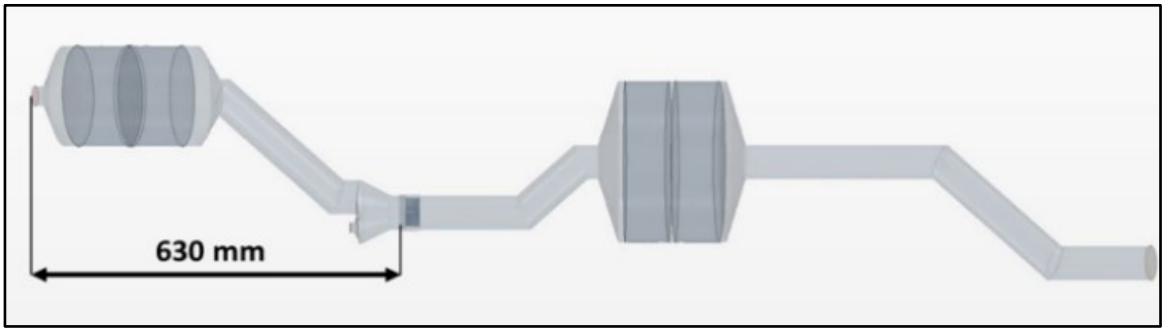

Figure 6.11: Mixer position in an SCR system

Figure 6.12 depicts the mixture quality of the six examples as determined by mass flux-based ammonia uniformity indices. The ammonia homogeneity on the catalyst inlet did not considerably improve from the prior findings for type-II and type-III. The ammonia uniformity rose greatly for type-IV, type-V, and type-VI, suggesting that mixers enhance the mixture quality such that ammonia flows into the catalyst more consistently.

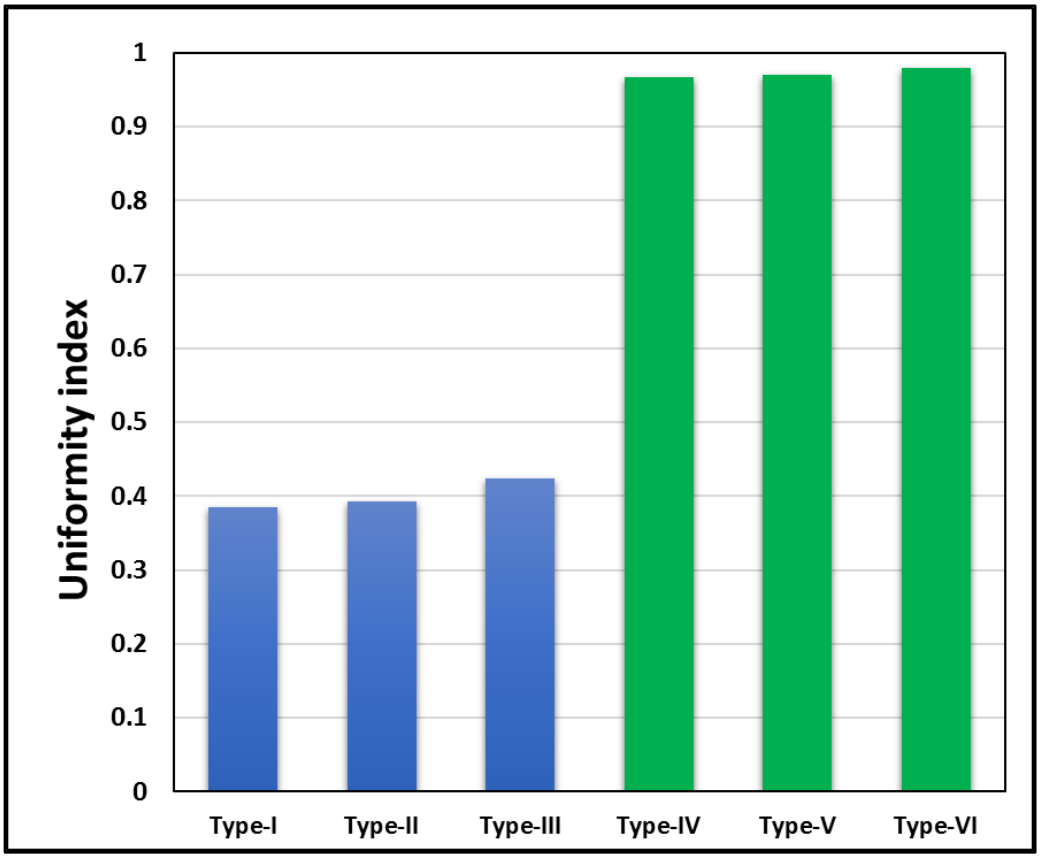

Figure 6.12: Ammonia uniformity at different engine speeds and mixer usage at the catalyst entrance

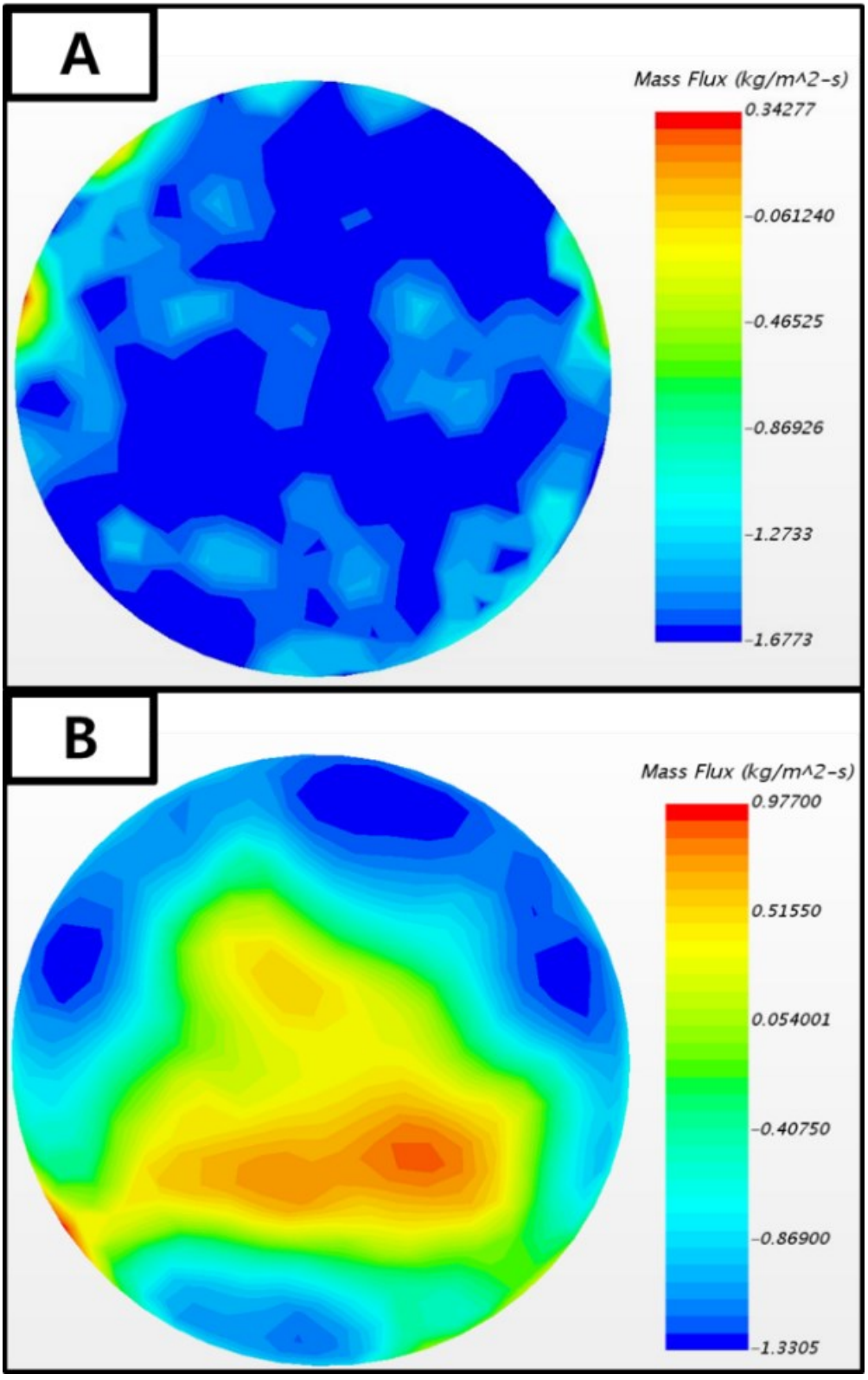

Figure 6.13: Ammonia uniformity from type-I (without mixer) and type-IV (with mixer) at the catalyst entrance

The difference in NH3 homogeneity without a mixer (type I) and with a mixer (type II) is seen in Figure 6.13. (type IV). The ammonia diffused to the input catalyst in the figure for type 1; with low

airflow, the quantity of ammonia connected to the catalysts was modest. This is due to the fact that ammonia and multi-component gas were unable to reach the catalyst inlet. Figures 6.4 and 6.5 demonstrate this observation. The dispersion of ammonia and multi-component gas across the catalyst inlet was insufficient due to the poor mixing reaction between ammonia and other gases at the pipe wall, as well as low pressure and velocity. The ammonia mass flow has a high concentration at the catalyst input, as shown in the figure for the type IV technique. This is due to the higher flow velocity of the gas from the mixer, which causes the ammonia and multi-component gas to spread more widely and completely occupy the input catalyst. In the experiment, 19 sensors in the SCR catalyst were used to detect ammonia homogeneity. The sensor data was analyzed in a gas analyzer to determine which gas was present in the catalyst. The sample data from the 19 sensors was then converted into a hexagram pattern, which was colored based on the amount of gas detected. As a result, comparing ammonia uniformity in simulation and experiment can better mimic real-world diesel engine circumstances.

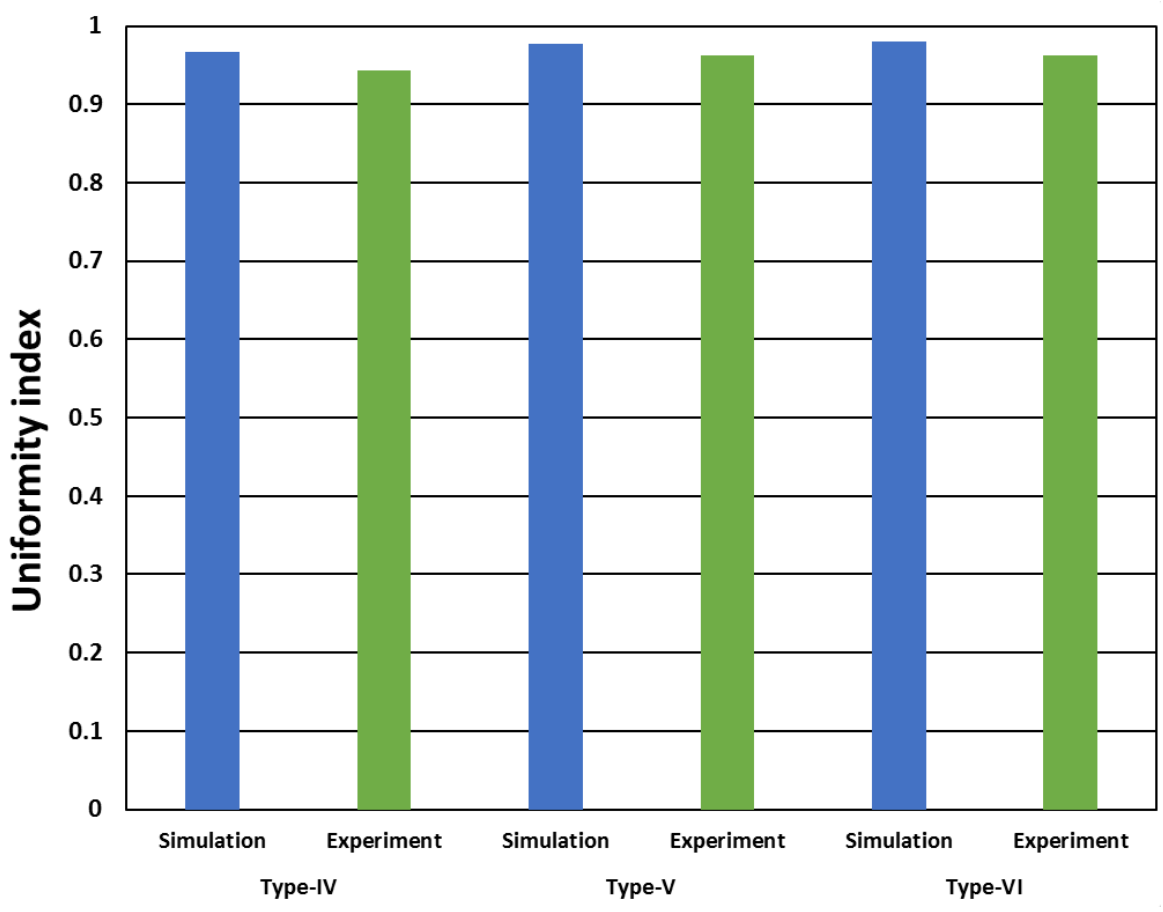

Figure 6.14: Comparison of ammonia uniformity from simulation and experiment results at the catalyst entrance

Without a mixer at the catalyst intake, it was impossible to illustrate the ammonia uniformity result for type I, type II, and type III. The gas pressure and flow velocity were too low, and the gas

analyzer could not identify the dispersion of ammonia into the catalyst. As a result, comparing the observations to the modeling findings was extremely challenging. Figure 6.14 shows a comparison of experiment and simulation findings for type-IV, type-V, and type-VI, demonstrating ammonia homogeneity at the catalyst input from simulation and experiment. The modeling result for the type-IV model was 97.7%, while the experimental result was 96.2% when the SCR catalyst was installed. Dust and other pollutants had no effect on the catalytic converter, mixer fan, pipe, or exhaust gas in simulation. The reaction was simulated, despite the fact that the experimental reaction included various pollutants and temperatures. If there is a 1.5% discrepancy in ammonia uniformity between the simulation result and the experimental result, the simulation result is credible.

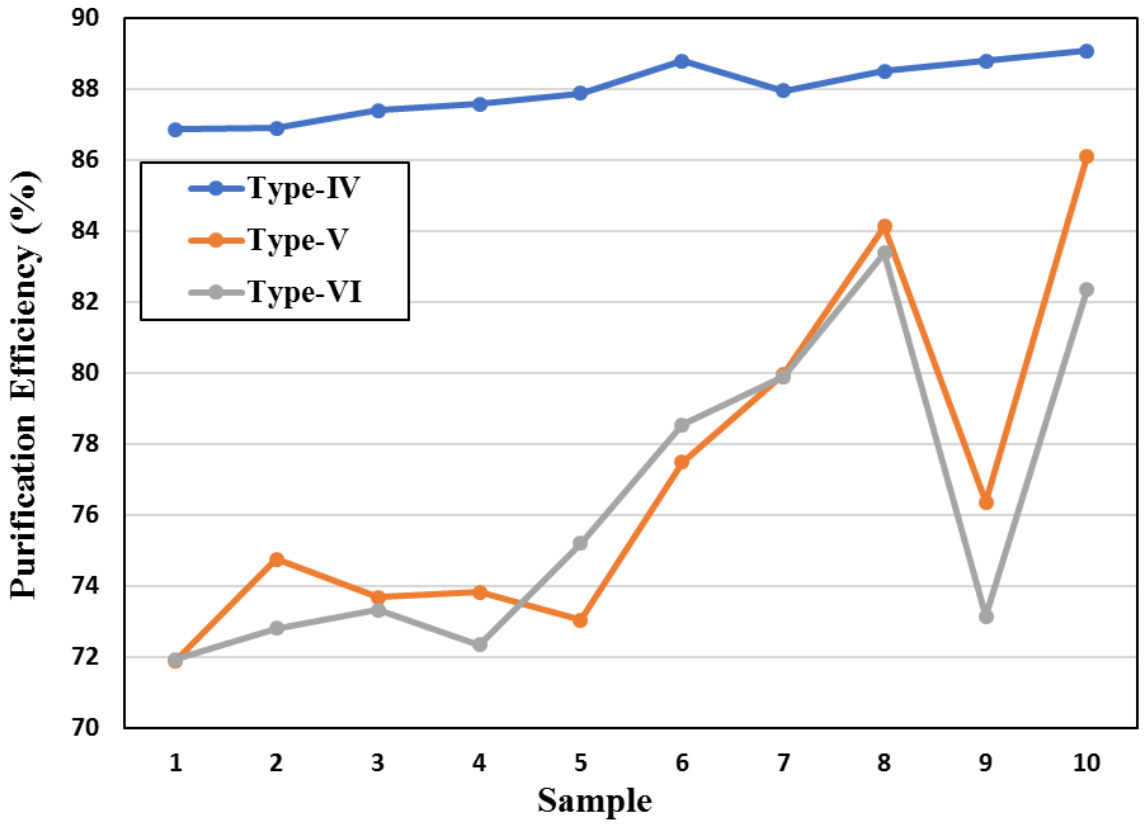

Figure 6.15: The comparison of purification efficiency of NOx at engine operation speeds of 1500 rpm, 2000 rpm, and 3000 rpm using a mixer at the system

The effectiveness of NOx purification after filtering at 1500, 2000, and 3000 rpm using a mixer with 10 repetitions is depicted in Figure 6.15. In this graph, the Y axis represents the % effectiveness of NOx purification, while the X axis represents each sample (1-10) in the experiment. Because dust and other impurities impacted the process, the purification effectiveness of NOx differed in each sample of the experiment. The NOx level was dramatically lowered when the engine was operated at 2000 rpm. At 2000 rpm, the engine and mixer's pressure and velocity magnitude generate strong flow and increase

turbulence in the pipe. Ammonia atomization can be improved by increasing flow and turbulence during the mixing process. As previously noted, reducing the bulk of non-vaporized ammonia particles can greatly increase catalyst performance. Furthermore, the functioning at 3000 rpm was quite comparable to that at 2000 rpm; The NOx level, on the other hand, was lowered even more, although the enhanced flow and turbulence responses in the mixing process were identical. This shows that raising engine speed and utilizing a mixer can result in high pressure and velocity in the exhaust line, which can promote ammonia atomization in the mixing process [51].

6.5 Summary

The study of ammonia uniformity is used to assess mixture quality, which has a significant impact on catalyst de-NOx performance. The low ammonia uniformity value was discovered without a mixer at 1500 rpm; so, this situation is extremely likely to result in poor de-NOx efficiency and excessive ammonia and isocyanic acid slips. The six combinations models were investigated to see if there were any ways to improve the mixing process and system performance. Type-II (2000 rpm without mixer) and type-III (3000 rpm without mixer) were discovered to have comparable effects to type-I (1500 rpm without mixer), such as a low level mixing reaction and poor SCR performance. The ammonia homogeneity rose greatly for type-IV (1500 rpm with mixer), type-V (2000 rpm with mixer), and type-VI (3000 rpm with mixer). This means that a 16-blade mixer may be used to optimize the mixing of UWS and NOx in order to create a very homogenous mixture for catalytic reaction. As a consequence of the consistent mixture, NOx reduction in the modeled 3L diesel engine will be improved. The urea evaporation model were studied in 3L diesel engines difficult to apply on the larger engines. Based on that situation, the investigation of ammonia generation process with 2 model of urea injector in 12L heavy-duty diesel engine will shows in the next chapter.

Chapter 7

Investigation of Different Types of Urea Injectors in 12L Heavy-duty Diesel Engine SCR System

This chapter describes the investigation of different type of urea injector in 12L Heavy-duty diesel engine in order to increase NOx conversion in SCR system. This chapter shows the saturation and vaporization process to produce ammonia gas, urea distribution, gas distribution in the system, ammonia uniformity value and NOx conversion value in 12L Heavy-duty diesel engine.

7.1 Investigation of low Engine Operation Condition Phenomenon

7.1.1 CFD for SCR system 12L Heavy-duty Diesel engine

The CFD model from the D6CC commercial SCR system in this simulation study was shows in figure 7.1. The CFD parameter and dimension has same; however, the first CFD model used an original of urea injector (L-type urea injector), while the second CFD model used the suggestion urea injector to increase the performance (I-type urea injector). That varies urea injectors were analyzed the quality of ammonia homogenization and increase the NOx conversion quantity in the system.

The injector holes and urea value parameters were same for all types. The simulation parameter and the experimental parameter in this study was same, that similarity parameter was useful to get the fix validation value for this study. Thus, the dimensions and size of the system matched with the actual conditions by the D66CC diesel engine from Hyundai. That varies of urea injector had high 152mm, 6.5mm of diameter and three spray holes with 120 μm of hole diameter. Each hole of injector has a 7° cone angle and that hole can produce huge urea mass flow rate (8.05-E5 kg/s).

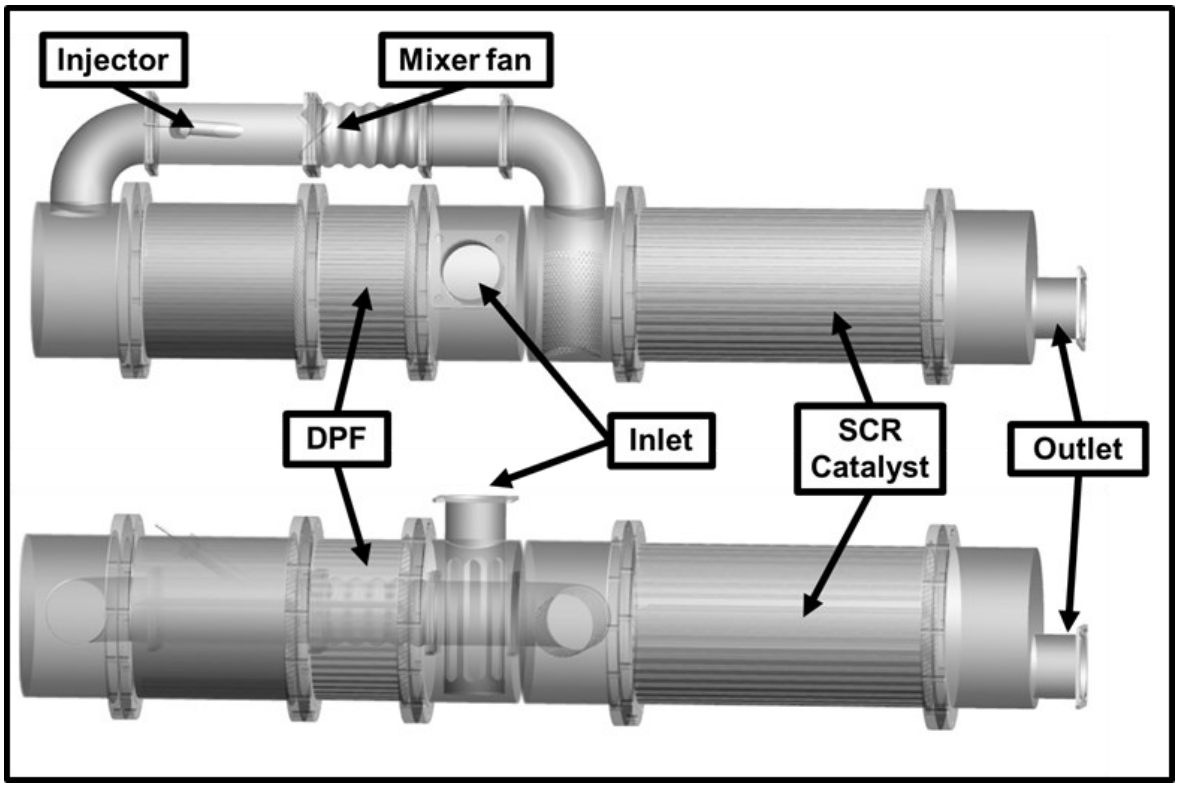

Figure 7.1: The CFD model from 12L Heavy-duty Diesel engine

7.1.2 UWS Saturation And Vaporization Processes

A simulation study is a way to clearly evidence phenomena that are difficult to show experimentally, especially inside a system such as the commercial SCR system for a Hyundai D6CC used here. Figure 7.2 shows the simulated urea saturation phenomena; in this figure shows that droplet saturation pressure for urea injector model-I has higher value. Its mean that urea injector model-I can produce higher ammonia gas in the system; the gas flow quantity in the system and the exhaust gas temperature from the engine were the most important indicators to produce a good ammonia quantity in the system. The exhaust gas had a large impact in this simulation because the gas flow distribution from the heavy-duty diesel engine was high. The UWS from the injector was distributed to the system by the gas flow. This explains the ammonia generation process by the H2O and urea saturation results in the simulation; the UWS used in this study has 60% water and 40% urea; and with the investigation on H2O and urea saturation value, the quality of ammonia generation process can be predicted; and based on that result both of those phenomena showed a higher concentration near the SCR catalyst: the nearer to the catalyst, the higher of gas pressure happen. The catalyst surface had small pores (less than 50 nm) which made it an efficient filter that produced good NOx conversion; this condition is the reason of higher pressure at catalyst. These phenomena also could assist the mixing process between the ammonia gas and the NOx before application onto the surface of the catalyst.

Figure 7.3 shows the urea vaporization values in the system; the high gas temperature from the heavy-duty diesel engine assisted the vaporization process. These results were similar to those of Koebel et al [27], who explained that the thermal temperature and urea hydrolytic decomposition process occurred in the 150 °C to 500 °C temperature range. And Khristamto et al.[49] also explained that the temperature can assist urea evaporation process. In this study, the engine's 1,000 rpm speed produced 686 K of heat to assist the saturation and vaporizing process, as shown in Figs. 7.2 and 7.3. The different concentrations are shown by the colors, which clearly compare the different areas of the urea injector to optimize the saturation and vaporization of the UWS in the system. Based on this result, the urea injector model-I show the higher result than urea injector model-L; even the distribution not as uniform urea injector model-L; but the quantity of evaporation higher. This result can predict the improvement of ammonia generation process in this system.[62]

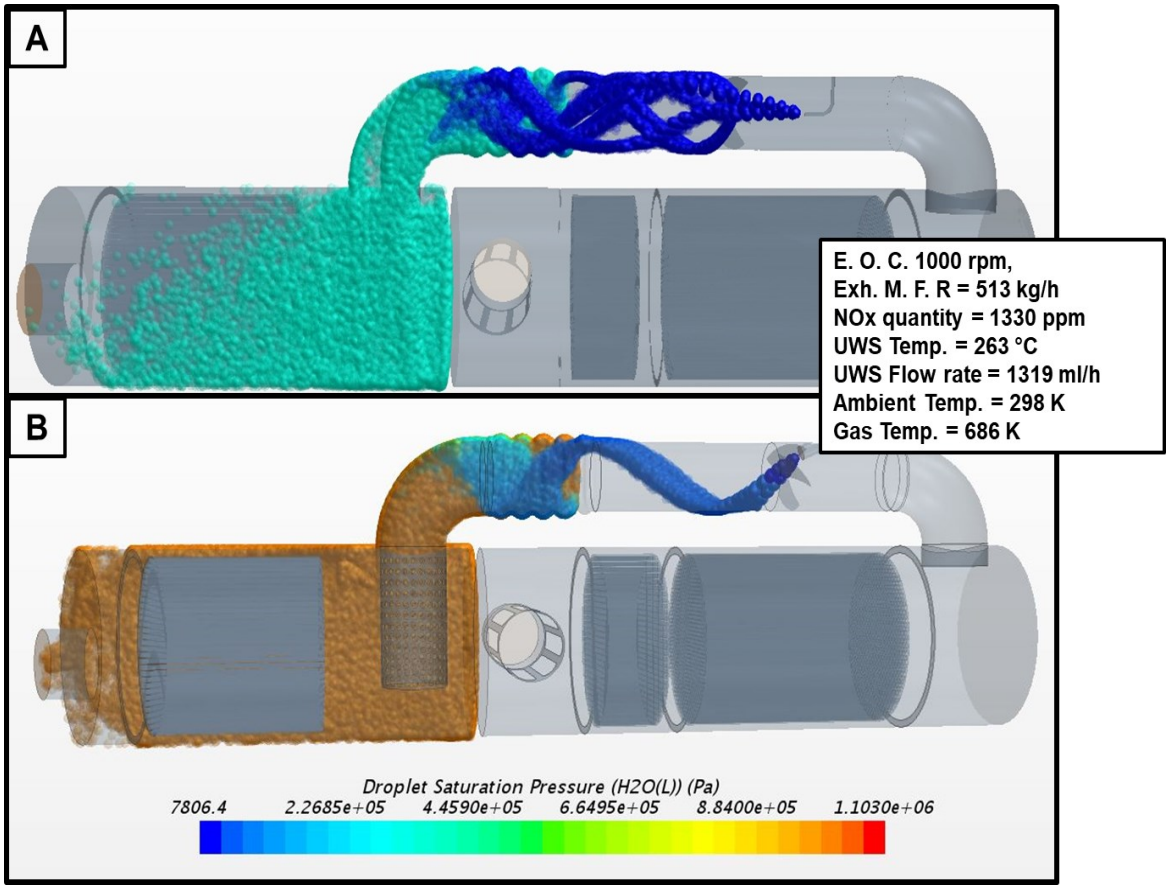

Figure 7.2: The UWS saturation value. (A) is urea injector model-L; (B) is model-I

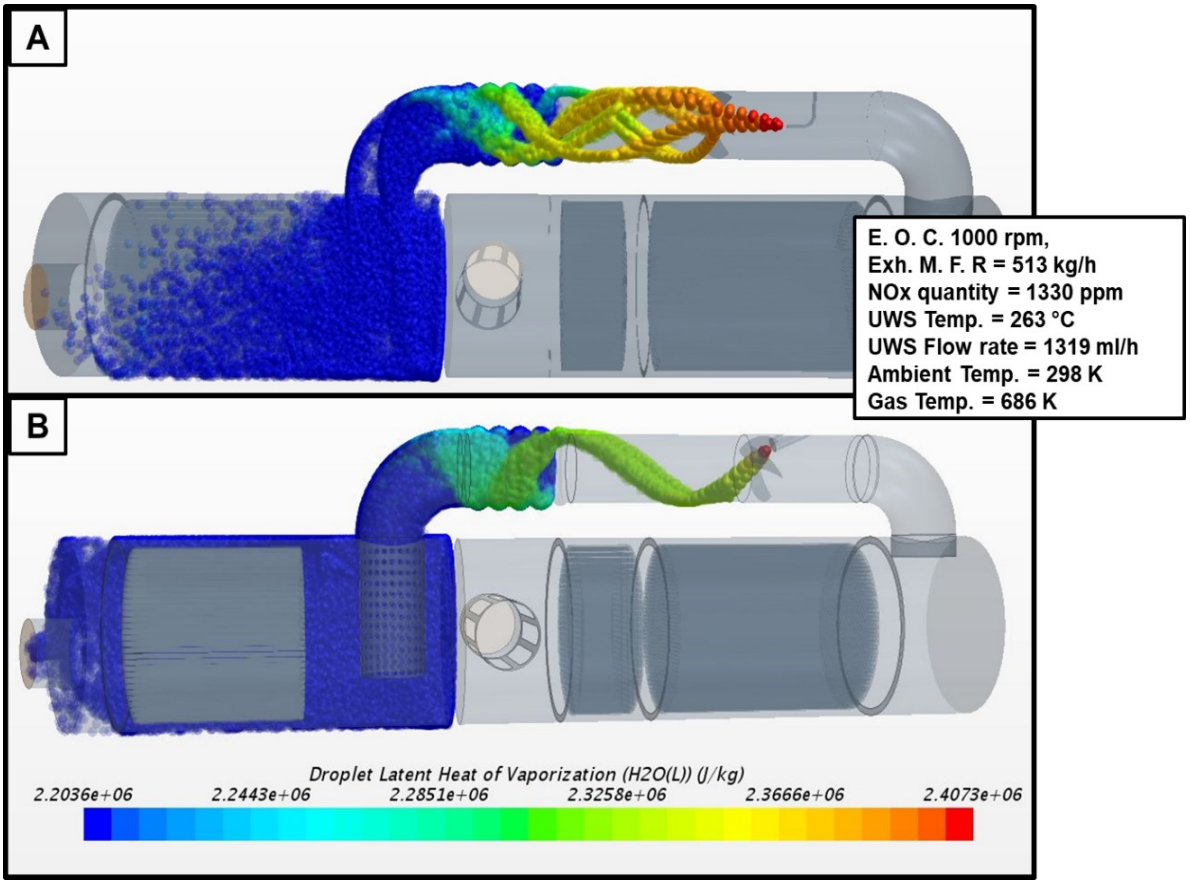

Figure 7.3 : The UWS vaporization values. (A) is urea injector model-L; (B) is model-I

7.1.3 UWS velocity distribution

The velocity magnitude pattern in our simulation elucidated the system gas distribution. As shown in Figure 7.4, the UWS in this simulation was easily distributed within the system, and the velocity pattern was aligned with the saturation and vaporization results in Figure 7.2. The pattern in Fig. 7.4 clearly shows how the UWS distribute to all system; this distribution pattern can predict the process of generate ammonia gas; based on the velocity, saturation and vaporization result, the higher value shows near on the injector inlet; this result predict the higher ammonia generation process occurred in that position; and making it possible to develop a strategy to increase the reducing of NOx emissions from diesel engines. The simulation parameters were based on experiments with an actual engine, so the simulation results and phenomena also occurred inside the experimental system.

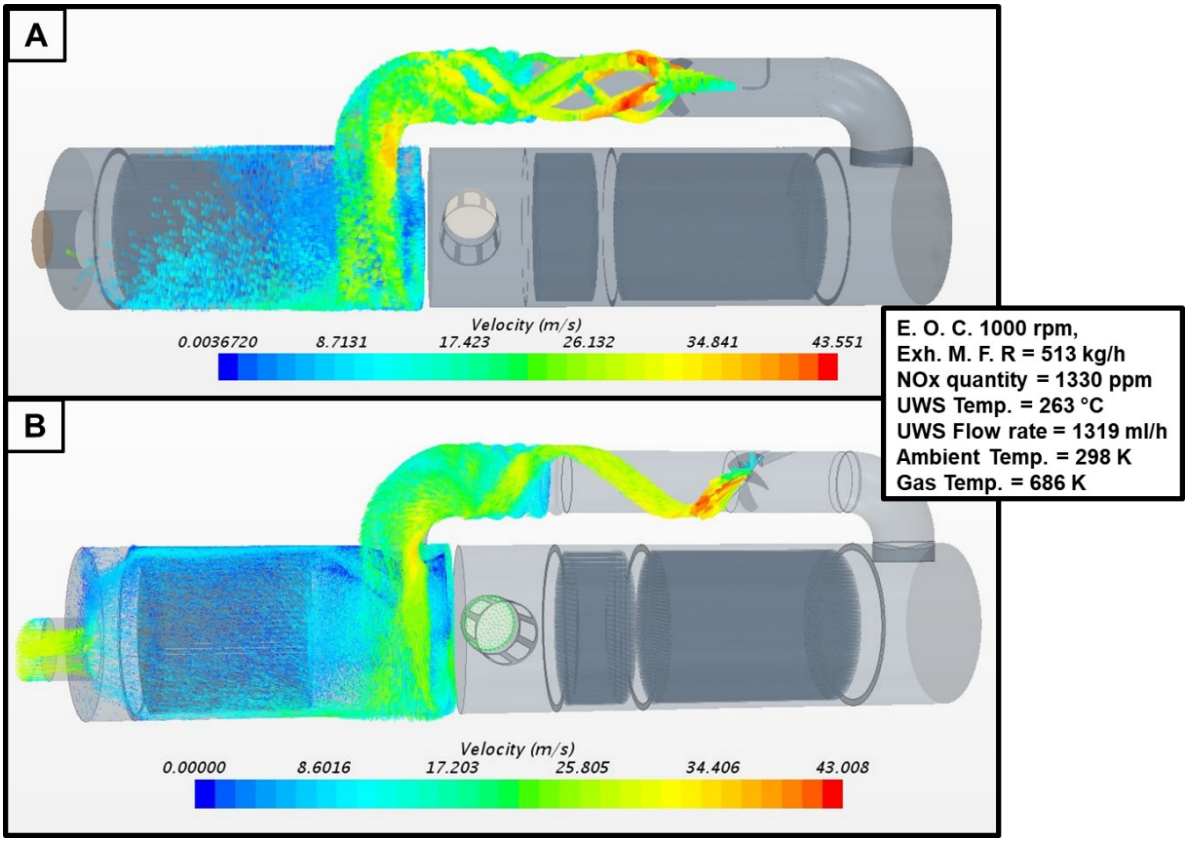

Figure 7.4: The pattern value of urea. (A) is urea injector model-L; (B) is model-I

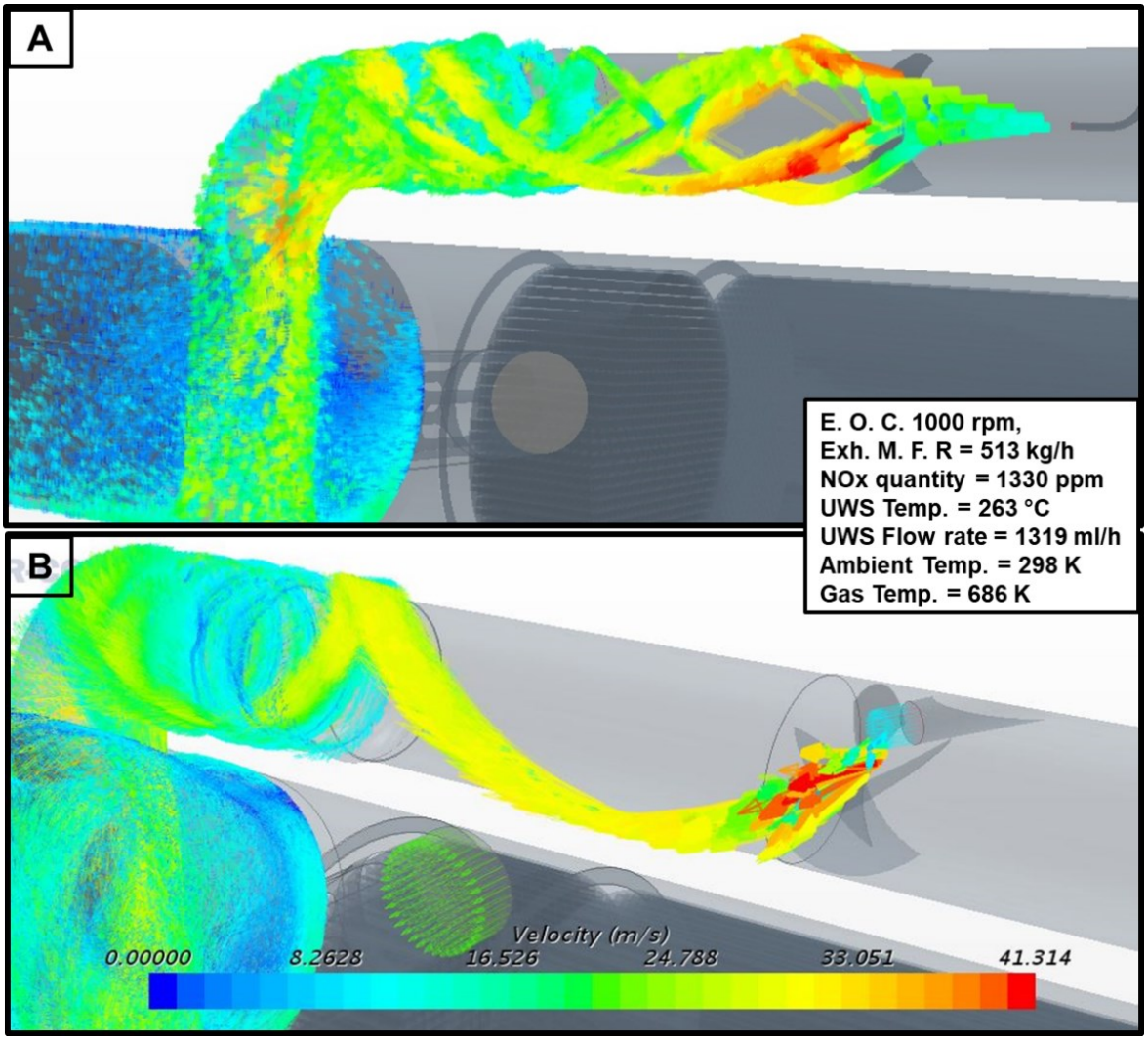

Figure 7.5: The distribution of urea. (A) is urea injector model-L; (B) is model-I

The urea distribution in the system can be affected by the amount of the exhaust gas. Here, the heavy-duty diesel engine produced a large exhaust mass (513 kg/h) and NOx mass (1,083 g/h). Those quantities of gas assisted the UWS distribution to the entire system (Fig. 7.5). In this section clearly shows the UWS distribution from urea injector model-I and model-L; and shows that model-L has a good shape of UWS distribution than model-I; and the result of urea distribution value explains the efficiency of ammonia generation process quality; and can predict the urea mechanism process in the system.

7.1.4 The quality of ammonia distribution

In the gas distribution described in the previous section (UWS saturation and vaporization processes), the urea injector model-I was shown to produce more ammonia than model-L; in that result, the vaporization and saturation processes performed better with the model-I injector. Figure 7.6 compares the gas properties in the SCR system based on time duration. The values are quite similar, reflecting the urea process conditions and the gas distribution inside the SCR system.

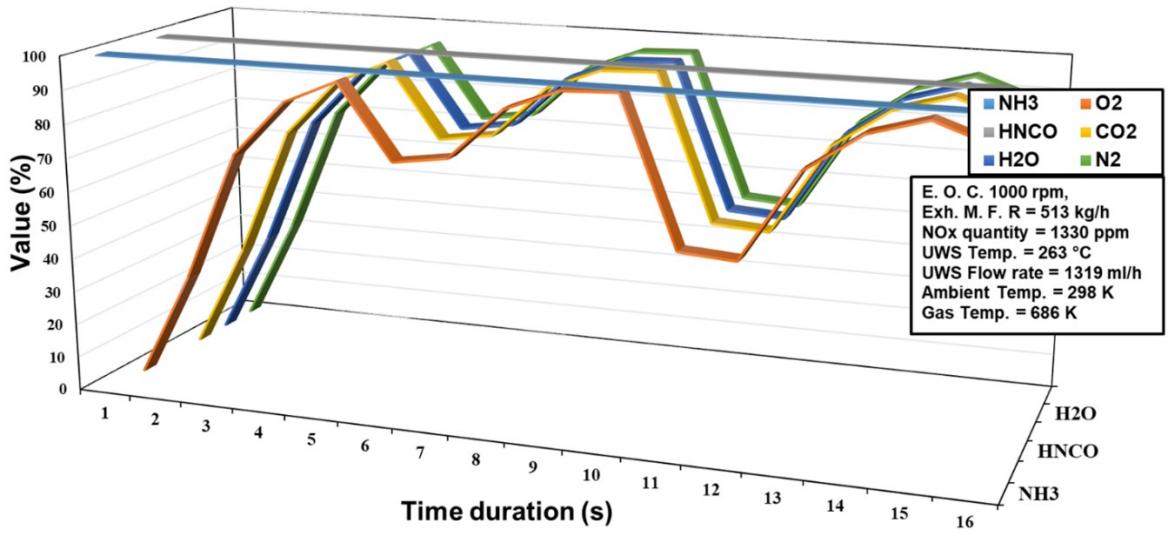

Figure 7.6: Various gas properties in the system

The primary objective of this study was to determine whether urea injector model-I is more effective than model-L (the original in the D6CC engine) in the urea decomposition process. Figures 7.7 show the two models studied here, and Fig. 7.8 shows the solid urea deposit inside the model-L injector. That deposit occurred because part of injector hindered the exhaust flow and was affected by the exhaust temperature, as shown in Fig. 7.7B, and lessened the distribution of urea into the system. This is why the model-L injector produced less urea than model-I injector.

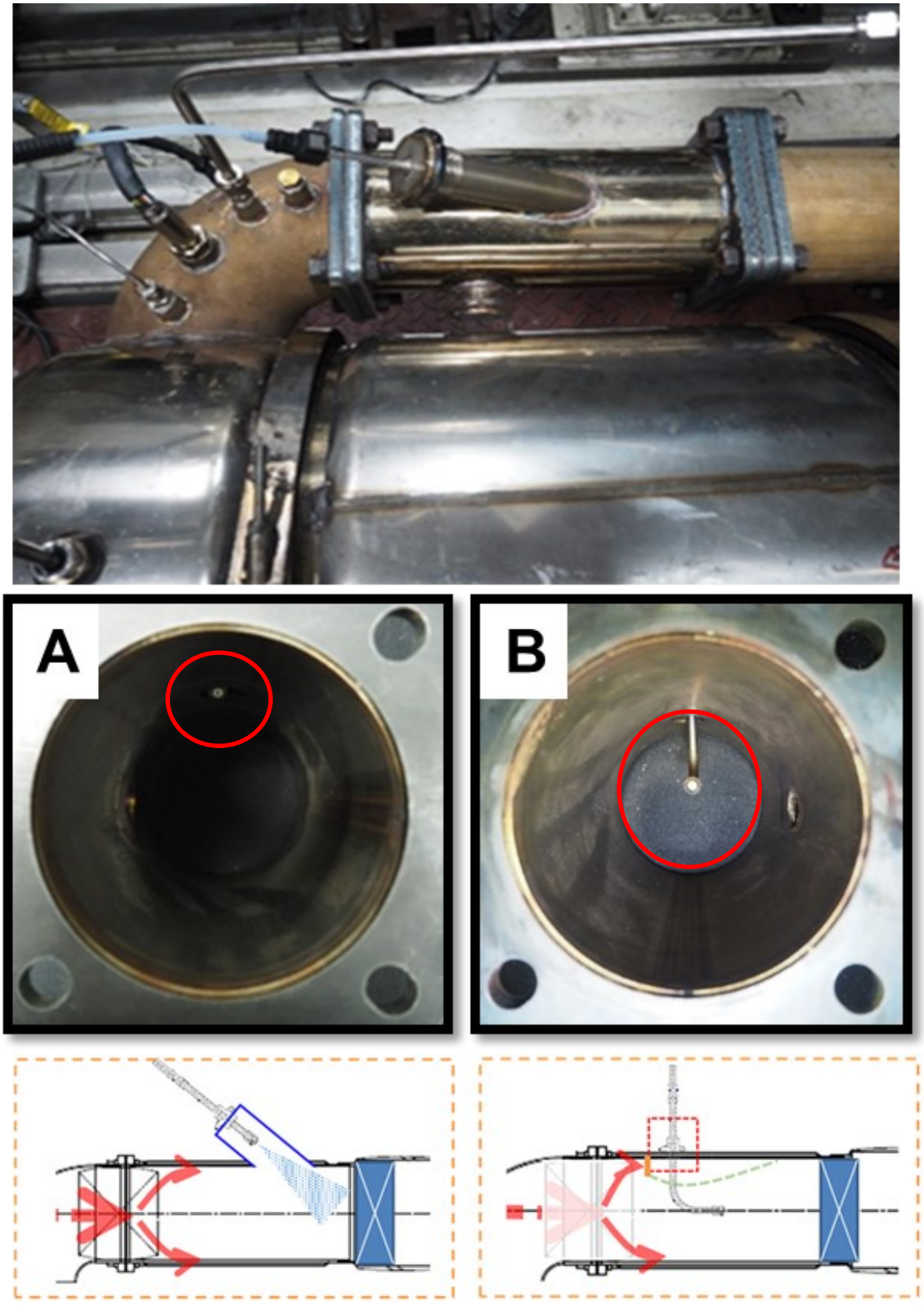

Figure 7.7: The urea injection model in the system; (A) Urea injector model-I (Suggestion injector) and (B) Urea injector model-L (original model from D6CC diesel engine)

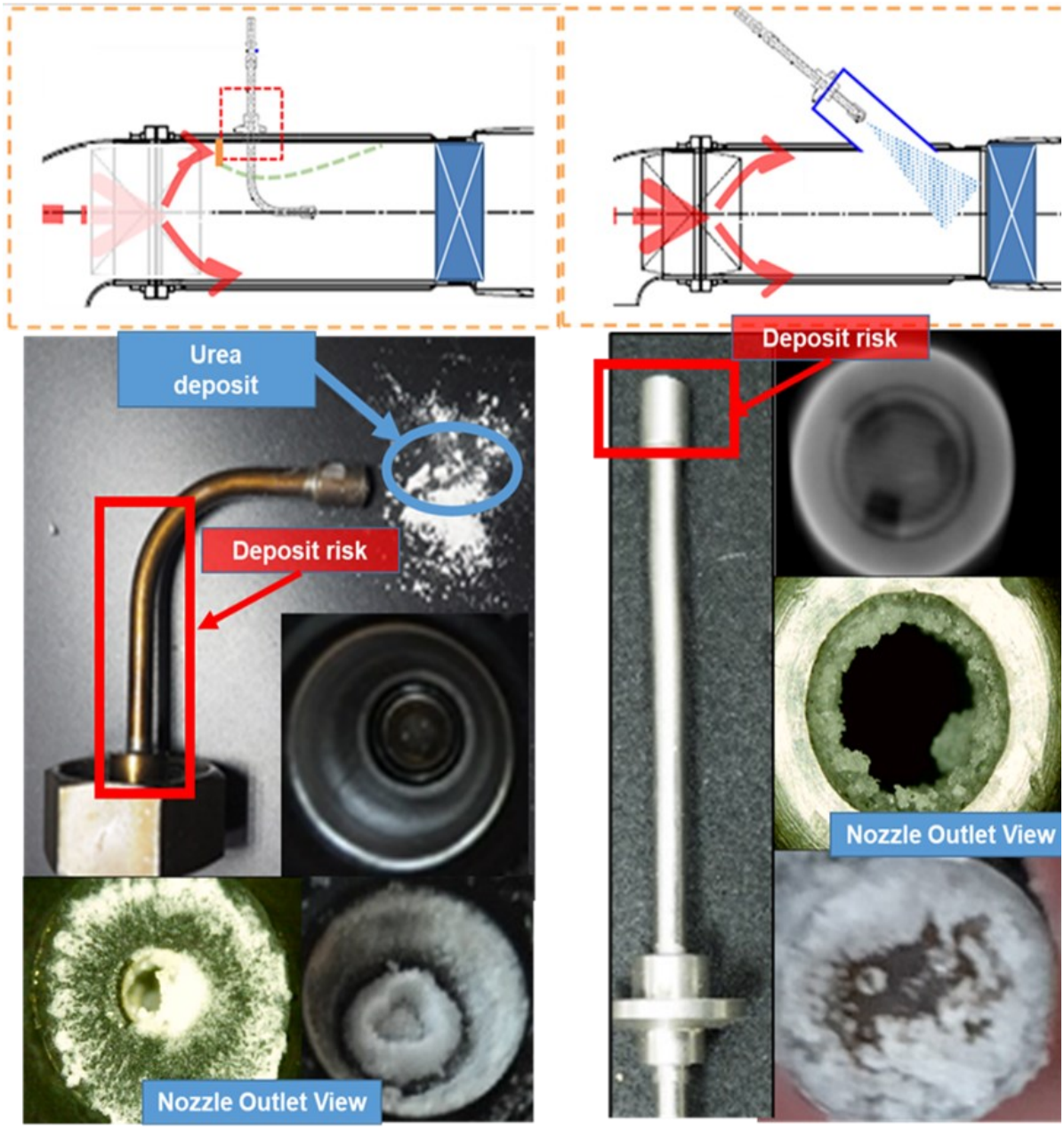

Figure 7.8: The solid deposit formation inside the Urea injector

Figure 7.9 shows the ammonia concentration value from various urea sensors in the outlets system. The simulation and experimental results showed that the urea injector model-I (blue bars in the figure) produced more ammonia than model-L (red bars). However, the ammonia homogenization in the catalyst surface for model-I was uneven. The ammonia homogenization in most SCR systems is the main indicator of high NOx conversion in a diesel engine; more ammonia in an SCR system is also indicative of higher NOx conversion quality.

Figure 7.10 compares the amounts of NOx conversion for the two injectors in the experiment. Model-I converted more NOx than model-L, and these data validate the simulation results in the previous section that model-I had higher saturation and better gas distribution in the system. This suggests that the urea injector model-I has a suitable shape for urea injection, enhancing the urea particle conversion into ammonia and minimizing solid deposits in the system. Additionally, with model-I the high pressure generated in the D6CC engine widely distributed the ammonia particles to mix more easily with the NOx. Therefore, the urea injector model-I is recommended to improve the quality of NOx reduction in heavy-duty diesel engines.

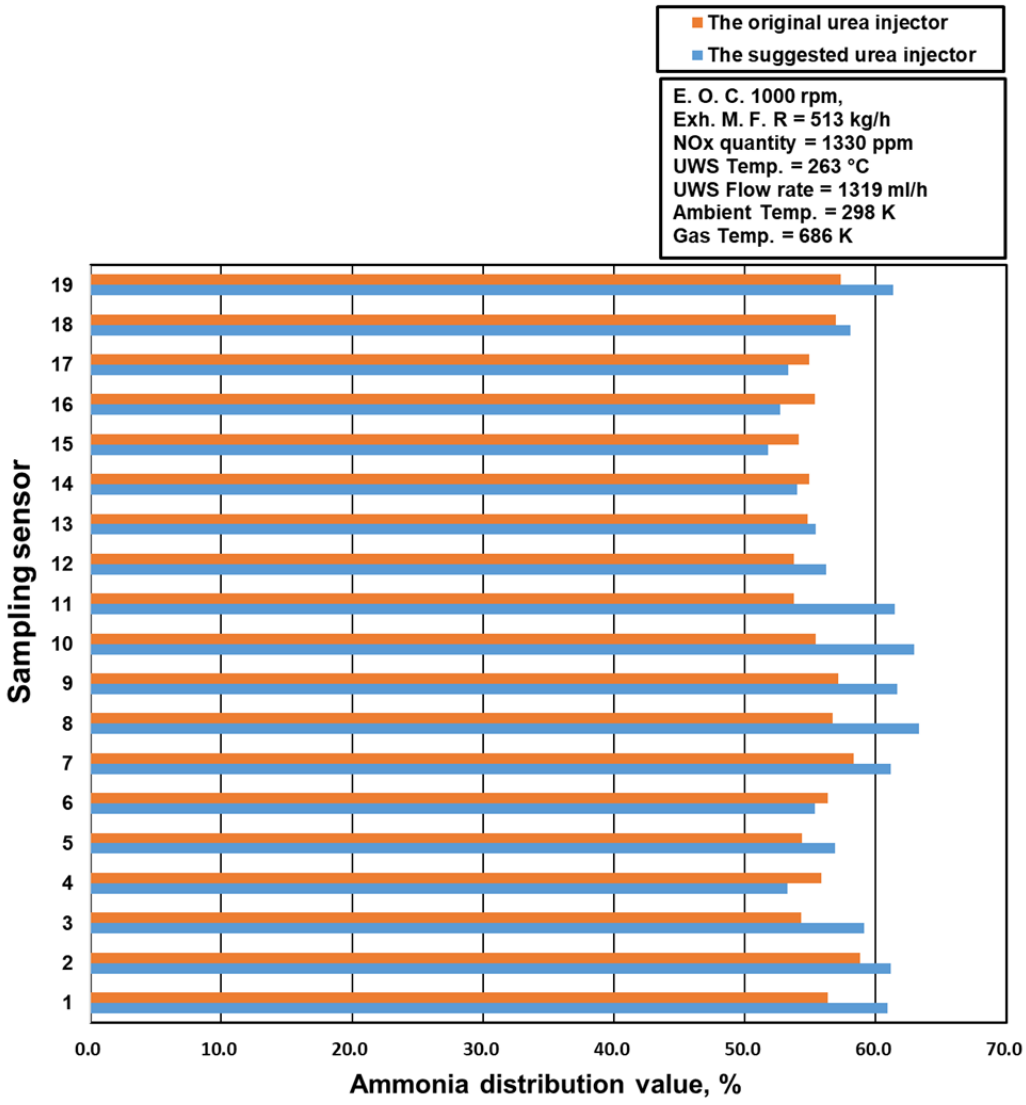

Figure 7.9: Sampled ammonia values in the catalyst inlet

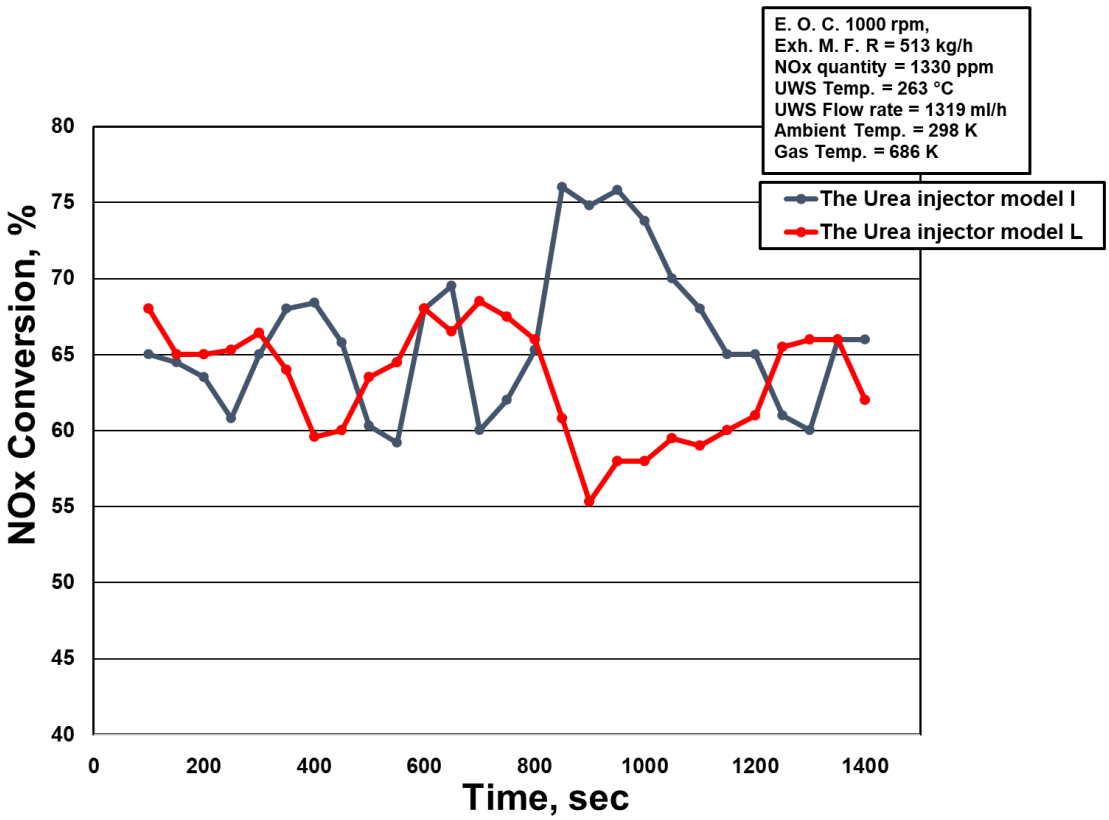

Figure 7.10: NOx conversion from urea injector model-I and model-L (MEXA-7100 gas analyzer)

7.2 Investigation of Variation Engine Operation Conditions Phenomenon

7.2.1 Ammonia generation processes

The urea evaporation value in the SCR system was the main indicator of NOx emissions. The quality of urea evaporation can impact the amount of ammonia gas in the system; that process also can impact to the urea solid deposit formation. Though the process is important, urea evaporation is difficult to investigate. The simulation study using a 3D model from STAR CCM+ can describe the urea evaporation process with saturation and vaporization values. The urea water solution (UWS) used in this study comprised 60% water and 40% urea. Thus, calculation of the water saturation value also will provide the urea saturation value. Figure 7.11 shows the saturation of water to explain the urea evaporation process in the system.

The simulation shows that in the figure 7.11a and 7.11c for model-L injector has lower saturation value than model-I; that's reaction happens because the model-L direct distribute the urea to the main flow of the system; some part from injector got direct hit by the gas main flow; the UWS inside the injector is easily solidified and deposited at high temperature; which can hamper urea distribution

from the injector and decrease the saturation value. The figure 7.11b and 7.11d for model-I injector has higher saturation value in this simulation result; that's value affected by the urea distribution quantity; the model-I injector position has in the top of the system; that position can reduce the possibility urea deposit solid inside the injector; based on that condition the amount of distribution urea for model-I injector was stable and produce high water saturation value.

The urea evaporation process also can affect by the temperature distribution in the system. The UWS has a temperature of 263°K, at which UWS is in liquid form at room temperature. The temperature of UWS will increase after inside to the system because effect of exhaust gas temperature; and that phenomena also described in this simulation study. Figure 7.12 shows the temperature of urea in the simulation, with Figure 7.12b and 7.12c showing urea temperature for the model-I injector. Figure 7.12c for 1700 rpm shows a higher temperature than for 1000 rpm. That relationship can affect urea evaporation quality because urea is easily evaporated at high temperature [27]**.** However, the result also can be influenced by other factors such as velocity and urea distribution.

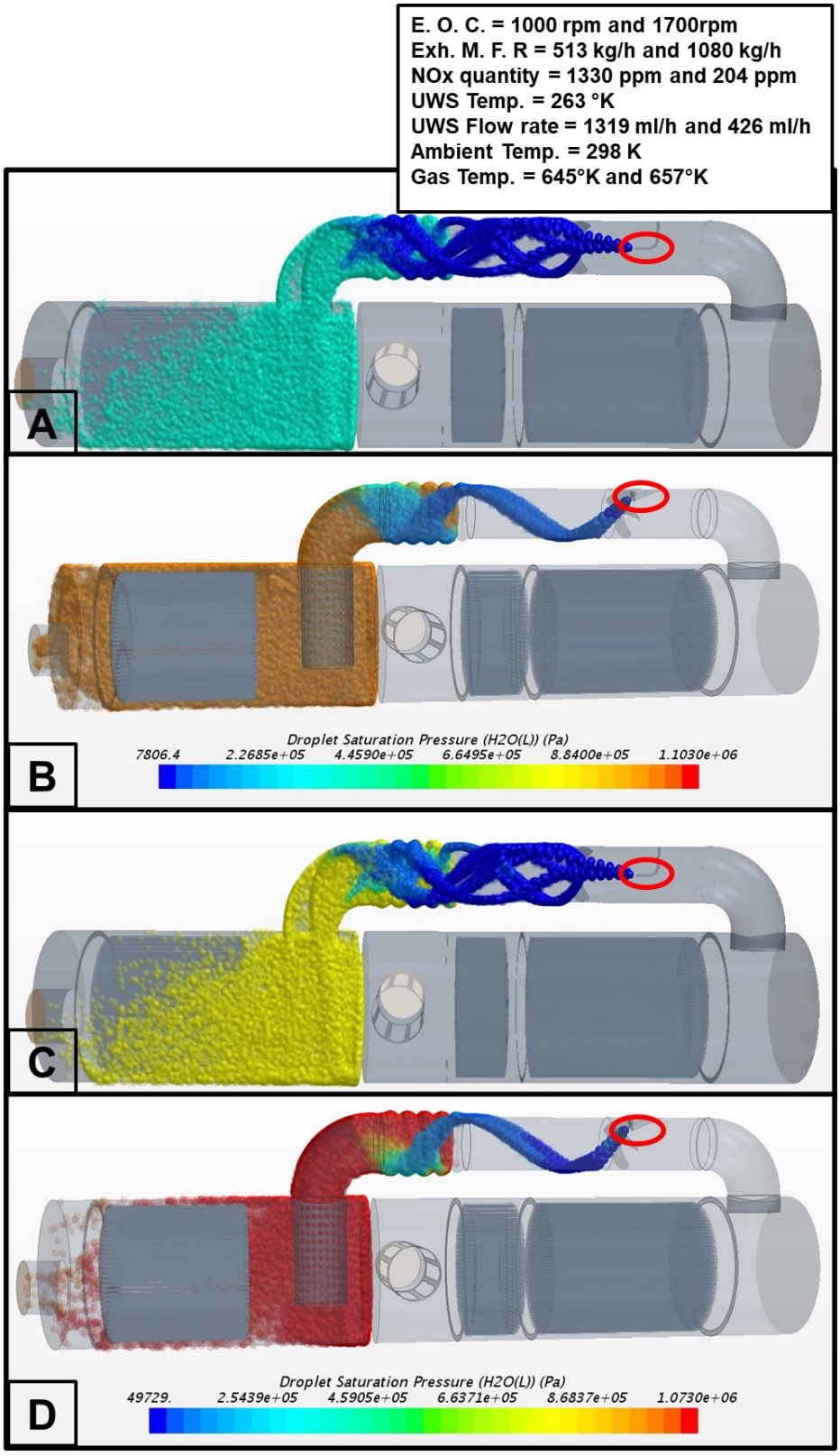

Figure 7.11: The saturation values using a) Urea injector model-L with 1.000rpm, b) Urea injector model-I with 1.000rpm, c) Urea injector model-L with 1.700rpm, and d) Urea injector model-I with 1.700rpm

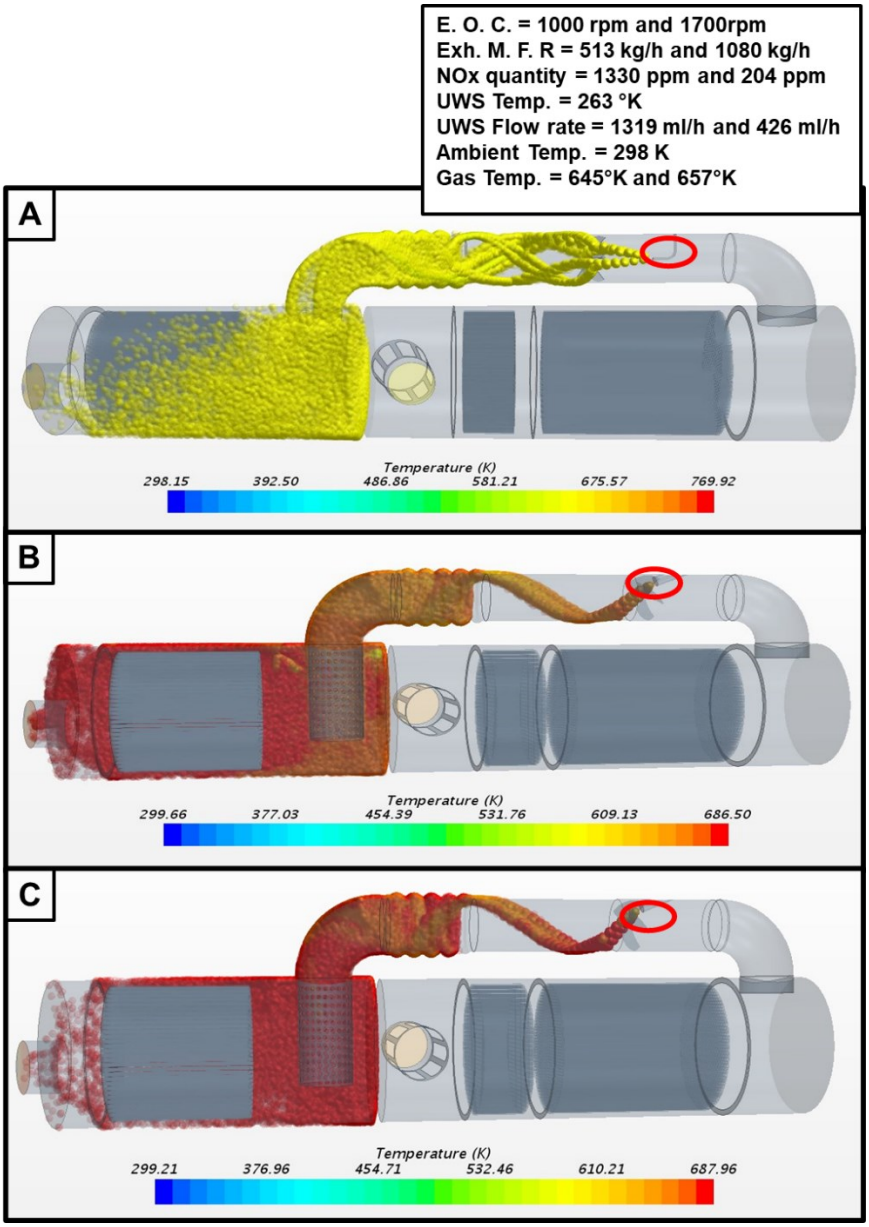

Figure 7.12: Urea temperature value a) Urea injector model-L with 1.000rpm, b) Urea injector model-I with 1.000rpm, and c) Urea injector model-I with 1.700rpm

7.2.2 Ammonia gas distribution

The chemical reaction between ammonia gaseous and NOx emission occurred inside the system from inlet injector to catalyst surface. The quality of chemical reaction can be affected when ammonia gas is distributed to all sides of the system. The distribution of gas can be shown with simulation, and the quantity of ammonia gas can be analyzed by the velocity pattern distribution from inlet injector to catalyst surface, as shown in Figure 7.13. The ammonia distribution shown in Figures 7.13a and 7.13b is the highest in this simulation study; the injector model-L can distribute ammonia to all side in the

system; that reaction occurred, because the position of inlet injector in the middle of system; based on that position the ammonia gaseous spread evenly.

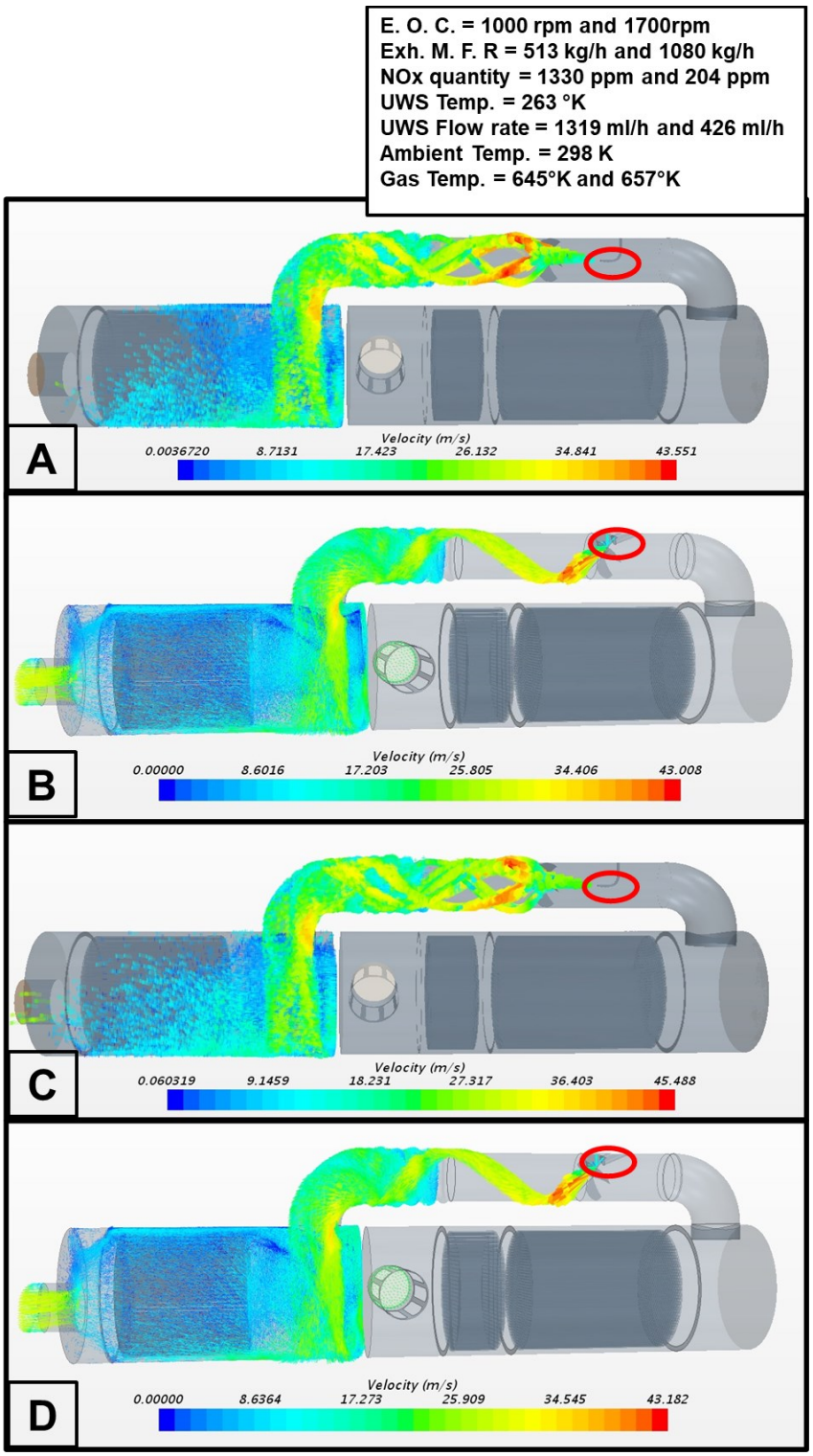

Figure 7.13: The gas distribution with a) Urea injector model-L with 1.000rpm, b) Urea injector model-I with 1.000rpm, c) Urea injector model-L with 1.700rpm, and d) Urea injector model-I with 1.700rpm

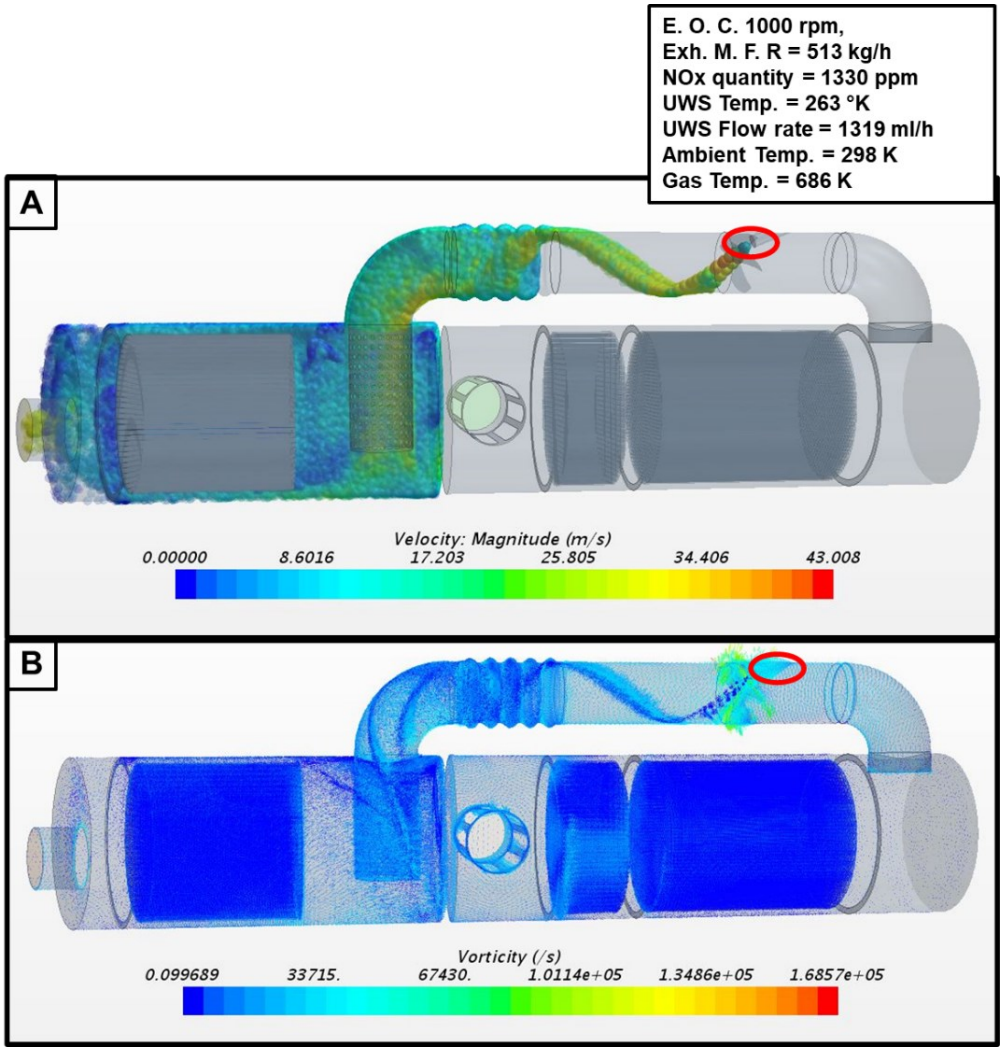

Figure 7.14: The ammonia distribution area

The I-shaped injector produce lowers value of ammonia gas distribution in figure 7.13; based on that result value, the investigation for urea injector model-I was showing in figure 7.14. The ammonia gaseous distribution for urea injector model-I was analyze by the velocity magnitude model and vorticity value. The position of this inlet injector is at the top of the system and limiting the angle of spray. The small angle produces uneven distribution of urea, which affects to the ammonia distribution gaseous value in this simulation study. The vorticity value from urea injector model-I can shows in figure 7.14b. Circulation of ammonia gas produces a small vortex in front of the injector inlet, affecting the main flow gas from the engine. When gaseous ammonia enters a system with a strong gas flow, the two streams collide, changing the shapes of both. These changed shapes are presented in Figure 7.13 and Figure 7.14 for the urea injector model-I.

7.2.3 Ammonia homogenization quality

Ammonia generation can be analyzed to determine the quality of urea evaporation in the system; the saturation value and temperature distribution indicate the quality of ammonia value in two shape of injector model at different engine operation conditions. However, that method is limited to capture the distribution of ammonia from the two injectors; the ammonia homogenization in the catalyst surface is the promising method to investigate the ammonia distribution value. Figure 7.15 shows the experimental and simulation values of ammonia homogenization. The uniformity index (UI) of the urea injector model-L is highest of the injectors because the position of urea injection in the center of the main flow, with which the ammonia gas can mix easily and be distributed to all sides of the system. Although the urea injector model-I has the lowest UI, it produces the highest quantity of ammonia, as demonstrated in Figures 7.11 and 7.12.

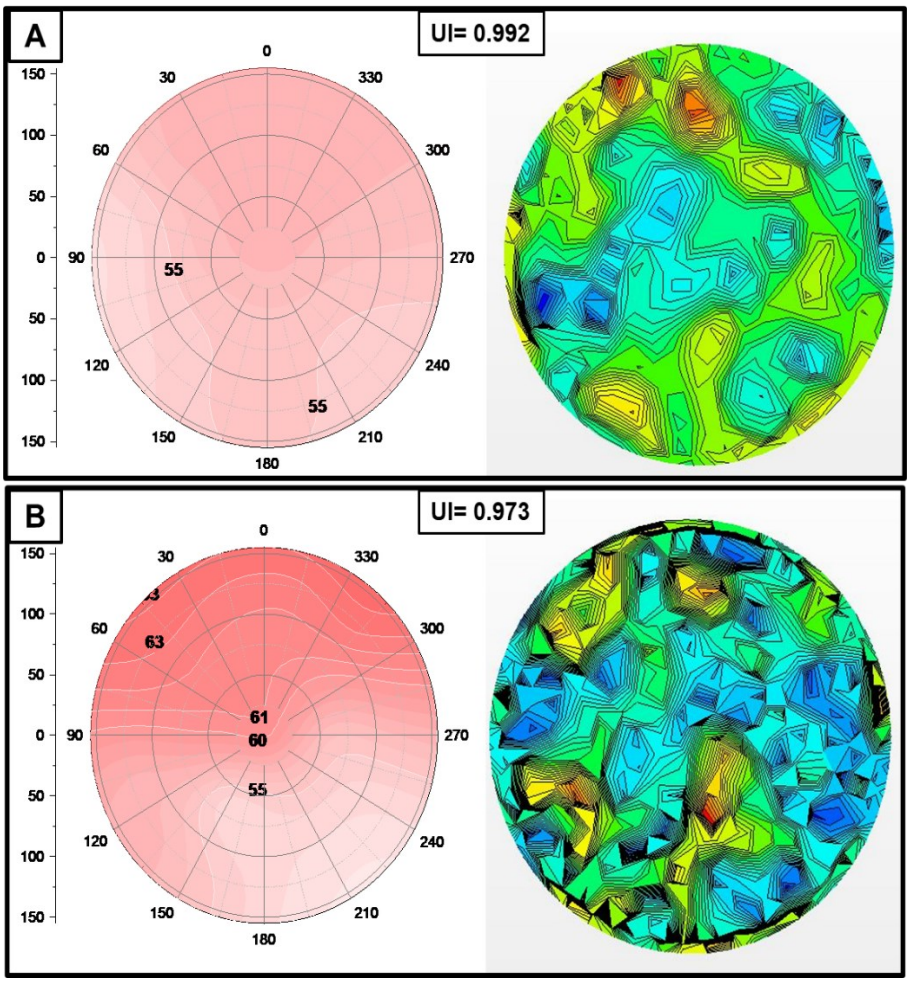

Figure 7.15: Ammonia homogenization in the catalyst surface, a) Urea injector model-L and b) Urea injector model-I

To increase ammonia homogenization in the urea injector model-I, this study used 4 mixer fan positions, as shown in Figure 7.16. The original mixer position is shown in Figures 7.16a and 7.16b, while Figure 7.16c shows the injector without a mixer fan, which is used as the reference to visualize the advantage of the mixer to increase ammonia homogenization. Figure 7.16d shows the mixer fan behind the injector, which can increase the air loop before urea injection and increase the ammonia distribution to all sides of the system.

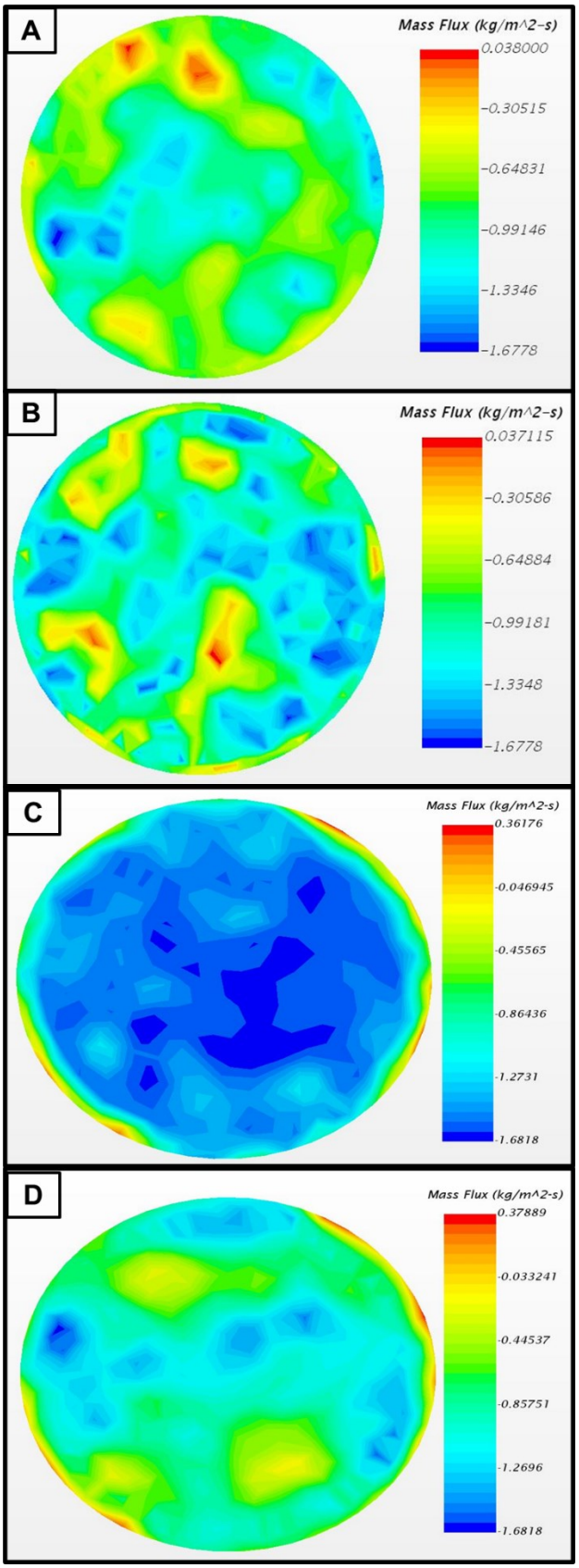

Figure 7.16: The gas distribution with a) Urea injector model-L with 1.000rpm, b) Urea injector model-I with 1.000rpm, c) Urea injector model-L with 1.700rpm, and d) Urea injector model-I with 1.700rpm

Ammonia homogenization with the 4 modifications is show in Figure 7.17, indicating the efficacy of the mixer fan position to increase ammonia homogenization in the system. Figure 7.17c shows the lowest ammonia homogenization without a mixer due to difficulty in distribution the ammonia gaseous in all side of system. However, in the figure 7.17d the ammonia homogenization for urea injector model-I was improve. The comparison between urea injector model-I with front mixer and urea injector model-I with back mixer position shows in the figure 7.18.

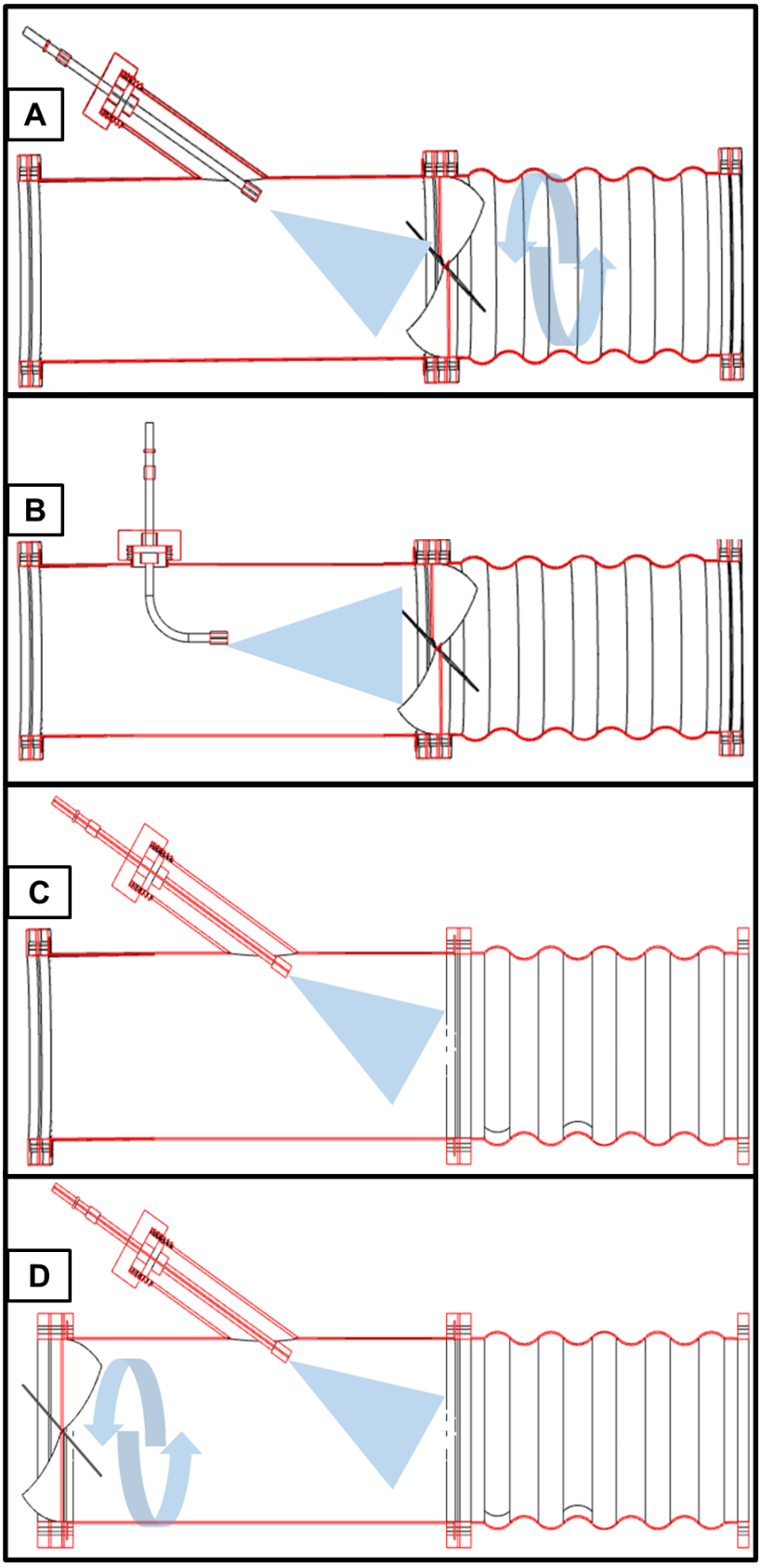

Figure 7.17: The model of modification mixer position, a) Urea injector model-I with front mixer position, b) Urea injector model-L with front mixer position, c) Urea injector model-I without mixer, and d) Urea injector model-I with back mixer position

Figure 7.18 shows the investigation of UI value from urea injector model-I based on the figure 7.17 result. The comparison result from simulation and experiment will shows the improvement value of ammonia homogenization in the catalyst surface. Figure 7.18a show the ammonia homogenization value with front mixer position; and figure 7.18b shows the ammonia homogenization value with back mixer position. Although the increasing value is not large, it is a reference for future study to increase ammonia homogenization value by increasing the air loop based on mixer position or by increasing the velocity and main flow pressure before urea injection.

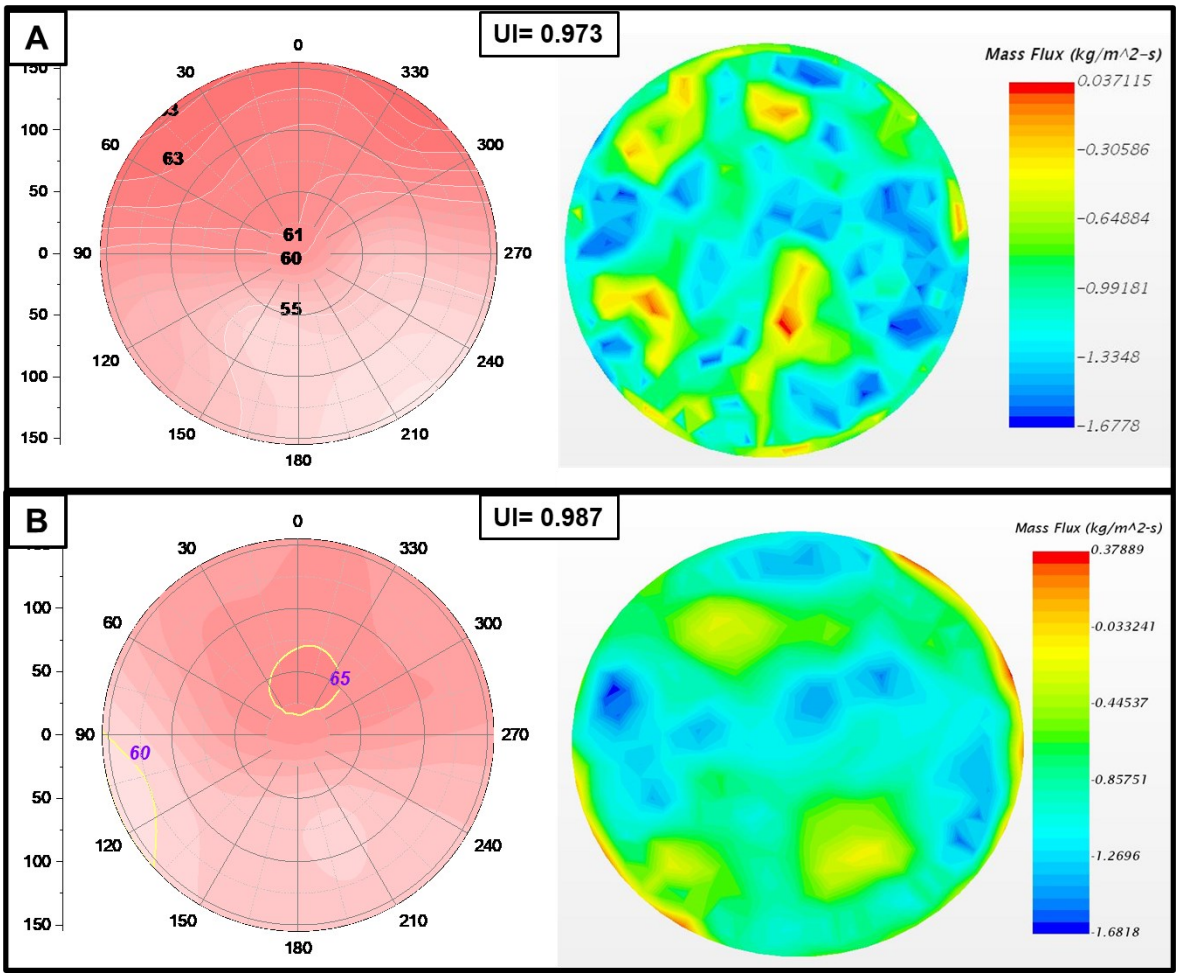

Figure 7.18: The ammonia distribution area

7.2.4 NOx Conversion quantity

NOx conversion is the main indicator to evaluate the quality of SCR system. The quantity of NOx will decrease after entering the system. To compute the NOx conversion value from the SCR system, the value of ammonia homogenization quality is needed from the simulation equation by the ammonia mass

flux value at the catalyst surface. The colorize of ammonia mass flux value also can predict the NO_x conversion quality in the system. To calculate the ammonia homogenization value and the utilization catalyst in the system, as follow:

$$\gamma_{mass\_flux} = 1 - \frac{\int_A (m''_{NH3} - \bar{m}''_{NH3})\, dA}{2\bar{m}''_{NH3}}, \qquad (21)$$

where m''_{NH3} is the value of ammonia mass flux on the *i*-direction , $\bar{m}''_{NH3}$ is mean value for ammonia mass flux in the system, and A is the area for ammonia mass flux attached. The equation 4 can compute the NO_x conversion value based on the NO_x quantity before and after inserted in the system [60]. The NO_x value without after treatment process (SCR system) is 100% or 1; that value was the original emission of NO_x from the engine. The NO_x conversion quality for compute the SCR system quality sometimes is different, that reaction happen because the concentration of inconstant the NO_x inlet value and the NO_x outlet value (SCR system performance). To find the NO_x concentration value for each SCR system, as follow:

$$NOx_{Conversion\ value} = \left(1 - \frac{NOx\ Outlet}{NOx\ inlet}\right) x\ 100\% \qquad (22)$$

The investigation of ammonia generation process and ammonia homogenization value in the previous section can inform the quality of ammonia gaseous in this study. In this section the NOx reduction value from urea injector model-I and urea injector model-L will investigate. The 1,000rpm engine operation condition is used for this analysis; be-cause this engine operation condition can produce 1,330ppm of NOx concentration value; and this value is higher than 1,700rpm.

Figure 7.19 shows the investigation of NOx concentration value from urea injector model-I and urea injector model-L; in this figure, the urea injector model-I and urea injector model-L has similar result; the average value from urea injector model-I is better than urea injector model-L to decrease NOx concentration from diesel engine. Figure 7.20 shows the NOx conversion value from urea injector model-I and urea injector model-L; this result demonstrating that the urea injector model-I with the largest amount of ammonia better reduced NOx from a heavy-duty diesel engine in this study. Improvement of gas distribution in the urea injector model-I is required to increase ammonia homogenization and NOx reduction quality.

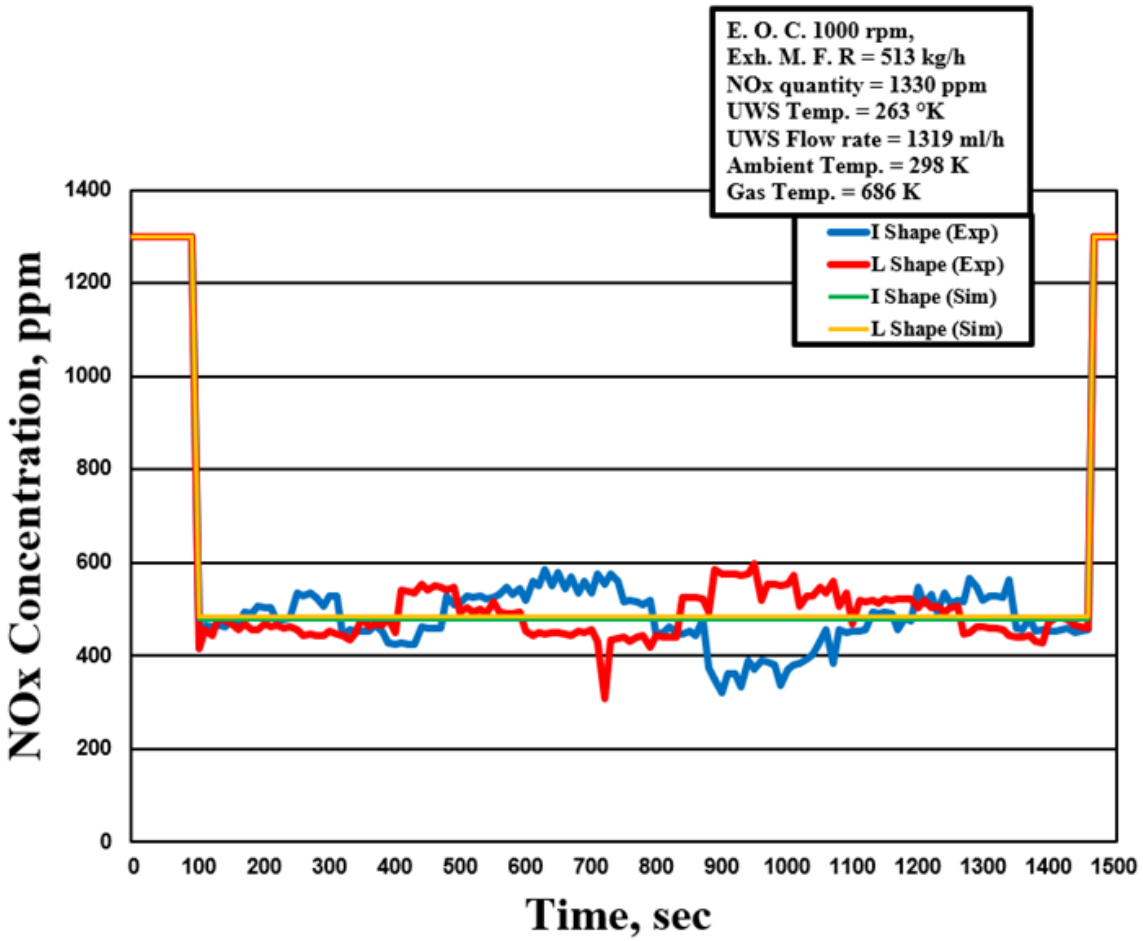

Figure 7.19: The NOx concentration for urea injector model-I and urea injector model-L

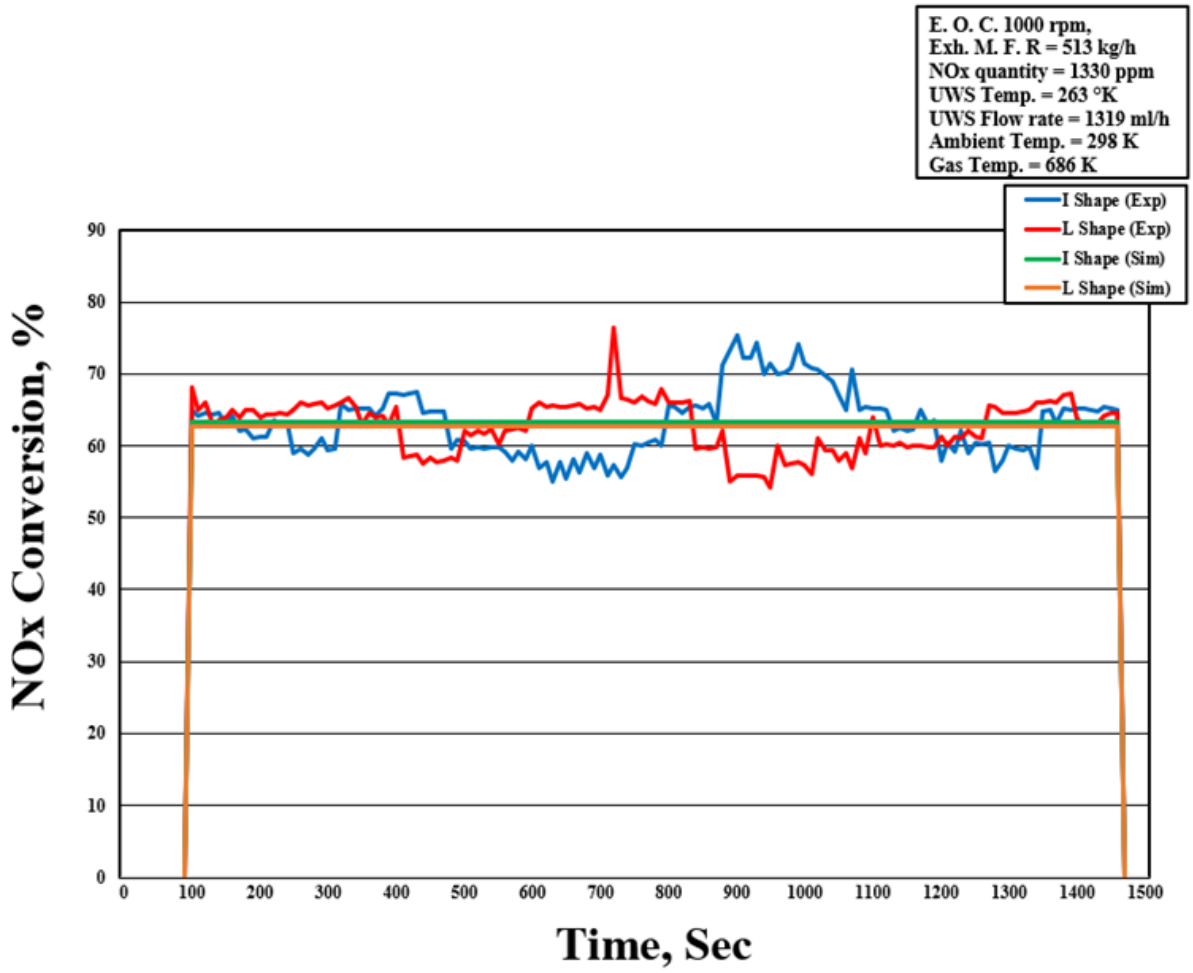

Figure 7.20: The NOx conversion for urea injector model-I and urea injector model-L

7.3 Summary

The urea evaporation model were studied in optical access and 3L diesel engines difficult to apply on the larger engines. Based on that situation, this study investigate 12L heavy-duty diesel engine with 513 kg/h exhaust mass flow rate, a 1,330 ppm NOx value, and a 686 K exhaust gas temperature in 1000rpm. The original urea injector (L-shaped) shows the compaction of urea inside the injector, thus inhibiting the urea injection process. This phenomenon has a negative effect on the NOx conversion efficiency in the SCR system. Based on that problem, the suggested urea injector (I-shaped) have to solve the solidification of urea inside the injector, because the shape and position of I-shaped urea injector were suitable for the SCR system. The study of ammonia generation and distribution showed that the I-shaped injector produced the highest amount of ammonia during saturation, while the L-shaped injector produce the highest ammonia distribution in this system. The investigation of urea solidification inside L-shaped injector also can validate the ammonia quantity values for that injector. The lowest ammonia quantity affected by the hampered distribution urea inside the injector. The urea

easily become solid when effected by the temperature in main flow gaseous; that reaction only occurred in L-shaped injector, because that injector directly blocked the exhaust main flow gaseous. The NOx conversion value from I-shaped injector also better than L-shaped injector in this study. That shows that the ammonia quantity can affect to NOx reduction in the SCR system. This NOx conversion value can increase if the ammonia gas quantity also increase.

Chapter 8

Summary and conclusion

This thesis was generally focus to improvement NOx conversion efficiency in SCR system. The investigation to measure NOx conversion was dealing with optical chamber and commercial SCR system from 3L diesel engine and 12L diesel engine. The experimental and simulation with changing the injector position to improve the spray phenomena; modified the mixer fan with 16 blades to increase the distribution and mixing gas inside the system; raising the suitable temperature to increase the evaporation process; injection timing strategy and adding the super-hydropobic material to prevent solid deposit formation; and using different injector models has been investigated to improve the NOx conversion value in SCR system. The following conclusions can be drawn from this study.

- The optical access and commercial SCR system used 3L diesel engine to produce 223 kg/h of flow mass and 362°C of exhaust temperature in 2000rpm. That parameter can achieve best quantity of mass flow and quality of temperature for urea injection at 20second after engine start-up. Those conditions resulted the best time for urea inject into the SCR system. The quality of urea decomposition process will improve and prevent the solid deposited formation in the system.
- This study used four types of design to investigate ammonia uniformity value. The stable condition was the condition after 20s engine start-up and unstable condition was ignore the temperature condition in the system. The simulation study with three dimensional model found type-I and type-II had a fairly ammonia uniform pattern, but low ammonia gas ratio in the SCR system; type-III and type IV had good ammonia uniformity pattern and high ammonia gas ratio. By the optimization of the urea injection timing, this study reach the ammonia uniformity value of 97.62% in type-IV. The SCR system with optimization of the urea injection timing conditions could reduce 75% of the NOx concentration from the diesel engine. These results imply that urea injection timing and wall temperatures is the first factors to improve NOx conversion efficiency in SCR system.

Type	The urea injection conditions	Mixer
1	Unstable	Without
2	Stable	Without
3	Unstable	With
4	Stable	With

- The second factor to improve NOx conversion efficiency in SCR system was the investigation of solid deposit formation in low and high wall impingement. This study shows the droplet

spray impingement was important role regarding the urea distribution and solid deposit formation. The low wall temperature (313 K) produce high droplets of urea-SCR reductant are adhered on the wall surface and high the urea crystallization in the system. At high wall temperature (> 453 K), an amount of ammonia gas is easily to produced. This is because, at high temperature heat transfer rate is very high from wall to droplets, thus droplet evaporation increases significantly. The improvement for urea droplet evaporation also can found by adding the super-hydrophobic surface. Based on the experiment, super-hydrophobic surface assist the urea break-up process after hit the plate and produces smaller size of urea particle. That particle easily to evaporate and produce high quality of ammonia in the system. By the increasing ammonia gas and reduce the solid deposit formation can assist the NOx conversion process in the SCR system.

- The third factor to improve NOx conversion efficiency in SCR system was the investigation of ammonia uniformity quantity in the catalyst surface. Ammonia uniformity was used to evaluate mixture quality, which greatly influences the catalyst de-NOx efficiency. The low uniformity was found when the study only used gas flow from 1500 rpm engine operation condition and without assist by mixer fan; this condition is very likely to yield poor de-NOx efficiency and high ammonia and isocyanic acid slips. Based on that result, this study investigate the improving of ammonia uniformity with two additional engine operation conditions (2000 rpm and 3000 rpm) were tested using a mixer fan with 16 blades. Each blade had an inclination angle of 35° to increase the pressure and creating better turbulence in the system.
- This study used six combination models to investigate the potential enhancements of the mixing process to produce high ammonia uniformity and NOx conversion efficiency. In the result shows type-II (2000 rpm without mixer) and type-III (3000 rpm without mixer) have similar results to type-I (1500 rpm without mixer), e.g., a low level mixing reaction and poor SCR performance. However, for type-IV (1500 rpm with mixer), type-V (2000 rpm with mixer), and type-VI (3000 rpm with mixer), the ammonia uniformity significantly increased.
- The forth factor to improve NOx conversion efficiency in SCR system was investigation the urea injectors model effect to urea evaporation process. The urea evaporation model were studied in optical access and 3L diesel engines difficult to apply on the larger engines. Based on that situation, this study investigate 12L heavy-duty diesel engine with 513 kg/h exhaust mass flow rate, a 1,330 ppm NOx value, and a 686 K exhaust gas temperature in 1000rpm. The investigation of original urea injector (L-shaped) shows the compaction of urea inside the injector, thus inhibiting the urea injection process. This phenomenon has a negative effect on the NOx conversion efficiency in the SCR system. Based on that problem, the suggested urea injector (I-shaped) have to solve the solidification of urea inside the injector, because the shape and position of I-shaped urea injector were suitable for the SCR system.

- The study of ammonia generation and distribution showed that the I-shaped injector produced the highest amount of ammonia during saturation, while the L-shaped injector produce the highest ammonia distribution in this system. The investigation of urea solidification inside L-shaped injector also can validate the ammonia quantity values for that injector. The lowest ammonia quantity affected by the hampered distribution urea inside the injector. The urea easily become solid when effected by the temperature in main flow gaseous; that reaction only occurred in L-shaped injector, because that injector directly blocked the exhaust main flow gaseous. Although produce lowest ammonia value, the L-shaped injector can distribute the ammonia gaseous to all side of system; that result can be proved by the ammonia homogenization quantity in the surface of catalyst. The NOx conversion value from I-shaped injector is better than L-shaped injector to decrease NOx concentration in the system. That shows that the ammonia quantity can affect to NOx conversion in the SCR system.
- Based on 4 model of study with optical access, 3L diesel engine and 12L Heavy-duty diesel engine was found that temperature as has a big effect to assist urea evaporation process in the system; the super-hydrophobic is the valuable material for urea particle break-up and reduce solid deposit formation; the modification of urea injector model and position can improve the spray quality and increase the ammonia gas quantity in the system; and by adding a mixer fan with 16 blades can increase the distribution gas inside the system and assist the mixing process between ammonia gas and NOx emission. These results explains that to improving NOx conversion efficiency in SCR system, it is necessary to optimize important factors such as temperature, gas flow, wall material, urea injection distribution, urea evaporation, ammonia gas distribution and mixing process as shown in this study. Thus, this study is a good reference for future research into increasing NOx conversion efficiency in SCR system from diesel engine and heavy-duty diesel engines, especially engines with similar parameters.

References

[1] Johnson T V. Vehicular emissions in review. SAE Int J Engines 2012;5:216–34.

[2] Cho SM. Properly apply selective catalytic reduction for NOx removal. Chem Eng Prog 1994;90:39–45.

[3] Optimization of ammonia source for SCR applications. Proc. 2003 Mega Symp., n.d.

[4] Fritz A, Pitchon V. The current state of research on automotive lean NOx catalysis. Appl Catal B Environ 1997;13:1–25.

[5] Weeks CL, Ibeling DR, Han S, Ludwig L, Ayyappan P. Analytical investigation of urea deposits in SCR system. SAE Int J Engines 2015;8:1219–39.

[6] Dong H, Shuai S, Wang J. Effect of urea thermal decomposition on diesel NOx-SCR aftertreatment systems. SAE Technical Paper; 2008.

[7] Zheng G, Fila A, Kotrba A, Floyd R. Investigation of urea deposits in urea SCR systems for medium and heavy duty trucks. SAE Technical Paper; 2010.

[8] Munnannur A, Chiruta M, Liu ZG. Thermal and fluid dynamic considerations in aftertreatment system design for SCR solid deposit mitigation. SAE Technical Paper; 2012.

[9] Strots VO, Santhanam S, Adelman BJ, Griffin GA, Derybowski EM. Deposit formation in urea-SCR systems. SAE Int J Fuels Lubr 2010;2:283–9.

[10] Wardana MKA, Lim O. Investigation of Solid Deposit Inside L-Type Urea Injector and NOx Conversion in a Heavy-Duty Diesel Engine. Catalysts 2021;11:595. https://doi.org/10.3390/catal11050595.

[11] Mera Z, Matzer C, Hausberger S, Fonseca N. Performance of selective catalytic reduction (SCR) system in a diesel passenger car under real-world conditions. Appl Therm Eng 2020;181:115983. https://doi.org/10.1016/j.applthermaleng.2020.115983.

[12] Maunula T, Kinnunen T, Kanniainen K, Viitanen A, Savimaki A. Thermally Durable Vanadium-SCR Catalysts for Diesel Applications. SAE Tech Pap 2013. https://doi.org/10.4271/2013-01-1063.

[13] Gao Y, Liu Q, Bian L. Numerical simulation and optimization of flow field in the SCR denitrification system on a 600 MW capacity units. Energy Procedia 2012;14:370–5. https://doi.org/10.1016/j.egypro.2011.12.944.

[14] Colombo M, Nova I, Tronconi E, Schmei??er V, Weibel M. Mathematical modelling of cold start effects over zeolite SCR catalysts for exhaust gas aftertreatment. Catal Today 2014;231:99–104. https://doi.org/10.1016/j.cattod.2014.01.044.

[15] Lee SI, Park SY. Numerical analysis of internal flow characteristics of urea injectors for SCR dosing system. Fuel 2014;129:54–60. https://doi.org/10.1016/j.fuel.2014.03.031.

[16] Saari S, Karjalainen P, Ntziachristos L, Pirjola L, Matilainen P, Keskinen J, et al. Exhaust particle and NOx emission performance of an SCR heavy duty truck operating in real-world conditions. Atmos Environ 2016;126:136–44. https://doi.org/10.1016/j.atmosenv.2015.11.047.

[17] Khair MK, Jääskeläinen H. Emission formation in diesel engines. SAE Eng Acad Lect Notes 2001.

[18] Forsthuber F, Krenek T, Marinitsch F, Lauer T, Weiss J, Raup M, et al. Investigations on the Tail-Pipe Emissions of Commercial Engines with Advanced One-Dimensional Simulation Methods 2013. https://doi.org/10.4271/2013-01-1117.

[19] Mehregan M, Moghiman M. Experimental investigation of the distinct effects of nanoparticles addition and urea-SCR after-treatment system on NOx emissions in a blended-biodiesel fueled internal combustion engine. Fuel 2020;262:116609. https://doi.org/10.1016/j.fuel.2019.116609.

[20] Weiss M, Bonnel P, Kühlwein J, Provenza A, Lambrecht U, Alessandrini S, et al. Will Euro 6 reduce the NOx emissions of new diesel cars?–Insights from on-road tests with Portable Emissions Measurement Systems (PEMS). Atmos Environ 2012;62:657–65.

[21] Delphi. Delphi-Emissions for Heavy Duty and Off-Highway Vehicles 2018-2019 2018.

[22] Iodice P, Senatore A. Air Pollution and Air Quality State in an Italian National Interest Priority Site. Part 2: The Pollutant Dispersion. Energy Procedia 2015;81:637–43. https://doi.org/10.1016/j.egypro.2015.12.048.

[23] Song Y, Hashemi H, Christensen JM, Zou C, Marshall P, Glarborg P. Ammonia oxidation at high pressure and intermediate temperatures. Fuel 2016;181:358–65. https://doi.org/10.1016/j.fuel.2016.04.100.

[24] Koebel M, Elsener M, Kleemann M. Urea-SCR: a promising technique to reduce NOx emissions from automotive diesel engines. Catal Today 2000;59:335–45.

[25] Birkhold F, Meingast U, Wassermann P, Deutschmann O. Modeling and simulation of the injection of urea-water-solution for automotive SCR DeNOx-systems. Appl Catal B Environ 2007;70:119–27.

[26] Yim SD, Kim SJ, Baik JH, Nam IS, Mok YS, Lee J-H, et al. Decomposition of Urea into NH3 for the SCR Process. Ind Eng Chem Res 2004;43:4856–63.

[27] Koebel M, Strutz EO. Thermal and Hydrolytic Decomposition of Urea for Automotive Selective Catalytic Reduction Systems: Thermochemical and Practical Aspects. Ind Eng Chem Res 2003;42:2093–100. https://doi.org/10.1021/ie020950o.

[28] Wärmeatlas VDI. VDI-Gesellschaft Verfahrenstechnik und Chemieingenieurwesen 2006.

[29] Fischer S. Simulation of the Urea-water-solution Preparation and Ammonia-homogenization with a Validated CFD-model for the Optimization of Automotive SCR-systems. na; 2012.

[30] Crowe CT. Multiphase flow handbook. vol. 59. CRC press; 2005.

[31] Samuelsson E, Holmberg S. A CFD study of the urea supply, droplet breakup and mixing in a pipe upstream of a SCR catalyst 2013.

[32] Bai C, Gosman AD. Development of methodology for spray impingement simulation. SAE Technical Paper; 1995.

[33] Bernardin JD, Mudawar I. The Leidenfrost point: experimental study and assessment of existing models. J Heat Transfer 1999;121:894–903.

[34] Dunand P, Castanet G, Gradeck M, Maillet D, Lemoine F. Energy balance of droplets impinging onto a wall heated above the Leidenfrost temperature. Int J Heat Fluid Flow 2013;44:170–80.

[35] Kuhnke D. Spray/wall interaction modelling by dimensionless data analysis. Shaker; 2004.

[36] Birkhold F, Meingast U, Wassermann P, Deutschmann O. Analysis of the injection of urea-water-solution for automotive SCR DeNOx-systems: modeling of two-phase flow and spray/wall-interaction. SAE Technical Paper; 2006.

[37] Qi F, Xiong S, Liao Y, Dang H, Yang S. A novel dual layer SCR catalyst with a broad temperature window for the control of NOx emission from diesel bus. Catal Commun 2015;65:108–12. https://doi.org/10.1016/j.catcom.2015.03.002.

[38] Crowe CT, Schwarzkopf JD, Sommerfeld M, Tsuji Y. Multiphase flows with droplets and particles. CRC press; 2011.

[39] Lefebvre AH. Atomization and sprays, combustion: an international series. Hemisph Pub Corp 1989.

[40] Xu L, Watkins W, Snow R, Graham G, McCabe R, Lambert C, et al. Laboratory and engine study of urea-related deposits in diesel urea-SCR after-treatment systems. SAE Technical Paper; 2007.

[41] Liao Y, Nocivelli L, Eggenschwiler PD, Spiteri A. Experimental investigation of urea-water sprays in selective catalytic reduction (SCR) systems. 15. Int. Stuttgarter Symp., Springer; 2015, p. 953–66.

[42] Hsieh M-F, Wang J. Development and experimental studies of a control-oriented SCR model for a two-catalyst urea-SCR system. Control Eng Pract 2011;19:409–22.

[43] Nishioka A, Sukegawa Y, Katogi K, Mamada H, Kowatari T, Mukai T, et al. A study of a new aftertreatment system (2): control of urea solution spray for Urea-SCR. SAE Technical Paper; 2006.

[44] Birkhold F. Selektive katalytische Reduktion von Stickoxiden in Kraftfahrzeugen: Untersuchung der Einspritzung von Harnstoffwasserlösung. Shaker; 2007.

[45] Smith H, Zöchbauer M, Lauer T. Advanced Spray Impingement Modelling for an Improved Prediction Accuracy of the Ammonia Homogenisation in SCR Systems. SAE Tech Pap 2015. https://doi.org/10.4271/2015-01-1054.

[46] Baleta J, Mikulčić H, Vujanović M, Petranović Z, Duić N. Numerical simulation of urea based selective non-catalytic reduction deNOx process for industrial applications. Energy Convers Manag 2016. https://doi.org/10.1016/j.enconman.2016.01.062.

[47] Chun DM, Ngo CV, Lee KM. Fast fabrication of superhydrophobic metallic surface using

nanosecond laser texturing and low-temperature annealing. CIRP Ann - Manuf Technol 2016;65:519–22. https://doi.org/10.1016/j.cirp.2016.04.019.

[48] Ngo CV, Chun DM. Control of laser-ablated aluminum surface wettability to superhydrophobic or superhydrophilic through simple heat treatment or water boiling post-processing. Appl Surf Sci 2018;435:974–82. https://doi.org/10.1016/j.apsusc.2017.11.185.

[49] Khristamto M, Wardana A, Oh K, Lee YJ, Woo YM, Lim O. EFFECTS OF UREA INJECTION TIMING ON PREDICTING NO X CONVERSION IN SCR SYSTEMS. Int J Automot Technol 2020;21:137–45. https://doi.org/10.1007/s12239.

[50] Shahariar GMH, Khristamto M, Wardana A, Lim OT. Investigation of urea-water solution spray impingement on the hot surface of automotive SCR system. J Mech Sci Technol 2018;32:2935–46. https://doi.org/10.1007/s12206-018-0550-9.

[51] Khristamto M, Wardana A, Shahariar GMH, Oh K, Lim O. AMMONIA UNIFORMITY TO PREDICT NOX REDUCTION EFFICIENCY IN AN SCR SYSTEM. Int J Automot Technol 2019;20:313–25. https://doi.org/10.1007/s12239.

[52] Senecal PK, Richards KJ, Pomraning E, Yang T, Dai MZ, McDavid RM, et al. A new parallel cut-cell Cartesian CFD code for rapid grid generation applied to in-cylinder diesel engine simulations. SAE Technical Paper; 2007.

[53] Ström H, Lundström A, Andersson B. Choice of urea-spray models in CFD simulations of urea-SCR systems. Chem Eng J 2009;150:69–82. https://doi.org/10.1016/j.cej.2008.12.003.

[54] Drennan S, Kumar G, Quan S, Wang M. Application of Automatic Meshing to Urea-Water Injection Simulation for Engine Aftertreatment. SAE Technical Paper; 2015.

[55] STAR CCM+ version 1104 Theory Guide, (2016). n.d.

[56] Zhang X, Romzek M, Morgan C. 3-D Numerical Study of Mixing Characteristics of NH3 in Front of SCR, 2006. https://doi.org/10.4271/2006-01-3444.

[57] Yi Y. Development of a 3D Numerical Model for Predicting Spray , Urea Decomposition and Mixing in SCR Systems. SAE Int 2017. https://doi.org/10.4271/2007-01-3985.

[58] Schaber PM, Colson J, Higgins S, Dietz E, Thielen D, Anspach B, et al. Study of the urea thermal decomposition (pyrolysis) reaction and importance to cyanuric acid production. Am Lab 1999;31:13–21.

[59] Li Z, Deng J, Li L, Cao L, Wu Z. A study on the factors affecting heated wall impinging characteristics of SCR spray. SAE Technical Paper; 2011.

[60] STAR-CCM+ Guide. STAR-CCM + ® Documentation 2018.

[61] Chae HJ, Choo ST, Choi H, Nam I. Direct Use of Kinetic Parameters for Modeling and Simulation of a Selective Catalytic Reduction process. Ind Eng Chem Res 2000;39:1159–70. https://doi.org/10.1021/ie9907270.

[62] Wardana MKA, Oh K, Lim O. Investigation of urea uniformity with different types of urea injectors in an SCR system. Catalysts 2020;10:1–14. https://doi.org/10.3390/catal10111269.

Publications

International Publications

[1] G M Hasan Shahariar, **Muhammad Khristamto Aditya Wardana** and Ock Taeck LIM, "Investigation of urea-water solution spray impingement on the hot surface of automotive SCR system", JMST, 32:2935-2946. https://doi.org/10.1007/s12206-018-0550-9. **Journal of Mechanical Science and Technology (JMST).**

[2] **Khristamto M, Wardana A,** Oh K, Lee YJ, Woo YM, Lim O. EFFECTS OF UREA INJECTION TIMING ON PREDICTING NO X CONVERSION IN SCR SYSTEMS. Int J Automot Technol 2020;21:137–45. https://doi.org/10.1007/s12239**. International Journal Automotive Technology (IJAT)**

[3] **Khristamto M, Wardana A**, Shahariar GMH, Oh K, Lim O. AMMONIA UNIFORMITY TO PREDICT NOX REDUCTION EFFICIENCY IN AN SCR SYSTEM. Int J Automot Technol 2019;20:313–25. https://doi.org/10.1007/s12239. **International Journal Automotive Technology (IJAT)**

[4] **Khristamto M, Wardana A**, Oh K, Lim O. Investigation of urea uniformity with different types of urea injectors in an SCR system. Catalysts 2020;10:1–14. https://doi.org/10.3390/catal10111269. **CATALYST Journal**.

[5] **Khristamto M, Wardana A** and Lim O. Investigation of solid deposit inside L-type urea injector and NOx conversion in a heavy-duty diesel engine. Catalysts 2021, 11, 595. https://doi.org/10.3390/catal11050595. **CATALYST Journal**.

[6] **Khristamto M, Wardana A**, Oh K, Lim O. The investigation of ammonia homogenization and NOx reduction quantity by remodeling urea injector shapes in heavy duty diesel engines. **Applied Energy Journal.** (under review)

[7] G M Hasan Shahariar, **Muhammad Khristamto Aditya Wardana** and Ock Taeck LIM, "A study on post impingement effects of urea-water solution spray on the heated wall of automotive SCR systems", **IOP Conference Series: Earth and Environmental Science**.

[8] **Khristamto M, Wardana A,** J Hyun, O Lim, A study of urea injection timing to predict the NOx conversion in SCR systems, **Energy Procedia** 158, 1942-1948.

[9] **Khristamto M, Wardana A,** LY Jae, W Youngmin, K Oh, O Lim, A study of optimization NOx reduction quality with different types of urea injectors in an SCR system, **2020 5th International Conference on Smart and Sustainable Technologies (SpliTech)** 1-5.

[10] **Khristamto M, Wardana A,** Hasan, S. GM, O Lim,A study about the effects of injection pressure and wall temperature to prediction decomposition of NH3 in SCR system, ", **IOP Conference Series: Earth and Environmental Science**

[11] **Khristamto M, Wardana A,** J Hyun, O Lim, THE VARIATIONS OF UREA INJECTOR TYPE TO OPTIMIZE THE NOX REDUCTION EFFICIENCY IN HEAVY DUTY DIESEL ENGINE, **International Conference on Applied Energy 2019 (ICAE 2019)**

[12] **Khristamto M, Wardana A,** Oh K, Lim O. The optimization of NOx reduction quality with 2 different types of urea injectors in heavy duty diesel engine, **International Conference on Applied Energy 2020 (ICAE 2020).**

[13] **Muhammad Khristamto Aditya Wardana** and Ock Taeck LIM, "The Effect Exhaust Temperature on the Urea Evaporation Process in SCR Systems", **Proceedings of the Korean Society of Automotive Engineers Conference, 98-98.**

International Conferences

[1] G M Hasan Shahariar, **Muhammad Khristamto Aditya Wardana** and Ock Taeck LIM, **2018 Asia Conference on Energy and Environment Engineering**.

[2] G M Hasan Shahariar, **Muhammad Khristamto Aditya Wardana** and Ock Taeck LIM, **2018 IOP Conference Series: Earth and Environmental Science**.

[3] **Khristamto M, Wardana A,** Hasan, S. GM, **2018 IOP Conference Series: Earth and Environmental Science**

[4] **Khristamto M, Wardana A,** J Hyun, O Lim, **International Conference on Applied Energy 2019 (ICAE 2019), Västerås, Sweden, 2019.**

[5] **Khristamto M, Wardana A**, Oh K, Lim O, **International Conference on Advanced Automotive Technology (ICAT) 2019, Gwangju, Republic of Korea, 2019**

[6] **Khristamto M, Wardana A,** Oh K, Lim O. **International Conference on Applied Energy 2020 (ICAE 2020), Bangkok, Thailand, 2020.**

[7] **Khristamto M, Wardana A,** LY Jae, W Youngmin, K Oh, O Lim, **2020 5th International Conference on Smart and Sustainable Technologies (SpliTech 2020)** 1-5.

Domestic Conferences

[1] Muhammad Khristamto Aditya Wardana, G M Hasan Shahariar and Ock Taeck LIM**, Korea Hydrogen & New Energy Conference 2016 Fall Conference, Gwangju, 2016.**

[2] G M Hasan Shahariar**, Muhammad Khristamto Aditya Wardana** and Ock Taeck LIM, **Korea Hydrogen & New Energy Conference 2016 Fall Conference, Gwangju, 2016.**

[3] G M Hasan Shahariar, **Muhammad Khristamto Aditya Wardana** and Ock Taeck LIM, "A Numerical study on urea-water solution spray impingement on the heated wall of automotive SCR DeNox-systems", **KSAE Spring conference 2017**.

[4] Muhammad Khristamto Aditya Wardana, G M Hasan Shahariar and Ock Taeck LIM, "A study about the effects of Exhaust pressure to prediction temperature and decomposition of NH3 in SCR system", **KSAE Spring conference 2017**.

[5] Muhammad Khristamto Aditya Wardana, G M Hasan Shahariar and Ock Taeck LIM, KSME 2017 Spring Conference at Ulsan Division, UNIST, Ulsan, Korea, 2017.

[6] G M Hasan Shahariar, **Muhammad Khristamto Aditya Wardana**, and Ock Taeck LIM, KSME 2017 Spring Conference at Ulsan Division, UNIST, Ulsan, Korea, 2017

[7] **Muhammad Khristamto Aditya Wardana** and Ock Taeck LIM, KSAE 2018 Annual Spring Conference and Exhibition, Busan, Korea, 2018.

[8] **Muhammad Khristamto Aditya Wardana** and Ock Taeck LIM, KSAE 2018 Annual Autumn Conference, Changwon, Korea, 2018.

[9] **Muhammad Khristamto Aditya Wardana** and Ock Taeck LIM, KSME 2018 Spring Meeting at Ulsan Division, University of Ulsan, Ulsan, Korea, 2018.

[10] **Muhammad Khristamto Aditya Wardana** and Ock Taeck LIM, KSAE 2019 Annual Spring Conference, Jeju, Korea, 2019.

[11] **Muhammad Khristamto Aditya Wardana** and Ock Taeck LIM, " THE IMPROVEMENT UREA UNIFORMITY QUALITY WITH I-TYPE INJECTOR IN HEAVY DUTY DIESEL ENGINE",

Korean Society of Automotive Engineers Autumn Conference and Exhibition, 215-215, KSAE 2019 Autum Conference, Gyoengju, Korea, 2019.

[12] **Muhammad Khristamto Aditya Wardana** and Ock Taeck LIM, “INVESTIGATION OF UREA EVAPORATION PROCESS WITH 2 TYPE OF UREA INJECTOR IN SCR SYSTEM”, Korean Society of Automotive Engineers Spring Conference, 167-167, KSAE 2020 Annual Spring Conference, Gangwondo, Korea, 2020.

[13] **Muhammad Khristamto Aditya Wardana** and Ock Taeck LIM, “ The Effect Exhaust Temperature to decrease Solid deposit phenomena in SCR Systems”, Korean Society of Automotive Engineers Spring Conference, 343-343, KSAE 2020 Annual Autumn Conference, Jeju, Korea, 2020.

[14] **Muhammad Khristamto Aditya Wardana** and Ock Taeck LIM, “The Investigation of Exhaust Gas to Predict Urea Injection Timing in SCR Systems”, Korean Society of Automotive Engineers Spring Conference, 265-265, KSAE 2020, Busan, Ulsan, and Gyeongnam, 2020

Appendix

Design of the optical box

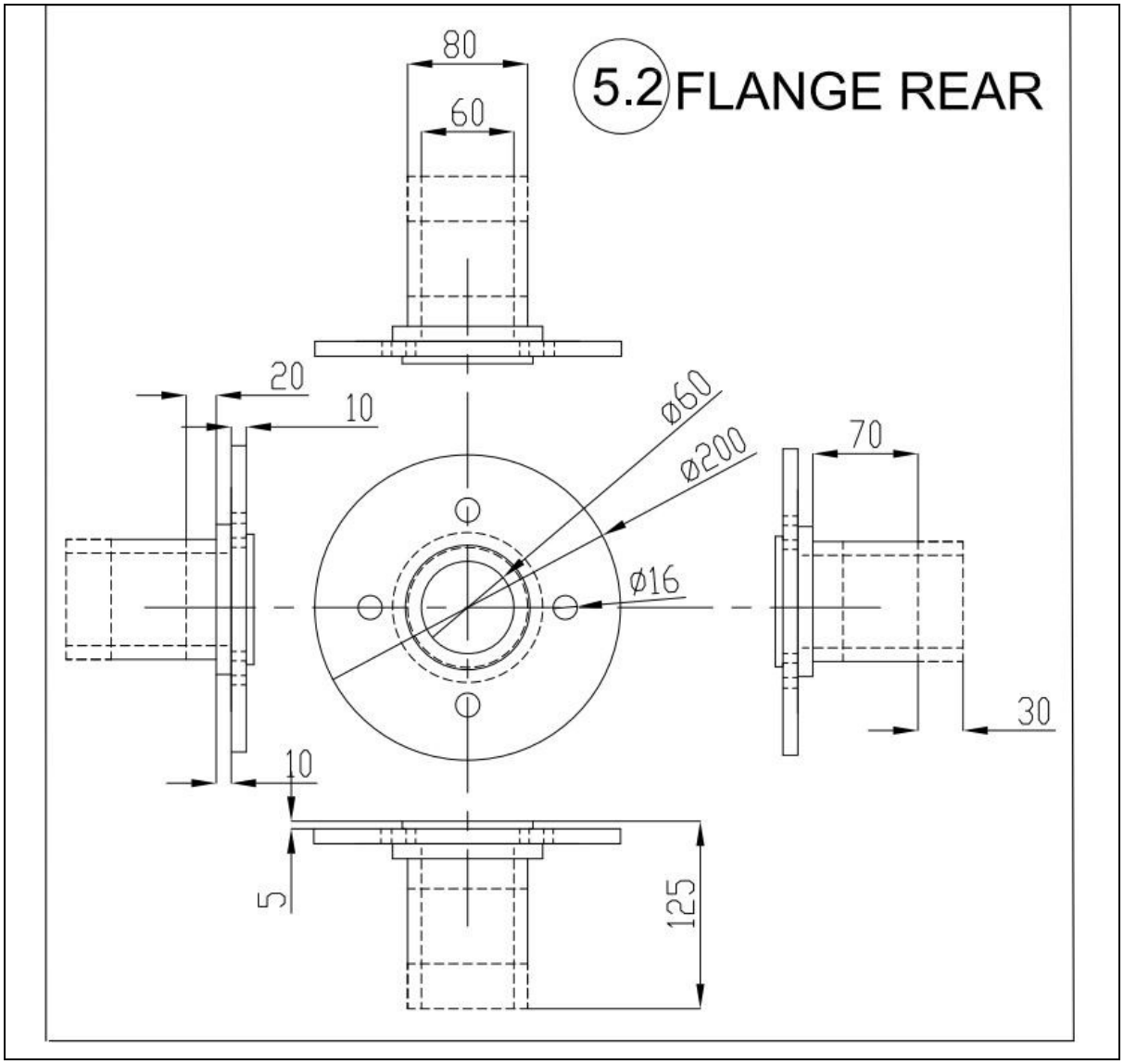

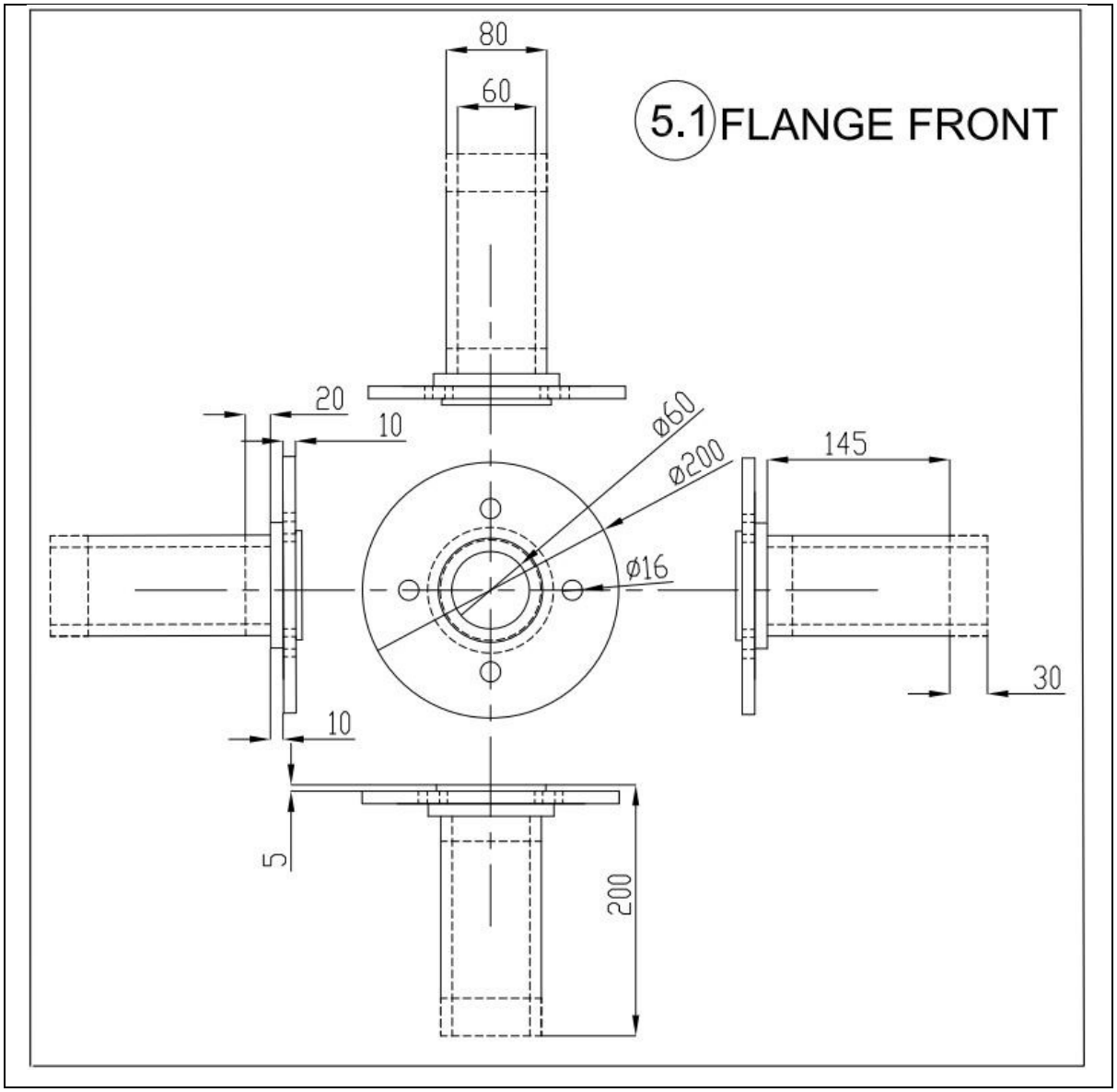
5.1 FLANGE FRONT
80
60
20
10
ø60
ø200
145
ø16
30
10
5
200

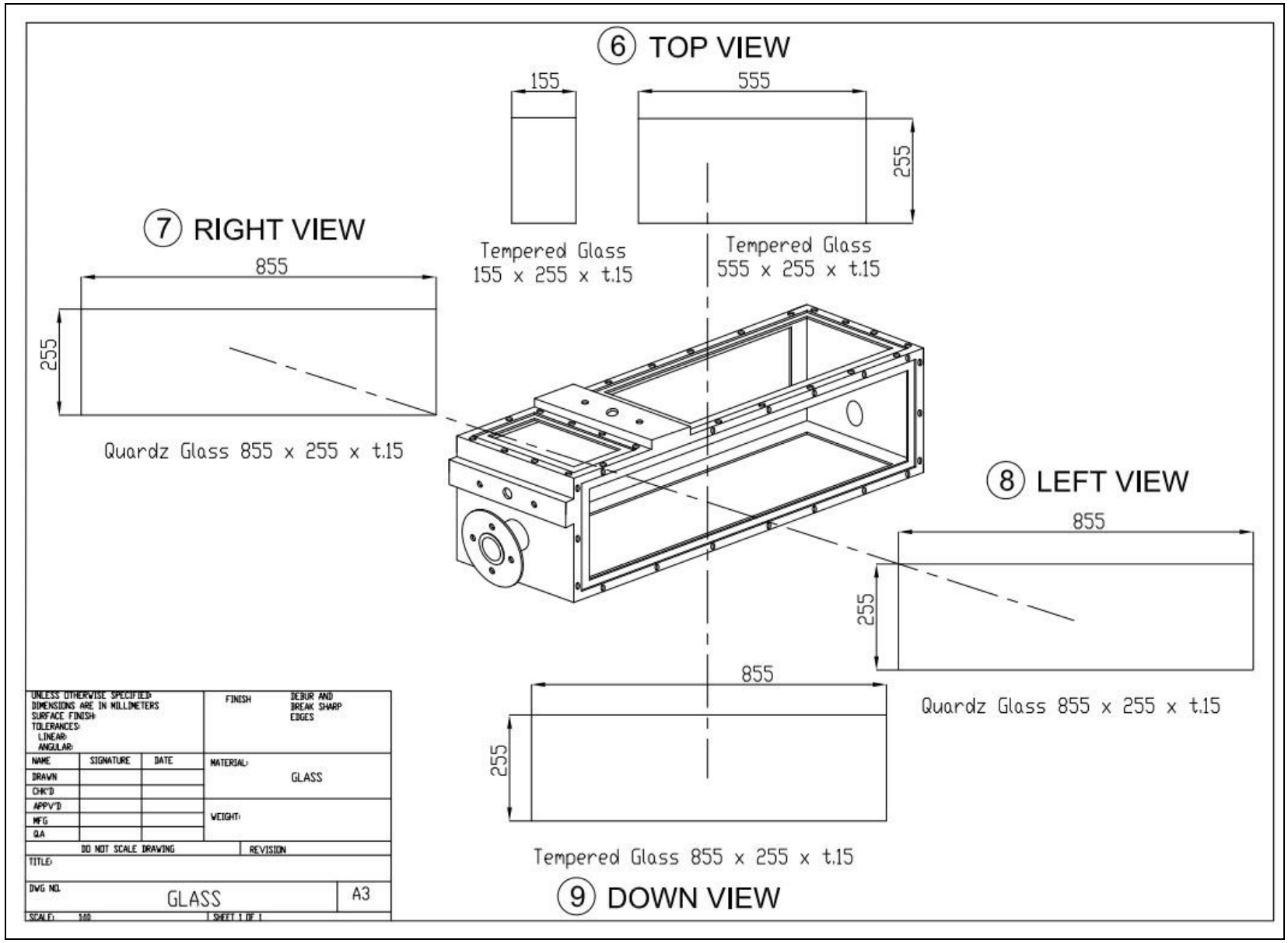
6 TOP VIEW
155
555
255
Tempered Glass
155 x 255 x t.15
Tempered Glass
555 x 255 x t.15
7 RIGHT VIEW
855
255
Quardz Glass 855 x 255 x t.15
8 LEFT VIEW
855
255
Quardz Glass 855 x 255 x t.15
855
255
Tempered Glass 855 x 255 x t.15
9 DOWN VIEW
UNLESS OTHERWISE SPECIFIED:
DIMENSIONS ARE IN MILLIMETERS
SURFACE FINISH:
TOLERANCES:
LINEAR:
ANGULAR:
FINISH
DEBUR AND
BREAK SHARP
EDGES
NAME
SIGNATURE
DATE
DRAWN
CHK'D
APPV'D
MFG
QA
MATERIAL:
GLASS
WEIGHT:
DO NOT SCALE DRAWING
REVISION
TITLE:
DWG NO.
GLASS
A3
SCALE: 1:10
SHEET 1 OF 1

② LEFT SIDE AND ③ RIGHT SIDE FRAME

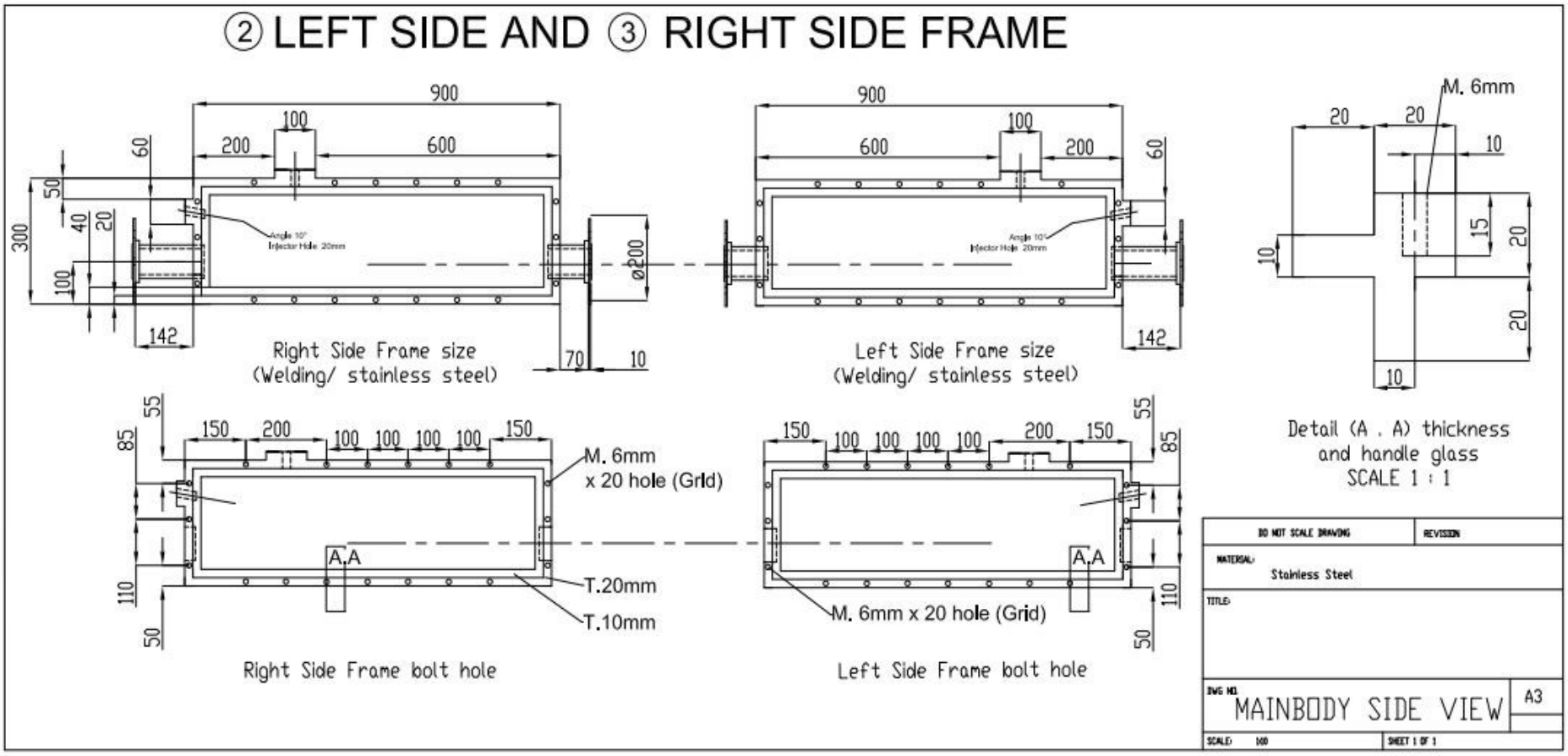

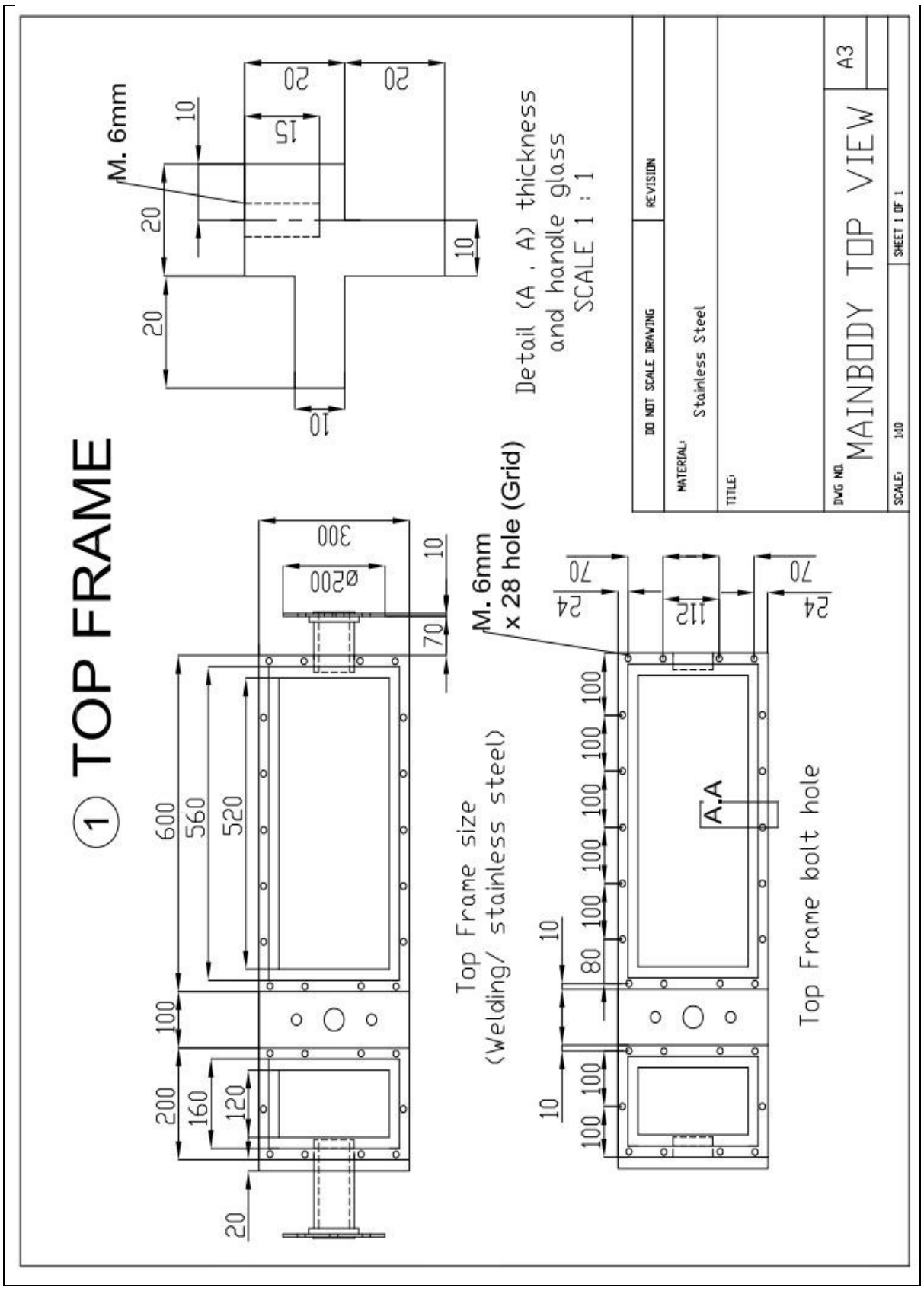
① TOP FRAME
M. 6mm
Detail (A . A) thickness
and handle glass
SCALE 1 : 1
M. 6mm
x 28 hole (Grid)
Top Frame size
(Welding/ stainless steel)
Top Frame bolt hole
A.A
DO NOT SCALE DRAWING
REVISION
MATERIAL:
Stainless Steel
TITLE:
DWG NO.
MAINBODY TOP VIEW
A3
SCALE: 1:10
SHEET 1 OF 1

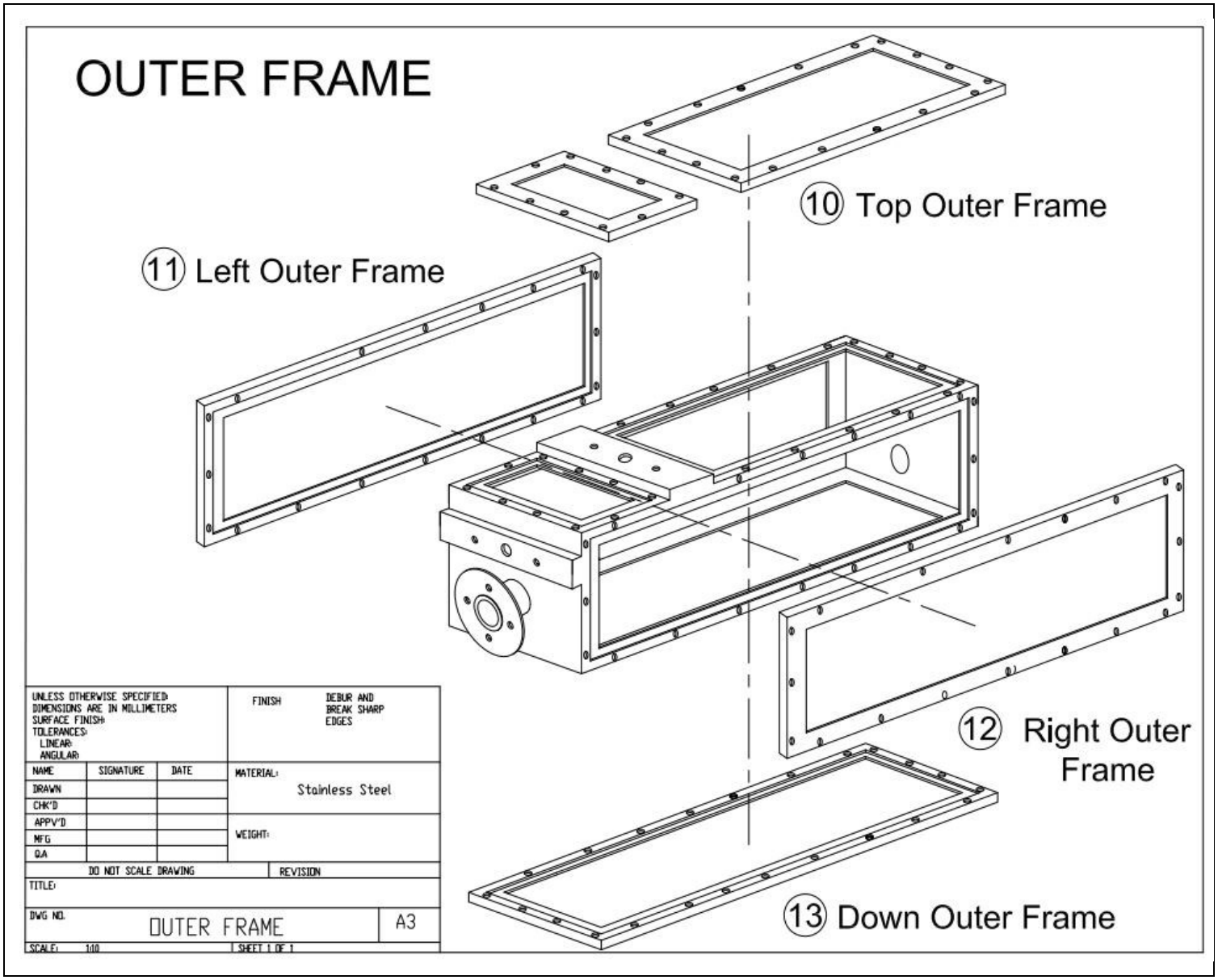
OUTER FRAME
10 Top Outer Frame
11 Left Outer Frame
12 Right Outer Frame
13 Down Outer Frame
UNLESS OTHERWISE SPECIFIED:
DIMENSIONS ARE IN MILLIMETERS
SURFACE FINISH:
TOLERANCES:
LINEAR:
ANGULAR:
FINISH
DEBUR AND BREAK SHARP EDGES
NAME
SIGNATURE
DATE
DRAWN
CHK'D
APPV'D
MFG
Q.A
MATERIAL:
Stainless Steel
WEIGHT:
DO NOT SCALE DRAWING
REVISION
TITLE:
DWG NO.
OUTER FRAME
A3
SCALE: 1:10
SHEET 1 OF 1

Design of the injector holder and other mountings

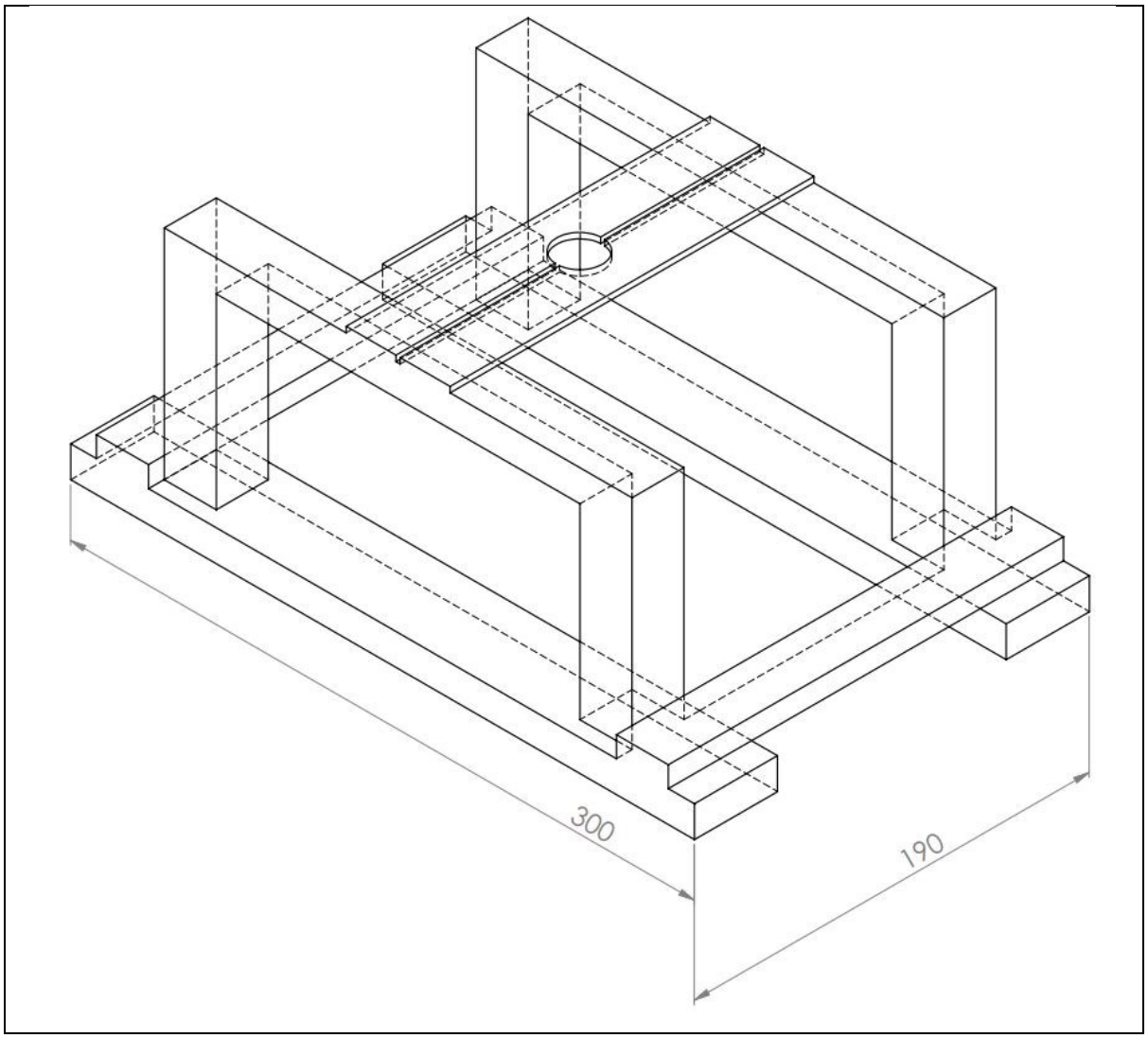

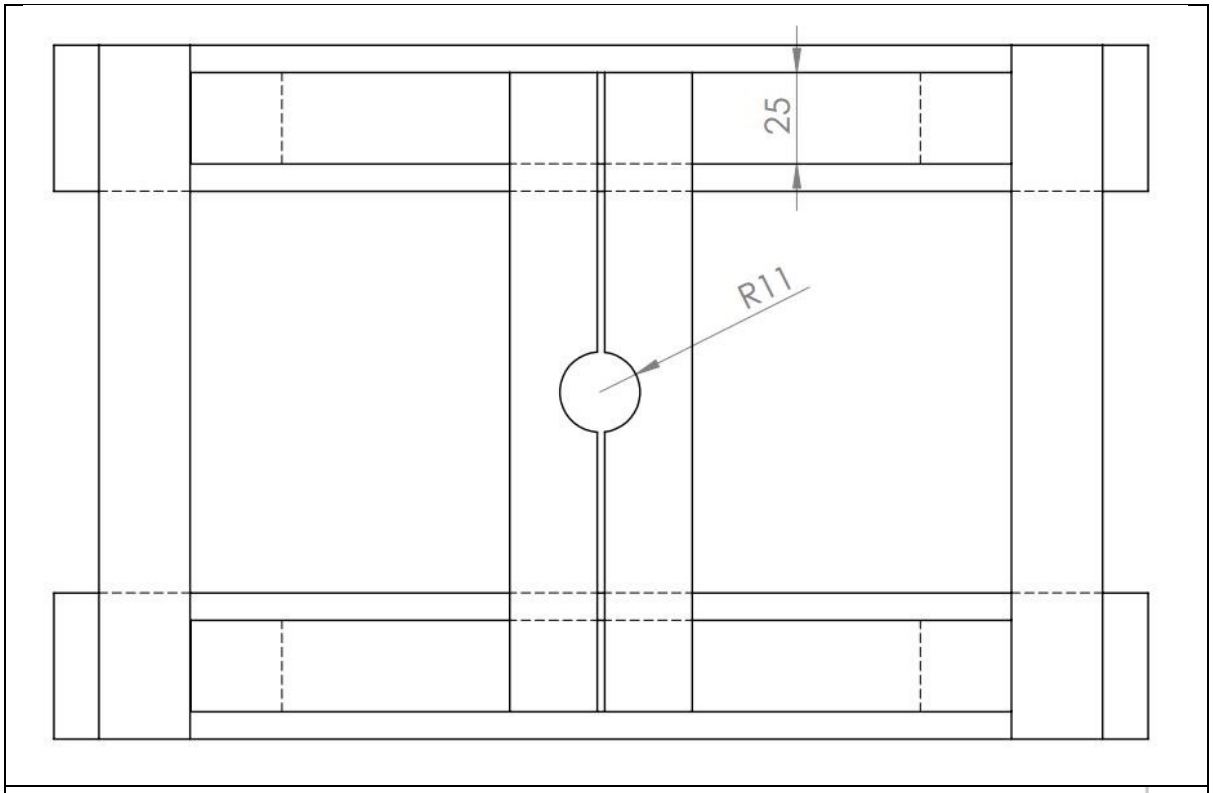
25
R11

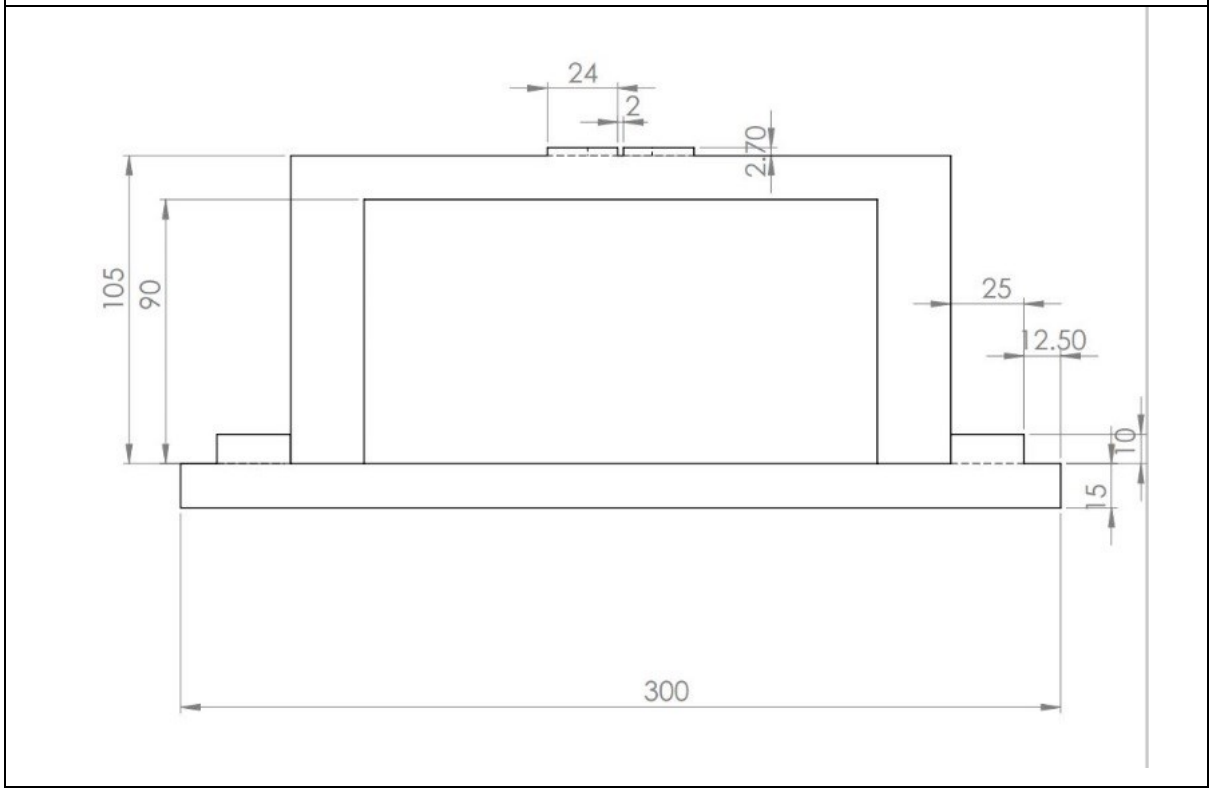
24
2
2.70
105
90
25
12.50
10
15
300

Exhaust outlet

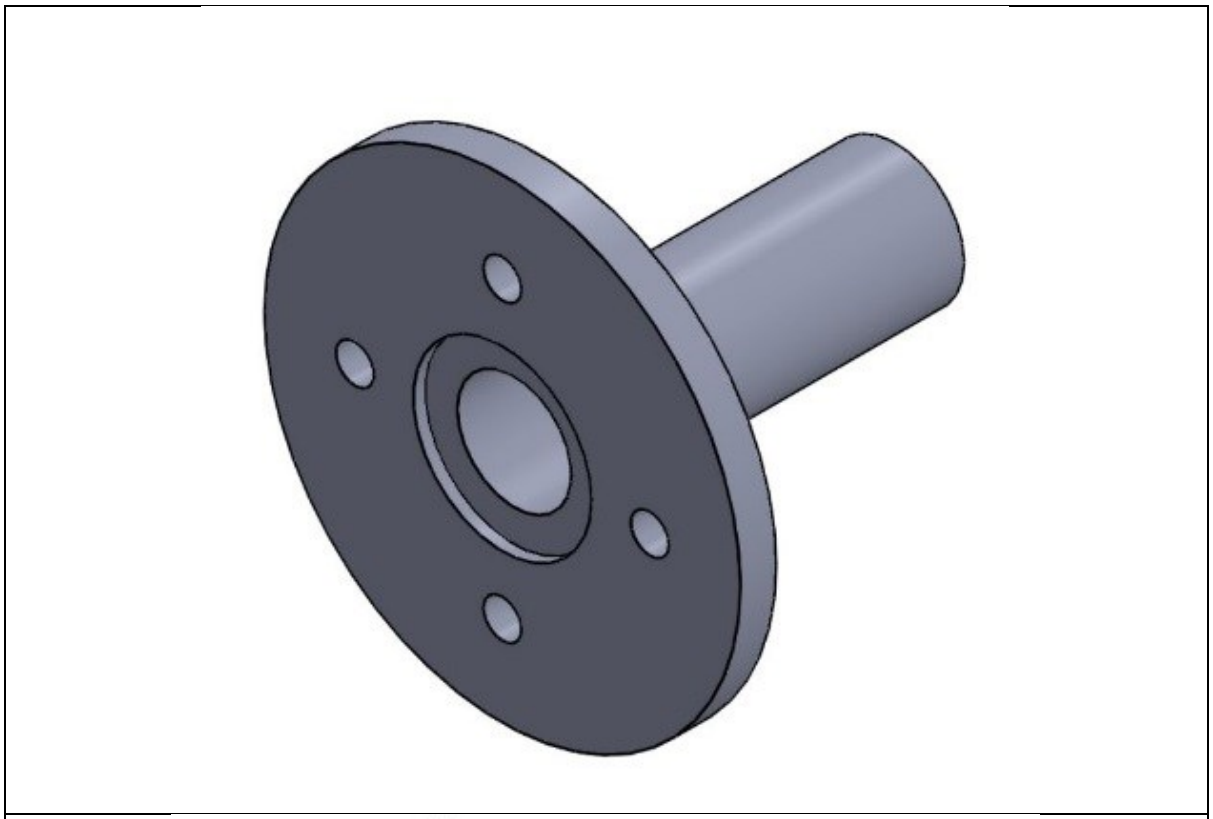

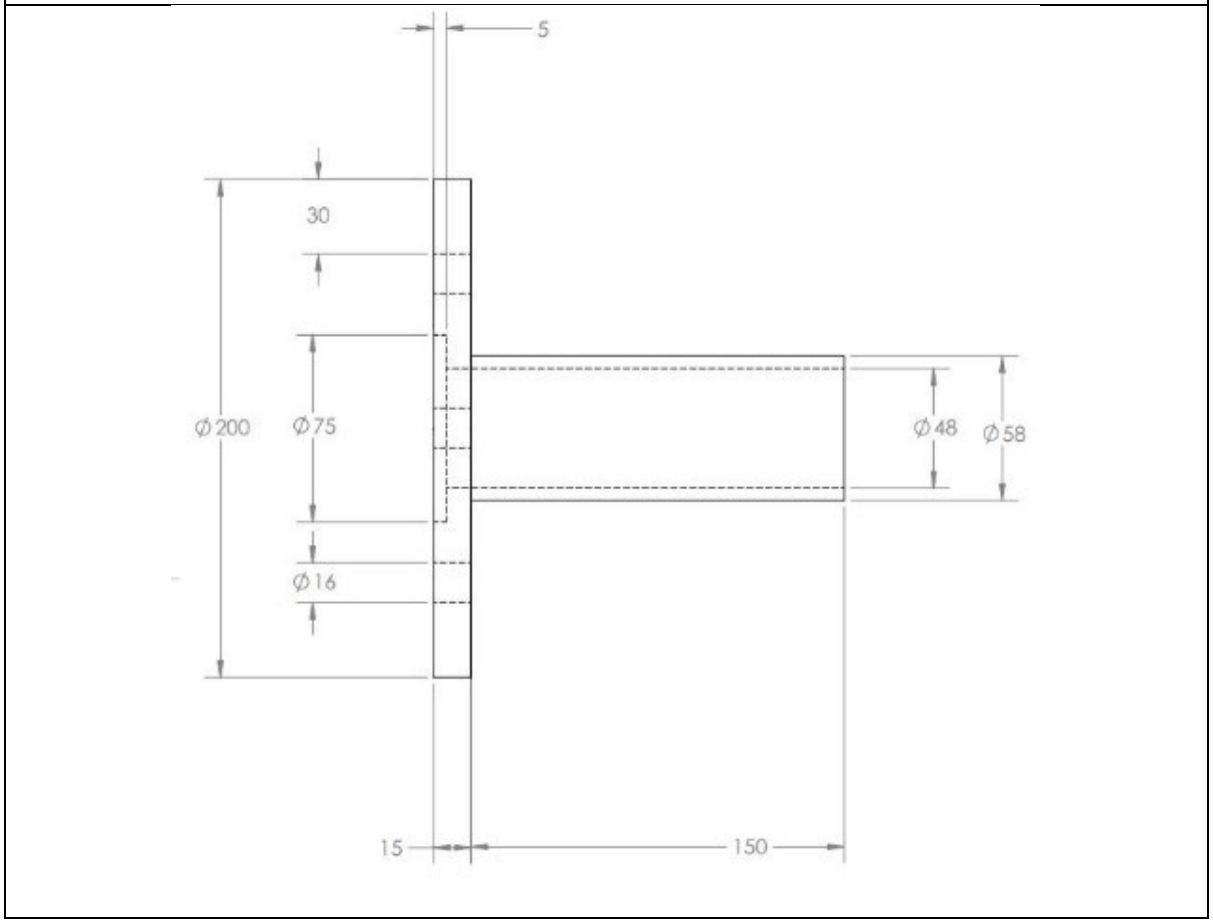

Heater connector

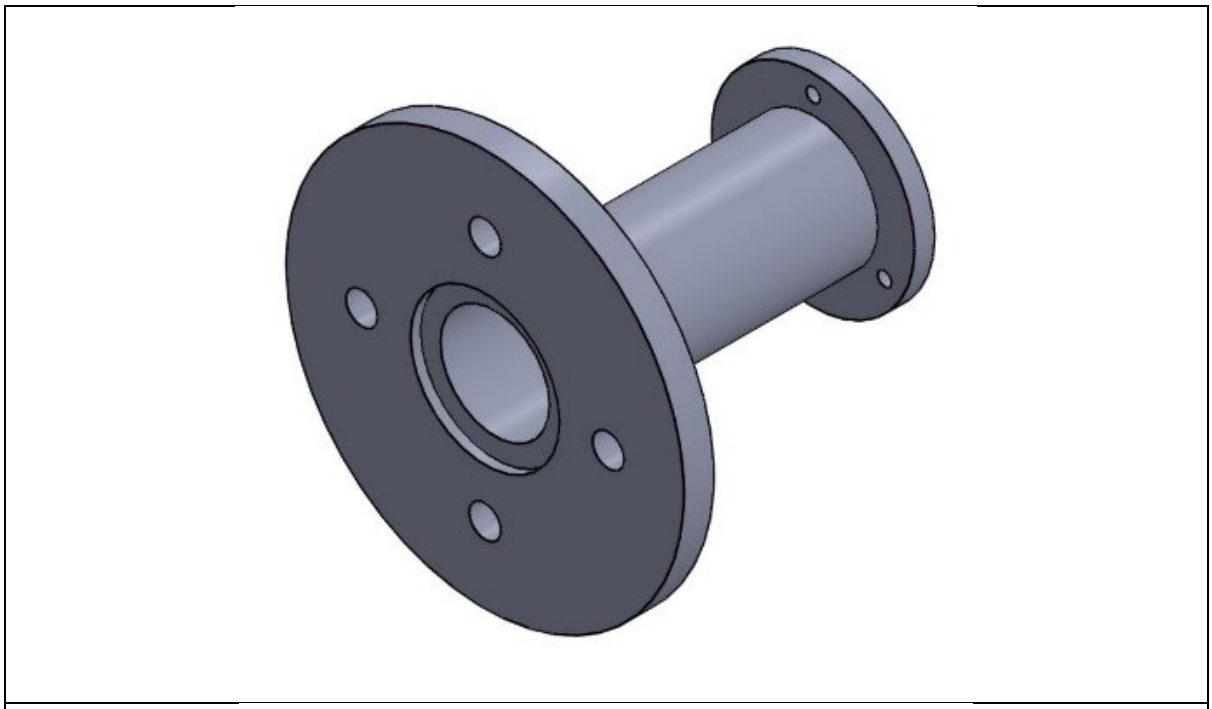

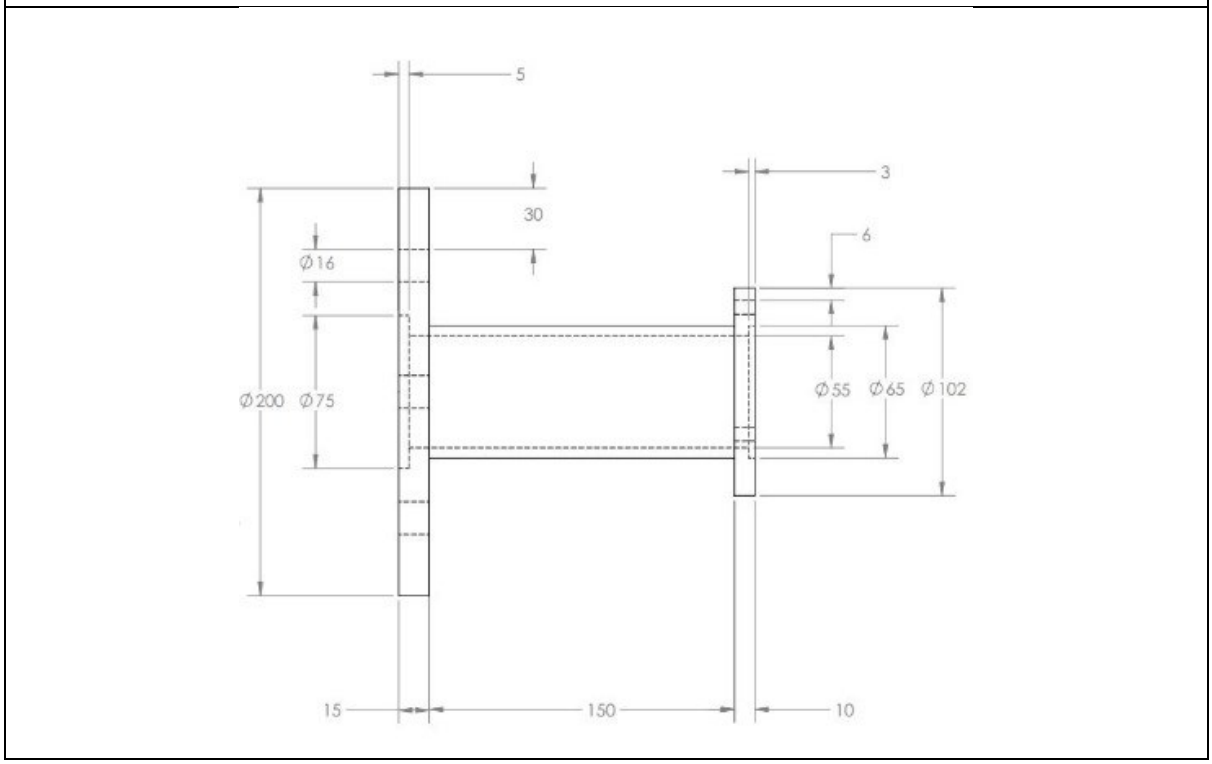

Air flow line-heater connector